

THE EFFECT OF HOT-DEFORMATION ON MECHANICAL PROPERTIES  
AND AGE HARDENING CHARACTERISTICS OF Al-Mg-Si BASED  
WROUGHT ALUMINUM ALLOYS

A THESIS SUBMITTED TO  
THE GRADUATE SCHOOL OF NATURAL AND APPLIED SCIENCES  
OF  
MIDDLE EAST TECHNICAL UNIVERSITY

BY

EVREN TAN

IN PARTIAL FULFILLMENT OF THE REQUIREMENTS  
FOR  
THE DEGREE OF MASTER OF SCIENCE  
IN  
METALLURGICAL & MATERIALS ENGINEERING

DECEMBER 2006

Approval of the Graduate School of Natural and Applied Sciences

---

Prof. Dr. Canan ÖZGEN  
Director

I certify that this thesis satisfies all the requirements as a thesis for the degree of Master of Science.

---

Prof. Dr. Tayfur ÖZTÜRK  
Head of Department

This is to certify that we have read this thesis and that in our opinion it is fully adequate, in scope and quality, as a thesis for the degree of Master of Science.

---

Prof. Dr. Bilgehan ÖGEL  
Supervisor

**Examining Committee Members**

Prof. Dr. Şakir BOR (METU, METE) \_\_\_\_\_

Prof. Dr. Bilgehan ÖGEL (METU, METE) \_\_\_\_\_

Assoc. Prof. Dr. Kadri AYDINOL (METU, METE) \_\_\_\_\_

Assoc. Prof. Dr. C. Hakan GÜR (METU, METE) \_\_\_\_\_

Dr. Yusuf Ziya KARABAY (TUBİTAK, SAGE) \_\_\_\_\_

**I hereby declare that all information in this document has been obtained and presented in accordance with academic rules and ethical conduct. I also declare that, as required by these rules and conduct, I have fully cited and referenced all material and results that are not original to this work.**

Name, Last name : Evren TAN

Signature :

# **ABSTRACT**

## **THE EFFECT OF HOT-DEFORMATION ON MECHANICAL PROPERTIES AND AGE HARDENING CHARACTERISTICS OF Al-Mg-Si BASED WROUGHT ALUMINUM ALLOYS**

Tan, Evren

M.Sc., Department of Metallurgical and Materials Engineering

Supervisor : Prof. Dr. Bilgehan Ögel

December 2006, 105 pages

Microstructural and mechanical characterizations of heat treatable Al-Mg-Si-Cu based wrought aluminum alloys have been studied. The aim of this work was to produce fine grained, high strength alloy by adjusting processing conditions: deformation, solutionizing and aging.

First, primary characterization was carried out via SEM-EDS analyses and tensile tests. Then an extensive experimental study has been carried out on two sets of samples. The first set has been studied to determine the ideal conditions for solutionizing and aging processes by analyzing the variation of hardness with different solutionizing and aging time and temperature. The second set, have first been mechanically deformed by swaging at four different deformations and four different temperatures, then heat treated. The hardness measurements have been

carried out before and after solutionizing and also after aging. Finally, recrystallization behavior has been investigated by measuring grain size before and after solutionizing treatment using image analyzer software.

The initial characterizations showed that  $Mg_2Si$  and complex iron, manganese bearing intermetallics were the primary particles observed in the  $\alpha$ -Al matrix. Nearly 140HB hardness could be obtained with solutionizing at 530°C and aging at 175°C for 8 hours which was determined as the optimum treatment for obtaining peak hardness. When shaping (deformation) was concerned; strength loss was the overall outcome of any hot or cold deformation before solutionizing; which was most probably due to the destruction of the initial microstructure. Improvement in the percent elongation was the promising aspect of this application. Strength loss was increased for samples deformed at higher temperatures and higher reductions.

**Keywords:** Al 6xxx; heat treatment; hot-deformation; grain size; microstructural characterization

## ÖZ

### SICAK ŞEKİLLENDİRMEİNİN Al-Mg-Si BAZLI İŞLENİK ALÜMİNYUM ALAŞIMLARININ MEKANİK ÖZELLİKLERİNE VE YAŞLANMA KARAKTERİSTİĞİNE ETKİSİ

Tan, Evren

Yüksek Lisans, Metalurji ve Malzeme Mühendisliği Bölümü

Tez Yöneticisi : Prof. Dr. Bilgehan Ögel

Aralık 2006, 105 sayfa

Isıl işlem uygulanabilir Al-Mg-Si-Cu bazlı alüminyum alaşımlarının iç yapı ve mekanik karakterizasyonu inceleme konusudur. Bu çalışmanın amacı; deformasyon, çözeltiye alma ve yaşlandırma gibi üretim ve ısıl işlem parametrelerinin ayarlanması ile küçük taneli, yüksek mukavemete sahip 6066 serisi alüminyum alaşımlarının üretimidir.

İlk olarak, ön karakterizasyon amacıyla taramalı elektron mikroskopisi (SEM), enerji dağılımlı x-ışını spektroskopisi (EDS) ve çekme testleri yapılmıştır. Daha sonra, geniş kapsamlı deneysel çalışmalar iki seri numunelerle yürütülmüştür. Birinci seri, çözeltiye alma ve yaşlandırma işlemlerinin ideal koşullarının bulunması amacıyla; farklı zaman ve sıcaklıklarda çözeltiye alınmış ve yaşlandırılmış numuneleri kapsamaktadır. Bu bağlamda, sertlik değişiminin ısıl işlem süresi ve sıcaklığına bağlı

değişimi incelenmiştir. İkinci seri numuneler ise; önce dört farklı sıcaklık ve oranda dövücü yardımıyla mekanik deformasyona (şekillendirme) maruz bırakılmış; daha sonra çözeltiliye alınarak yaşlandırılmıştır. İşlem aralarında alınan sertlik ölçümleriyle; alaşımın mekanik özelliklerindeki gelişim takip edilmiştir. Son olarak; yeniden kristallenme davranımı, çözeltiliye alma işlemi öncesi ve sonrası yapılan tane boyu ölçümleriyle incelenmiştir.

Ön karakterizasyon çalışmalarıyla  $\alpha$ -Al matrisin içinde  $Mg_2Si$  ve kompleks demir, mangan intermetalikleri tespit edilmiştir. Yaklaşık 140HB sertlik; optimum işlem olan  $530^\circ C$  de çözeltiliye alınmayı takiben  $175^\circ C$  de 8 saat yaşlandırmayla elde edilmiştir. Şekillendirme (deformasyon) düşünüldüğünde; çözeltiliye alma öncesi uygulanan sıcak ya da soğuk deformasyonun mukavemet düşüşüne sebebiyet verdiği saptanmıştır. Bu uygulamanın iyi yönü yüzde uzamadaki gelişmedir. Yapılan çalışma mukavemet kaybının yüksek sıcaklıklardaki yüksek deformasyon oranlarında arttığını göstermiştir.

**Anahtar Kelimeler:** Al 6xxx; ısıl işlem; sıcak-deformasyon; tane boyutu; içyapı karakterizasyon

*To TANS  
İbrahim, Sema, Elvan*

## ACKNOWLEDGEMENTS

I would like to express my sincere appreciation to Prof. Dr. Bilgehan Ögel for his supervision, patience, guidance throughout the study.

I am sincerely grateful to Prof. Dr. Şakir Bor for his valuable guidance, moral support and motivation.

I also want to express thanks to Prof. Dr. David Embury for his valuable suggestions in the final stages of the study.

I must also thank to my sister Elvan Tan for her never-ending patience, motivation, physical and moral support in the completion of this thesis. I can never renumerate her for labor at home and at department. These years would be intolerable without her.

I am grateful to my roommate Güher Kotan, for her support, motivation, helps and Reiki; she deserves all by withstanding a man like me. I am also grateful to my friend Fatih Gürçağ Şen, for his brotherly behavior and friendship. Thanks to Ziya Esen for conversations at sleepless nights and special thanks to my roommate Serdar Karakaş, for his support and motivation throughout the study.

I would like to thank Cengiz Tan, for his kind interest during maintenance of the oil-bath, without which I could not continue my work.

Special thanks to Muhimmatsan and the employee especially to director Muammer Çimen and the chief engineer Faruk Çalık for their help about material provision.

Thanks to my friends Alper Kınacı, Barış Okatan, Melih Topçuoğlu, Gül Çevik, Selen Gürbüz, Tufan Güngören, Caner Şimşir, Kemal Davut and the others, I will not able to record all their names at the Department of Metallurgical and Materials Engineering, METU, for creating a warm working place.

I owe a depth to my parents, İbrahim and Sema Tan, for their never-ending devotion, support and encouragements from far away lands of Turkmenistan and trust in me throughout my life.

I would also thank to technical staff of Middle East Technical University, Department of Metallurgical and Materials Engineering, especially the atelier and mechanical testing lab, for their contributions to my study.

# TABLE OF CONTENTS

PLAGIARISM .....	iii
ABSTRACT .....	iv
ÖZ .....	vi
ACKNOWLEDGEMENTS .....	ix
TABLE OF CONTENTS .....	xi
LIST OF TABLES .....	xiii
LIST OF FIGURES .....	xv
CHAPTER	
1. INTRODUCTION .....	1
2. THEORY AND LITERATURE SURVEY .....	3
2.1. Aluminum Alloys.....	4
2.1.1. Alloying Elements and Phases in Aluminum Alloys.....	4
2.1.2. Alloys and Temper Designations .....	6
2.1.3. Heat Treatment Strengthening .....	10
2.2. 6xxx Al-Si-Mg Alloys.....	13
2.2.1. Effect of Alloying Elements .....	13
2.2.1.1. Effect of Silicon and Magnesium Content.....	13
2.2.1.2. Effect of Copper.....	15
2.2.1.3. Effect of Iron and Intermetallics .....	16
2.2.1.4. Effect of Chromium-Manganese.....	17
2.2.2. Phases and Phase Diagrams .....	17
2.2.3. Precipitation Sequence .....	20
2.2.3.1. Sequence with Excess Si.....	21
2.2.3.2. Sequence with Cu.....	23
2.2.4. Strengthening in 6xxx .....	25
2.3. Precipitation Hardening Mechanisms .....	28
3. EXPERIMENTAL PROCEDURE .....	30
3.1. Material Used.....	30

3.2. Initial Characterization.....	32
3.3. Determination of Ideal Heat Treatment .....	33
3.3.1. Solutionizing Temperature Determination.....	33
3.3.2. Aging Time and Temperature Determination .....	36
3.4. Deformation Tests.....	37
3.5. Specimen Notations .....	40
3.6. Microstructural Characterization .....	41
3.7. Mechanical Characterization.....	43
3.7.1. Hardness Tests .....	43
3.7.2. Tensile Tests .....	43
4. RESULTS AND DISCUSSION .....	45
4.1. Characterization of Al 6066 .....	45
4.1.1. Microstructural Investigations .....	45
4.1.2. Mechanical Properties.....	50
4.2. Heat Treatment Studies .....	53
4.2.1. Effect of Solutionizing Treatment.....	53
4.2.2. Aging Behavior of the Alloy.....	56
4.3. Effect of Deformation .....	58
4.3.1. Effect of Deformation on Microstructure .....	60
4.3.1.1. Recrystallization Behavior.....	63
4.3.1.2. Grain Morphology.....	64
4.3.2. Effect of Deformation on Mechanical Properties .....	73
4.3.2.1. Tensile Testing.....	73
4.3.2.2. Hardness Measurements .....	76
4.4. An Overview of Results .....	83
5. CONCLUSION.....	90
REFERENCES.....	92
APPENDIX.....	96

## LIST OF TABLES

Table 2.1 Basic temper designations [1].....	8
Table 2.2 Subdivision of H temper: strain hardened [1].....	8
Table 2.3 Subdivision of T temper: thermally treated [4].....	9
Table 2.4 Possible phases in 6xxx system (adapted from [3]).....	18
Table 2.5 Types of transition and metastable phases in Al-Mg-Si alloys [22].....	25
Table 2.6 Coherency of phases formed during aging of 6000 series aluminum alloys.....	25
Table 3.1 Spectral analysis of alloy and the composition ranges of Standard AA6066.....	30
Table 3.2 Mechanical properties of Al6066.....	32
Table 3.3 Soak times and max quench delays for solutionizing [3] .....	34
Table 3.4 Different solutionizing trials before quenching and aging at 175°C for 8 hours.....	35
Table 3.5 Different aging trials followed by solutionizing at 530°C for 95min and quenched .....	37
Table 3.6 Initial diameters of specimens and deformation scheme .....	38
Table 3.7 Sets of deformed samples .....	40
Table 3.8 The specimen notation system .....	41
Table 3.9 Composition of the etchant used.....	42
Table 4.1 The chemical compositions of the particles analysed with EDS .....	50
Table 4.2 Mechanical test results for O, T4 and T6 tempers .....	51
Table 4.3 Tabulated Brinell hardness values for different solutionizing treatment...	54
Table 4.4 Hardness values for different aging treatments .....	56
Table 4.5 The effect of deformation route on grain size.....	72
Table 4.6 Tensile test results for aged specimens subjected to various deformation routes .....	74
Table 4.7 Effect of 10% deformation on hardness of alloy .....	77

Table 4.8 Effect of 20% deformation on hardness of alloy .....	77
Table 4.9 Effect of 30% deformation on hardness of alloy .....	78
Table 4.10 Effect of 40% deformation on hardness of alloy .....	78
Table 4.11 Effect of deformation's order in the whole sequence .....	83
Table 4.12 Variation of mechanical properties and grain sizes with deformation.....	84
Table 4.13 Brinell hardness ranges obtained after various deformations .....	86
Table 4.14 Effect of heating to deformation and air-cooling on hardness.....	87
Table 4.15 Summary of yield and tensile strength values obtained in the study .....	89
Table A. 1 Survey of reported crystal structures of Al-Mg-Si-Cu alloy [24].....	98
Table A. 2 Hardness values for different solutionizing trials .....	101
Table A. 3 Hardness values for different aging trials .....	102
Table A. 4 Hardness values for different deformation steps.....	104

## LIST OF FIGURES

Figure 2.1 Solubility of alloying additions in aluminum (wt%) as a function of temperature [1].....	4
Figure 2.2 Principle aluminum alloys [3] .....	5
Figure 2.3 Effect of excess Si and Mg content on the tensile properties of alloy [8].....	14
Figure 2.4 Distribution of Cu atoms around Q' phase [11] .....	15
Figure 2.5 Aluminum-rich portion of Al-Mg <sub>2</sub> Si system [] .....	18
Figure 2.6 Line diagram of stable equilibrium phase fields in Al-Mg-Si-Cu system [17].....	19
Figure 2.7 Pseudo-binary phase diagram of (Al-0.55wt%Mg-1.58wt%Si)-Cu alloy [12].....	20
Figure 2.8 Schematic representation of clusters GP zones for (a) Si-excess alloy, (b) balance alloy [20].....	23
Figure 2.9 Aging curve and relevant phases during heat treatment at 190°C [6] .....	26
Figure 2.10 Aspect ratio change during aging [26] .....	27
Figure 2.11 TEM micrograph in the peakaged condition [27] .....	27
Figure 2.12 Particle – dislocation interactions (a)Orowan looping, (b)particle cutting [32].....	28
Figure 2.13 Role of major hardening mechanisms during age hardening [33].....	29
Figure 3.1 General experimental layout.....	31
Figure 3.2 Muffle furnace for solutionizing.....	34
Figure 3.3 Salt bath for solutionizing.....	35
Figure 3.4 Julabo heating circulator for aging .....	36
Figure 3.5 Operation scheme of swager.....	37
Figure 3.6 Swager and the dies used.....	38
Figure 3.7 Failure of 40% deformation at 200°C with single pass .....	39
Figure 3.8 Swaged aluminum rods .....	39
Figure 3.9 Grain size measurement with clemex software .....	42

Figure 3.10 Small-sized specimen proportional to standard tension specimen .....	43
Figure 3.11 Specimen dimensions according to ASTM B557M [36] .....	44
Figure 4.1 Microstructure of as-received Al 6066 (200X) .....	46
Figure 4.2 Microstructure of Al 6066 – T6 (200X) .....	47
Figure 4.3 XRD of the as-received alloy .....	47
Figure 4.4 The optical micrograph of as polished surface of the as-received alloy...	48
Figure 4.5 Backscatter SEM image of the alloy .....	48
Figure 4.6 The EDS analysis of gray script-like particles, .....	49
Figure 4.7 The EDS analysis of black particles, .....	50
Figure 4.8 Macroscopic fracture surfaces .....	51
Figure 4.9 Fracture surface of as-received alloy .....	52
Figure 4.10 Fracture surface of peak-aged alloy.....	52
Figure 4.11 Effect of solutionizing treatment on Brinell Hardness .....	55
Figure 4.12 Aging response of alloy solutionized at 530°C for 95 min .....	57
Figure 4.13 Backscatter SEM image of a deformed sample.....	59
Figure 4.14 (a) Back-scatter SEM image and (b) optical micrograph of as- received samples showing the particles on as-polished surface parallel to the deformation axis (LD).....	59
Figure 4.15 Optic micrographs from etched surfaces of as-received samples (a) TD, (b) LD .....	60
Figure 4.16 The optical micrographs of cold deformed samples (TD).....	61
Figure 4.17 Sample treated at 530°C for 65 min after 40% cold deformation (LD) .....	63
Figure 4.18 Sample treated at 450°C for 1 hr after 40% cold deformation (LD) .....	63
Figure 4.19 Sample treated at 350°C for 1 hr after 40% cold deformation (LD) .....	64
Figure 4.20 LD surface showing different grain.....	65
Figure 4.21 Optic micrographs obtained from LD sections of the specimens solutionized at 530°C and the corresponding grain size distributions; a)10% b)20% c)30% d)40% cold-deformed samples.....	67

Figure 4.22 Optic micrographs after solutionizing at 530°C and the corresponding grain size distributions; TD sections obtained from the specimens a)10% b)20% c)30% d)40% cold deformed .....	68
Figure 4.23 Optic micrographs after solutionizing at 530°C and the corresponding grain size distributions; TD sections obtained from the specimens a)10% b)20% c)30% d)40% deformed at 200°C .....	69
Figure 4.24 Optic micrographs after solutionizing at 530°C and the corresponding grain size distributions; TD sections obtained from the specimens a)10% b)20% c)30% d)40% deformed at 300°C .....	70
Figure 4.25 Optic micrographs after solutionizing at 530°C and the corresponding grain size distributions; TD sections obtained from the specimens a)10% b)20% c)30% d)40% deformed at 400°C .....	71
Figure 4.26 Variation of grain size of TD sections obtained from hot deformed specimens prior to soln and aging.....	72
Figure 4.27 Change of tensile strength of hot deformed specimens prior to soln and aging.....	75
Figure 4.28 Change of yield strength of hot deformed specimens prior to soln and aging.....	75
Figure 4.29 Effect of cold deformation with various %deformation on hardness .....	79
Figure 4.30 Effect of deformation at 200°C with various %deformation on hardness .....	80
Figure 4.31 Effect of deformation at 300°C with various %deformation on hardness .....	81
Figure 4.32 Effect of deformation at 400°C with various %deformation on hardness .....	82
Figure 4.33 Back-scatter SEM image of complex intermetallic broken during deformation.....	87
Figure 4.34 Evolution of microstructure during thermo-mechanical treatment of 6xxx [28].....	89
Figure A. 1 Al-Mg-Si phase diagram (liquidus) [2] .....	96
Figure A. 2 Al-rich portion of Al-Mg-Si system (solidus) [2].....	96

Figure A. 3 Al-rich portion of Al-Mg-Si system (solvus) [2].....	97
Figure A. 4 Al-Cu-Mg-Si system (97% Al section) [2].....	97
Figure A. 5 Specimen orientations.....	100

# CHAPTER 1

## INTRODUCTION

Aluminum alloys have been the candidate materials in aircraft and automotive industry since 1930s. Considerable industrial and scientific interest on the aluminum alloys of 6xxx series because nearly two-third of all extrusions are made from aluminum alloys and most of them are of the 6xxx type. 6xxx (Al-Si-Mg-Cu) series aluminum alloys has lots of benefits including high strength / weight ratio, formability, weldability, corrosion resistance, and low cost. This heat treatable alloy derives its strength from the precipitation hardening phase,  $Mg_2Si$ . Investigation of the effects of microstructure on mechanical properties showed that; obtaining homogeneously distributed  $Mg_2Si$  precipitates in fine grain sized aluminum matrix is a must. Hence for optimum mechanical properties; production method gains great importance. Although solutionizing time and temperature; aging time and temperature; are the main parameters to be controlled; for preserving fine grain structure, deformation amount and temperature are the other prerequisite parameters.

In this study; microstructural and mechanical characterization of AA6066 bars were performed; which were heat treated and deformed differently. At first, the relation between mechanical properties and solutionizing-aging treatments were established via brinell hardness tests. Secondly; the effect of shaping (deformation) process on the final product was evaluated. Consequences of hot and cold deformations prior to solutionizing and artificial aging were investigated with the use of swaged specimens. Recrystallization behavior with varying amounts and temperatures of deformation was criticized with microstructure image analysis.

The following chapter, theory and literature review on 6xxx alloys, were written to remind key points about the topic. Preceding chapters, starting with experimental

procedure were recorded to bound the method and its outcomes. In the results chapter; hardness and tensile test data obtained for different deformation and artificial aging routes were visually presented via graphs and also their effects on microscopic evaluations were examined. Results obtained were discussed with use of the physical metallurgy tools in terms of strengthening mechanisms.

## CHAPTER 2

### THEORY AND LITERATURE SURVEY

The development of civilization is closely linked with that of metals. Among the common metals, aluminum now cedes first place only to steel. If measured by volume rather than weight, it now exceeds in quantity all other non-ferrous metals combined, including copper and its alloys, lead, tin and zinc. Because of its unique properties, from the beginning aluminum has competed with and replaced much older, established materials, such as wood, copper and steel. Aluminum has won this position even though its industrial production began only in the late 19<sup>th</sup> century; therefore, it is a latecomer among common metals [1].

The properties of aluminum that contribute to its widespread use can be summarized as: [1]

- Aluminum is light; its density is only one third that of steel.
- Aluminum is resistant to weather, common atmospheric gases, and a wide range of liquids.
- Aluminum can be used in contact with a wide range of foodstuffs.
- Aluminum has a high reflectivity and, therefore, finds many decorative uses.
- Aluminum alloys can equal or even exceed the strength of normal construction steel.
- Aluminum has high elasticity, which is an advantage in structures under shock loads.
- Aluminum keeps its toughness down to very low temperatures, without becoming brittle like carbon steels.
- Aluminum is easily worked and formed; it can be rolled to very thin foil.
- Aluminum conducts electricity and heat nearly as well as copper.

## 2.1. Aluminum Alloys

Today more than half of the semi-finished production is delivered in alloys, most of the remainder in commercial purity aluminum with only a small quantity of super-purity aluminum being produced [1].

### 2.1.1. Alloying Elements and Phases in Aluminum Alloys

No element is known to have complete miscibility with aluminum in the solid state. Of all elements, zinc has the greatest solid solubility in aluminum: a maximum of 66.4 at%. In addition to zinc, three elements have solid solubilities greater than 10 at%: silver, magnesium and lithium. Gallium, germanium, copper and silicon have maximum solubilities of less than 10 but greater than 1 at%. All other elements are less soluble [2].

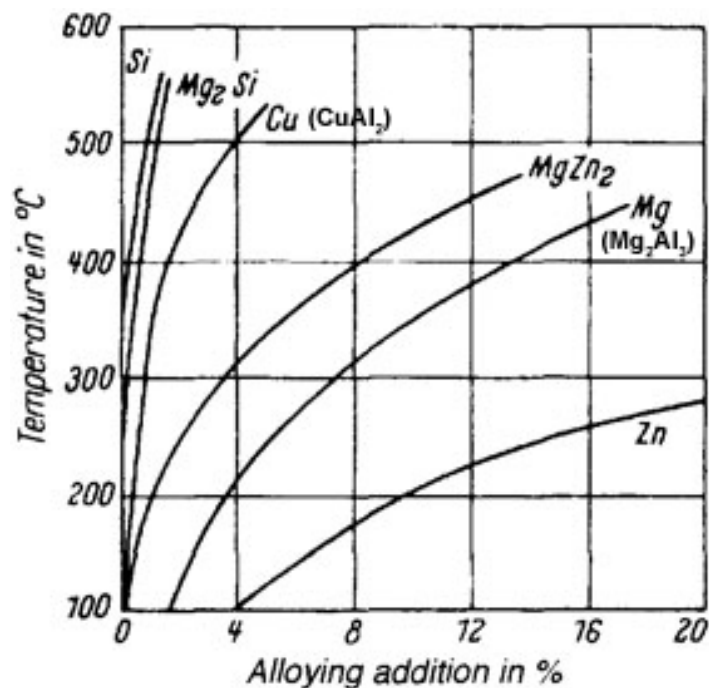
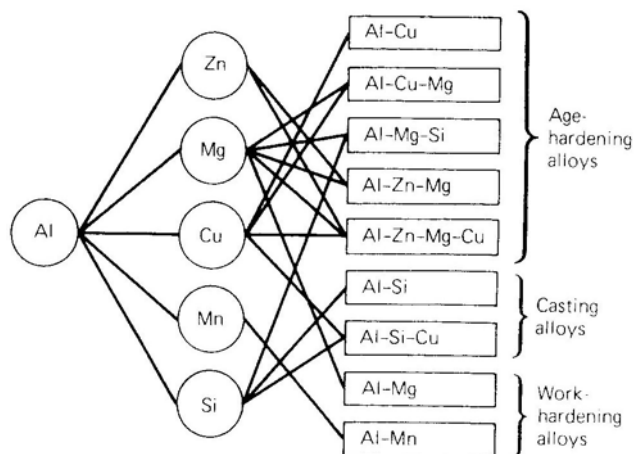


Figure 2.1 Solubility of alloying additions in aluminum (wt%) as a function of temperature [1]

Maximum solid solubility in aluminum alloys occurs at the eutectic, peritectic or monotectic temperature. With decreasing temperature, the solubility limits decrease. (Figure 2.1). This decrease from appreciate concentrations at elevated temperatures to relatively low concentrations at low temperatures is the fundamental characteristic that provides the basis for increasing substantially the hardness and strength of aluminum alloys by solution heat treatment and subsequent precipitation aging operations [2].

The elements that are most commonly present in commercial aluminum alloys to provide increased strength – particularly when coupled with strain hardening by cold working or with heat treatment, or both – are copper, magnesium, manganese, silicon and zinc. Figure 2.2 shows the principle aluminum alloys based on these elements which are used in various combinations [3].



**Figure 2.2 Principle aluminum alloys [3]**

When the content of an alloying element exceeds the solubility limit, the alloying element produces second-phase microstructural constituents that may consist of either the pure alloying ingredient or an intermetallic compound phase. In the first group are silicon, tin and beryllium. Manganese and chromium are included in the other group.

### **2.1.2. Alloys and Temper Designations**

The production of semifabricated products utilizes three different types of aluminum, namely super purity, commercial purity and alloys. Alloys are used for producing castings or fabricating wrought products. The alloys used for casting contain a greater amount of alloying additions than those used for wrought products. The addition of alloying elements has the effect of strengthening the wrought alloys and improving the castability of the casting alloys [1].

Hence, it is convenient to divide aluminum alloys into two major categories: casting compositions and wrought compositions. A further differentiation for each category is based on the primary mechanism of the property development. Cast and wrought alloy nomenclatures have been developed by Aluminum Association which is the most widely recognized one [3].

A system of four-digit numerical designations is used to identify wrought aluminum and wrought aluminum alloys. The first digit indicates the alloy group. The last two digits identify the aluminum alloy or indicate the aluminum purity. The second digit indicates modifications of the original alloy or impurity limits [1].

The alloy groups are as follows: [3]

- 1xxx Controlled unalloyed (pure) composition used primarily in electrical and chemical industries
- 2xxx Alloys in which copper is the principle alloying element, though notably magnesium may be specified which are widely used in aircraft
- 3xxx Alloys in which manganese is the principle alloying element. Used as a general purpose alloy for architectural applications
- 4xxx Alloys in which silicon is the principle alloying element. Used in welding rods and brazing sheets.
- 5xxx Alloys in which magnesium is the principle alloying element. Used in boat hulls, gangplanks and other products exposed to marine environments
- 6xxx Alloys in which magnesium and silicon is the principle alloying elements. Commonly used for extrusions.

- 7xxx Alloys in which zinc is the principle alloying element, but elements such as copper, magnesium, chromium and zirconium may be specified. Used in aircraft structural components and other high strength applications.
- 8xxx Alloys including tin and some lithium compositions, characterizing miscellaneous compositions
- 9xxx Reserved for future use

Wrought alloy compositions with a wide variety of strengths and other properties related to the alloying element content. The properties of wrought alloys can be described by adopting two basic classes: non-heat treatable alloys and heat treatable alloys. Non-heat treatable alloys include all the various grades of pure aluminum and all those other alloys in which the strength is developed largely by strain hardening from the basic annealed temper. They are in the 1xxx, 3xxx, 4xxx and 5xxx series. Heat treatable alloys are those containing appreciable amounts of the elements that are soluble in solid aluminum. They are soluble in aluminum in considerable amounts at elevated temperatures, but to a much smaller degree at room temperature. This characteristic renders these alloys susceptible to heat treatment. They are designated in the 2xxx, 6xxx and 7xxx series [2].

Since wrought alloy products are offered for sale in a variety of conditions that determine strength and other characteristics; a uniform system of temper designations is a necessity. Temper designations are tabulated in Table 2.1 to Table 2.3 [1,4].

**Table 2.1 Basic temper designations [1]**

<i>Temper</i>	<i>Explanation</i>
F	<i>as-fabricated</i> applies to the products of shaping processes in which no special control over thermal conditions or strain hardening is employed.
O	<i>annealed</i> applies to wrought products that are annealed to obtain the lowest strength temper and to cast products that are annealed to improve ductility and dimensional stability.
H	<i>strain-hardened (wrought products only)</i> applies to products that have their strength increased by strain-hardening with or without supplementary thermal treatments to produce some reduction in strength.
W	<i>solution heat treated</i> applies to an unstable temper applicable only to alloys that spontaneously age at room temperature after solution heat treatment.
T	<i>thermally treated to produce stable tempers other than F, O, or H</i> applies to products that are thermally treated with or without supplementary strain-hardening.

**Table 2.2 Subdivision of H temper: strain hardened [1]**

<i>Temper</i>	<i>Explanation</i>
H1	<i>strain-hardened</i> only applies to products that are strain-hardened to obtain the desired strength without supplementary thermal treatment.
H2	<i>strain-hardened and partially annealed</i> applies to products that are strain-hardened more than the desired final amount and then reduced in strength to desired level by partial annealing.
H3	<i>strain-hardened and stabilized</i> applies to products that are strain hardened and whose mechanical properties are stabilized either by a low temperature thermal treatment or as a result of head introduced during fabrication.
H4	<i>strain-hardened and lacquered or painted</i> applies to products that are strain hardened and subjected to some thermal operation during the subsequent painting or lacquering operation.

**Table 2.3 Subdivision of T temper: thermally treated [4]**

<i>Temper</i>	<i>Explanation</i>
T1	<i>cooled from an elevated temperature shaping process and naturally aged to a substantially stable condition</i> applies to products that are not cold worked after an elevated temperature shaping process such as casting or extrusion and for which mechanical properties are stabilized by room-temperature aging.
T2	<i>cooled from an elevated temperature shaping process, cold worked, and naturally aged to a substantially stable condition</i> applies to products that are cold worked specifically to improve strength after cooling from a hot working process such as rolling or extrusion and for which mechanical properties are stabilized by room-temperature aging.
T3	<i>solution heat treated, cold worked, and naturally aged to a substantially stable condition</i> applies to products that are cold worked specifically to improve strength after solution heat treatment and for which mechanical properties are stabilized by room-temperature aging.
T4	<i>solution heat treated, and naturally aged to a substantially stable condition</i> applies to products that are not cold worked after solution heat treatment and for which mechanical properties are stabilized by room-temperature aging.
T5	<i>cooled from an elevated temperature shaping process and artificially aged</i> applies to products that are not cold worked after an elevated temperature shaping process such as casting or extrusion and for which mechanical properties or dimensional stability or both have been substantially improved by precipitation heat treatment.
T6	<i>solution heat treated and artificially aged</i> applies to products that are not cold worked after solution heat treatment and for which mechanical properties or dimensional stability or both have been substantially improved by precipitation heat treatment.

**Table 2.3(cont'd)**

<i>Temper</i>	<i>Explanation</i>
T7	<i>solution heat treated and stabilized / overaged</i> applies to products that have been precipitation heat treated to the extent that they are overaged to provide special characteristics such as enhanced resistance to stress-corrosion cracking.
T8	<i>solution heat treated, cold worked, and artificially aged</i> applies to products that are cold worked specifically to improve strength after solution heat treatment, and for which mechanical properties or dimensional stability or both have been substantially improved by precipitation heat treatment.
T9	<i>solution heat treated, artificially aged and cold worked</i> applies to products that are cold worked specifically to improve strength after they have been precipitation heat treated.
T10	<i>cooled from an elevated temperature shaping process, cold worked, and artificially aged</i> applies to products that are cold worked specifically to improve strength after cooling from a hot working process such as rolling or extrusion, and for which mechanical properties or dimensional stability or both have been substantially improved by precipitation heat treatment.

### **2.1.3. Heat Treatment Strengthening**

The commercial heat-treatable aluminum alloys are based on ternary or quaternary systems with respect to the solutes involved in developing strength by precipitation. Commercial alloys whose strength and hardness can be significantly increased by heat treatment include 2xxx, 6xxx and 7xxx series alloys. One essential attribute of a precipitation hardening alloy system is a temperature dependent equilibrium solid solubility characterized by increasing solubility with increasing temperature. Heat treatment to increase the strength of aluminum alloy is carried out in three successive steps:

- Solution heat treatment : dissolution of soluble phases
- Quenching : development of supersaturation

- Age hardening : precipitations of solute atoms either at room temperature (natural aging) or at elevated temperatures up to 200°C (artificial aging)

### Solution heat treating

To take the advantage of the precipitation hardening reaction, it is necessary first to produce a solid solution via solution heat treating. Its objective is to take into solid solution the maximum practical amounts of the soluble hardening elements in the alloy. The process consists of soaking the alloy at a temperature sufficiently high and for a time long enough to achieve a nearly homogeneous solid solution. Air is the usual heating medium but molten salt baths or fluidized beds are advantageous in providing more rapid heating.

The solutionizing temperature must be as high as possible for increased solution and diffusion rates. But; care must be exercised to avoid exceeding the initial eutectic melting temperature. If appreciable eutectic melting occurs as a result of overheating, properties such as tensile strength, ductility and fracture toughness may be degraded. Although maximum temperature must be restricted to avoid melting, the lower limit should be above the temperature at which complete solution occurs (solvus). In this case; solution is incomplete and strength is somewhat lower than expected. Besides temperatures; the soaking time is important for a satisfactory degree of solution of the undissolved or precipitated soluble phase constituents and to achieve good homogeneity of the solid solution [2,3]. The time required for solution heat treatment depends on product type, alloy, prior history and section thickness. Section thickness controls the heating time. Once the product is at the temperature, the length of the solution heat treatment depends primarily on the coarseness of the microstructure and the diffusion distance necessary to obtain sufficient homogenization [5].

### Quenching

Quenching is in many ways the most critical step in the sequence of heat treating operations. The objective of quenching is to preserve as nearly intact as possible the solid solution formed at the solution heat treating temperature, usually near room temperature. The solute atoms that diffuse to grain boundaries, as well as the

vacancies that migrate (with extreme rapidity) to disordered regions, are irretrievably lost for practical purposes and fail to contribute to the subsequent strengthening.

As a broad generalization, the highest strengths are attainable are those associated with the most rapid quenching rates. Both the degree of warpage or distortion that occurs during quenching and the magnitude of residual stress that develops in the products tend to increase with the rate of cooling [2].

### Age hardening

After solution treatment and quenching, hardness is achieved either at room temperature (natural aging) or with a precipitation heat treatment (artificial aging). In some alloys, sufficient precipitation occurs in a few days at room temperature to yield stable products with properties that are adequate for many applications. Other alloys with slow precipitation reactions at room temperature are always precipitation heat treated before being used.

Precipitation heat treatments generally are low-temperature, long term processes. Temperatures range from 115 to 190°C, times vary from 5 to 48h. Choice of time-temperature cycles for precipitation heat treatment should receive careful considerations. Larger particles of precipitate result from longer times and higher temperatures; however, the larger particles must, of necessity, be fewer in number with greater distances between them. The objective is to select the cycle that produces the optimum precipitate size and distribution pattern which provide the best combination of properties [3].

Aging at room or higher temperature leads to formation of metastable phases. Its coherency affects the strength and hardness of the alloy in such a manner: After GB zones, with the formation of coherent metastable phases; tensile strength and hardness are improved by effective hindering dislocation movement. As for long aging times or higher temperatures these phases become first semi-coherent (mismatch dislocation in one crystallographic direction) and later incoherent (no fit to any crystallographic direction of the host matrix), they do not hinder the

dislocation movement as effectively as before. Hence, the material will become softer again on overaging [6].

## **2.2. 6xxx Al-Si-Mg Alloys**

Aluminum alloys have been the material of choice for aircraft construction since the 1930s. The aerospace industry relies heavily on 2xxx and 7xxx alloys, while a wide variety of aluminum alloys are used by the automotive industry. 6xxx aluminum alloys are of particular interest to both the aerospace industry (for fuselage skins and other applications) and automotive industry (for body panels and bumpers) because of their attractive combinations of properties. According to Troeger [7]; the benefits of 6xxx alloys include medium strength, formability, weldability, corrosion resistance, and low cost. 6xxx alloys have corrosion resistance which is superior to 2xxx and 7xxx alloys, traditional aerospace alloys that are prone to intergranular attack. The low cost of 6xxx alloys is especially significant to the aerospace industry that relies heavily on the more expensive 2xxx and 7xxx alloys.

### **2.2.1. Effect of Alloying Elements**

Main components of heat treatable 6xxx series aluminum alloy are magnesium and silicon. It is known that; 6xxx derives its strength from the precipitation hardening phase,  $Mg_2Si$ . The alloy may also include small amounts of copper, manganese, chromium and iron, which provides different properties to the alloy system.

#### **2.2.1.1. Effect of Silicon and Magnesium Content**

In spite of historical bias against excess silicon because of brittleness, recent studies have shown that excess silicon can actually have the beneficial effect of dispersing slip within grain interior, thereby acting like incoherent dispersoids to raise the work hardening rate and elongation. However, silicon particles precipitated at the grain boundaries still contribute to an intergranular fracture process [8].

Dorward and Bouvier [8] explained the beneficial effect of excess silicon at constant strength as the homogenization of deformation which increases the work hardening

rate. They found that; excess silicon increased the strength dramatically whereas excess magnesium had a negative effect.

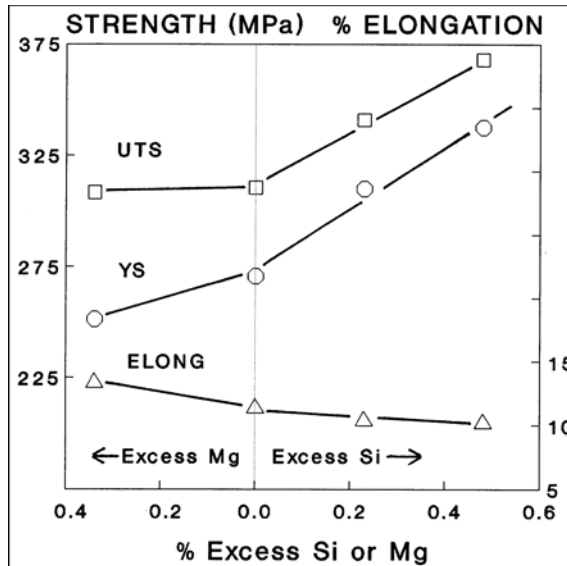


Figure 2.3 Effect of excess Si and Mg content on the tensile properties of alloy [8]

Another study by Hirth et al. [9] showed that; the level of Si within the alloy influences the solution heat treated (T4) strength and the subsequent aging response of 6xxx alloy through its effect on the volume fraction of  $Mg_2Si$ . A more complete removal of Mg from solid solution and a contaminant increase in Mg-Si cluster hardening were the reasons of strength increase with increase of Si. But at higher levels of Si, the strength was found to be saturated which was possibly due to less available Mg for the formation of  $Mg_2Si$ . Hence the volume fraction of  $Mg_2Si$  is primary dictated by the level of magnesium in the alloy.

The positive effect of excess silicon is somehow related to its effect on the precipitation sequence. Although this will be discussed deeply in following sections; a brief summary by Gupta et al [10] gives the key points. According to their research, excess Si reduces the time to initiate strengthening and increases the strength in both T4 and T6 tempers; which is caused by enhanced precipitation of

fine, uniformly distributed  $\beta''$  particles. They also concluded that, the reduction of Mg/Si ratio in the zones/clusters and  $\beta''$  precipitates with excess silicon allows higher levels of precipitation and strengthening.

#### 2.2.1.2. Effect of Copper

Matsuda and his colleague's study [11] on 6xxx series aluminum alloys show that addition of copper to Al-Mg-Si alloys enhances hardness and refines microstructure.

In the view of these reports, Cu is believed to form solid-solution in the matrix during the early stages of aging, and to contribute to the nucleation of metastable  $\beta''$ ,  $\beta'$  and  $Q'$  phases. As aging proceeds, Cu atoms are attracted to the region of lattice mismatch at the  $Q' \setminus \alpha$ -Al interface. (Figure 2.4) It is believed that, Cu segregation limit the diffusional growth of  $Q'$  phase producing finer microstructures.

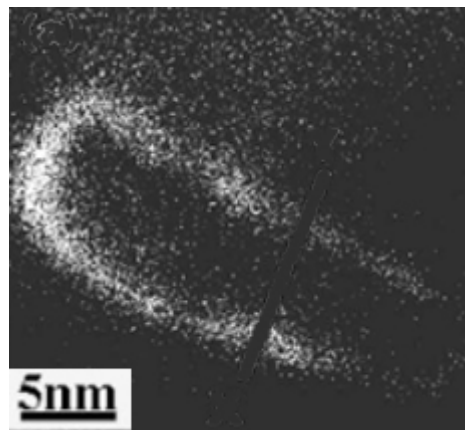


**Figure 2.4 Distribution of Cu atoms around  $Q'$  phase [11]**

The effect of Cu on the precipitation sequence of Al-Mg-Si has been investigated extensively by the researchers. It has been found that the addition of copper enhances the precipitation hardening kinetics and contributes to grain refinement [12]. Precipitation sequence with Cu will be discussed in the following sections.

### 2.2.1.3. Effect of Iron and Intermetallics

The main alloying elements in 6xxx series aluminum alloys are silicon and magnesium which are partly dissolved in solid solution of  $\alpha$ -Al matrix and partly dissolved in the form of intermetallics. Depending on alloy composition and solidification conditions, different intermetallics might form. The type, size, morphology and distribution of the intermetallics are very important in determination of the subsequent material properties.

Fe is known as an impurity in all commercial alloys which forms a variety of Al-Fe and Al-Fe-Si intermetallics during solidification. Except from Fe containing intermetallics, any Si which is not incorporated in  $\alpha$ -Al matrix and Al-Fe-Si intermetallics is thought to form  $Mg_2Si$  at the later stages of solidification. The possible mechanisms of  $Mg_2Si$  formation was discussed by Hsu et al. [13]. Among them, ternary eutectic reaction ( $L \rightarrow \alpha\text{-Al} + \alpha_c\text{-AlFeSi} + Mg_2Si$ ) was underlined by the authors; which was explained as the solidification of eutectic liquid droplets to form clustered  $\alpha_c\text{-AlFeSi}$  particles during partial melting and re-solidification, and solidification of residual liquid to form  $\alpha\text{-Al}$ ,  $\alpha_c\text{-AlFeSi}$  and  $Mg_2Si$  in the final stage.

Another study on intermetallics of 6xxx was carried by Sha et al. [14]. Most commercial 6xxx series wrought Al alloys are direct chill (DC) cast into sheet ingots or extrusion billets. In DC casting, local cooling rate variation from ingot center to ingot surface causes different intermetallic phases formed at different positions resulting variations in the final product properties. According to Sha [14];  $\alpha\text{-AlFeSi}$ ,  $\beta\text{-AlFeSi}$  and  $Mg_2Si$  were the three intermetallic phases in 6xxx series.  $\alpha\text{-AlFeSi}$  and  $Mg_2Si$  are thought to be the only phases with  $\alpha\text{-Al}$ , occurring under equilibrium solidification whereas  $\beta\text{-AlFeSi}$  is the metastable phase formed at intermediate growth velocities.

Iron is probably the most important element, because it forms brittle and hard intermetallic, which may act as stress raiser and become point of weakness that reduce the strength and ductility of alloys [15].

#### 2.2.1.4. Effect of Chromium-Manganese

The effects of Cr and Mn additions to aluminum alloys have been summarized by Dorward and Bouvier [8]. Brittleness of the 6xxx series alloys is associated with the elemental silicon particles and refined  $Mg_2Si$  precipitates at grain boundaries, which causes coarse slip behavior and dislocation pile-ups at the grain boundaries. However toughness can be improved through grain size refinement, non shearable particles and narrower precipitate free zones at grain boundaries by manganese and chromium additions.

Additions of these alloying elements inhibit the precipitation of magnesium and/or silicon at the grain boundaries, reducing intergranular fracture tendency. The manganese as a grain structure control agent has positive effect in grain refinement. Also Mn-containing dispersoids are effective in homogenization of deformation (slip), thereby reducing stress concentrations at grain boundaries [8].

#### 2.2.2. Phases and Phase Diagrams

Magnesium and silicon combine to form a compound  $Mg_2Si$ , which in turn forms a simple eutectic system with aluminum. The main ingredient of the 6xxx alloy is composed of  $\alpha$ -Al and  $Mg_2Si$  (Figure 2.5). The presence of Cu, Mn, Cr and Fe contributes to the formation of other particles. Cu mainly contributes to the hardening by precipitate phases as described in the following sections. Fe has a very low solid solubility in Al (maximum 0.05wt% at equilibrium). Virtually all Fe in Al alloys forms a wide variety of Fe-containing intermetallic phases [14]. If there is no manganese or chromium present, the iron-rich phases are  $Fe_3SiAl_{12}$ ,  $Fe_2Si_2Al_9$  or a mixture of two depending on the proportions of magnesium, silicon and iron. Manganese and chromium stabilize  $(Fe,Mn)_3SiAl_{12}$ ,  $(Fe,Cr)_3SiAl_{12}$ ,  $(Fe,Mn,Cr)_3SiAl_{12}$ . Besides the interchangeability of Fe, Mn, and Cr; this phase can probably contain Cu  $(Fe,Mn,Cu)_3SiAl_{12}$  [3].

The possible phases in the 6xxx alloy system are given in Table 2.4 and the related phase diagrams are presented in the appendix from Figure A. 1 to Figure A. 4.

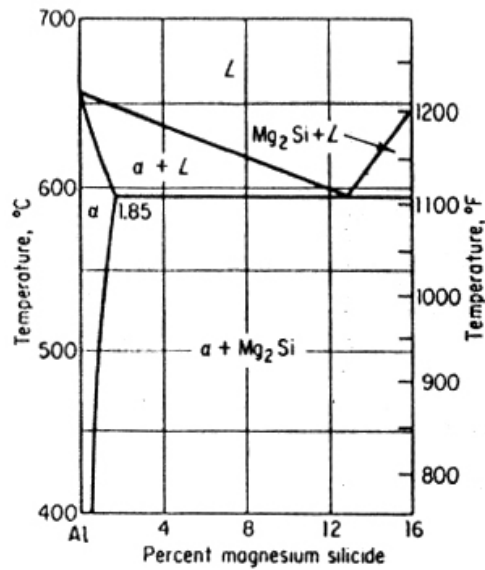


Figure 2.5 Aluminum-rich portion of Al-Mg<sub>2</sub>Si system [16]

Table 2.4 Possible phases in 6xxx system (adapted from [3])

Alloy System	Alloy Form	Phases
Al-Mg-Si-Cu-Fe-Mn	Ingot	Fe <sub>2</sub> Si <sub>2</sub> Al <sub>9</sub> , (Fe,Mn) <sub>3</sub> SiAl <sub>12</sub> , (Fe,MnCu) <sub>3</sub> SiAl <sub>12</sub> , Mg <sub>2</sub> Si, Si
	Wrought	(Fe,Mn) <sub>3</sub> SiAl <sub>12</sub> , (Fe,MnCu) <sub>3</sub> SiAl <sub>12</sub> , Mg <sub>2</sub> Si

According to alloy composition and aging procedure; different phases (particles and/or precipitates) can be observed in the microstructure which will affect the final mechanical properties.

In their report; Chakrabarti and Laughlin [17] had tried to place some of these precipitates on a phase diagram. Many commercial ternary Al-Mg-Si alloys have their compositions in a three phase field (at normal aging temperatures) consisting of

the equilibrium phases: primary aluminum (Al),  $\beta$  ( $\text{Mg}_2\text{Si}$ ) and primary Si (Si). On addition of Cu, the coexisting equilibrium three-phase fields expand into three tetrahedron composition spaces. A four-phase equilibrium is present inside each of these spaces consisting of the two common phases, namely (Al), and the quaternary intermediate phase Q, and two of the other three phases, namely  $\theta$  ( $\text{CuAl}_2$ ),  $\beta$  ( $\text{Mg}_2\text{Si}$ ) and (Si). This is schematically shown in the skeletal phase diagram representation in Figure 2.6. Three-phase fields in this diagram are schematically shown contained within the triangular faces, two-phase fields by compositions bound by the parallel lines and single phase fields as point compositions by the circles. Filled circles represent corners of the three four-phase tetrahedrons.

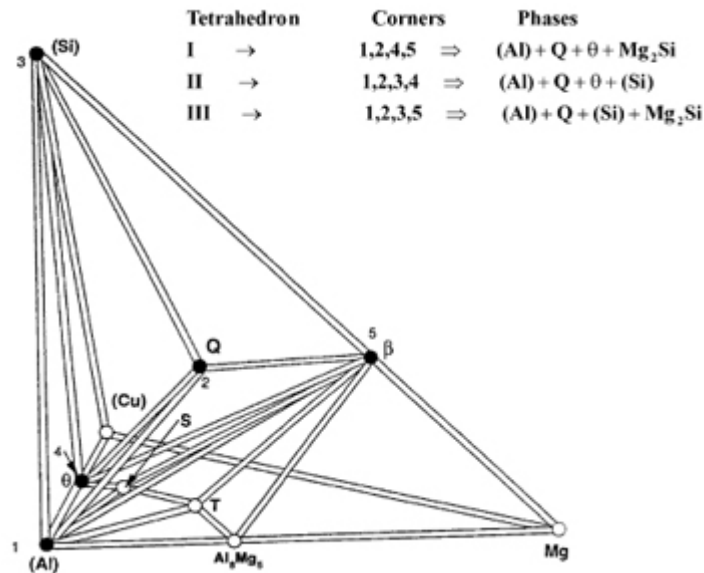


Figure 2.6 Line diagram of stable equilibrium phase fields in Al-Mg-Si-Cu system [17]

In the quaternary Al–Mg–Si–Cu system when the  $\text{Mg}/\text{Si} > 1$ , the compositions at artificial aging temperatures have been calculated to lie in Tetrahedron I, which has the coexisting phases, (Al), Q,  $\theta$  and  $\beta$ . When  $\text{Mg}/\text{Si} < 1$ , the compositions occupy Tetrahedron II, having the coexisting phases, (Al), Q,  $\theta$  and (Si). The tetrahedron III

composition field is occupied when the Cu level is low, the value of which varies with the Mg and Si.

Another representation of Al-Mg-Si-Cu phase diagram has been established by Miao et al. [12]. They have used a software to draw a pseudo-binary diagram (Al-0.55wt%Mg-1.28wt%Si)-Cu. The diagram (Figure 2.7) could be useful for determination of final phases in the system with varying amounts of Cu.

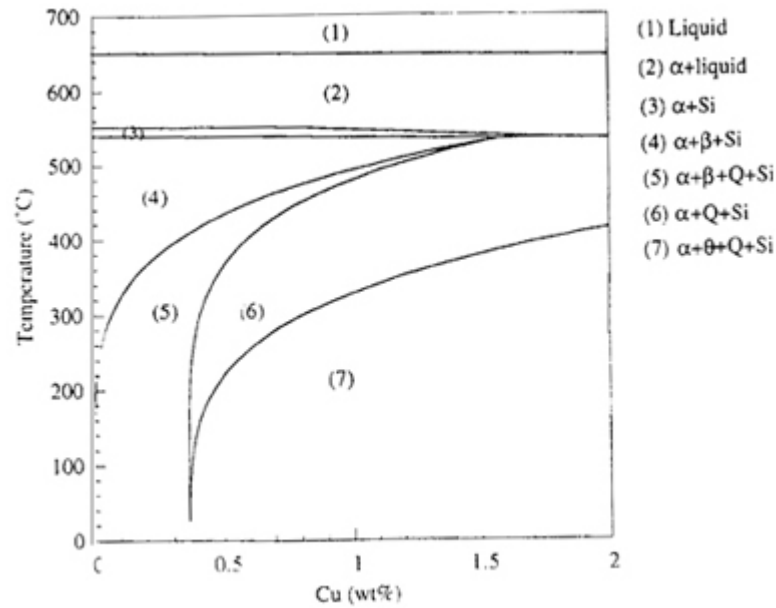


Figure 2.7 Pseudo-binary phase diagram of (Al-0.55wt%Mg-1.58wt%Si)-Cu alloy [12]

### 2.2.3. Precipitation Sequence

6xxx series aluminum alloys, containing magnesium and silicon as the major elements, are strengthened by precipitation of metastable precursors of the equilibrium  $\beta$  ( $Mg_2Si$ ) phase. Hence, the understanding and control of precipitation during artificial aging is critical for achieving optimum properties. The precipitation of these phases occurs in one or more complex sequences which are not fully agreed by authors. The confusions in literature are on the number, structure and composition of metastable phases involved in the sequences. Nevertheless it is generally agreed

that; the precipitation process in Al-Mg-Si alloys can be roughly divided into following steps:



similar to the sequence of Al-Cu system.

This general sequence was summarized by Miao et al. [12] with the morphology and crystal structures of metastable phases. The sequence starts with  $\alpha$  (sss), the super saturated solid solution formed after quenching. GP zones (also called clusters) are believed to be spherical with certain structure. The  $\beta''$  term represents fine needle shaped precipitates along  $\langle 100 \rangle_{\text{Al}}$  with a monoclinic structure. The  $\beta'$  term represents rod-like precipitates (circular cross section) along  $\langle 100 \rangle_{\text{Al}}$ , having hexagonal crystal structure with  $a = 0.705 \text{ nm}$  and  $c = 0.405 \text{ nm}$ . The  $\beta$  phase ( $\text{Mg}_2\text{Si}$ ) is usually formed as platelets on  $\{100\}$  of Al having the  $\text{CaF}_2$  structure with  $a = 0.639 \text{ nm}$ .

#### 2.2.3.1. Sequence with Excess Si

For strength and hardness improvement; some 6xxx series aluminum alloys contain an excess of Si which is required to form stoichiometric  $\text{Mg}_2\text{Si}$ . The effect of excess silicon on the precipitation sequence of Al-Mg-Si alloy became a topic of interests for authors. The decomposition of the supersaturated solid solution (sss) of Al-Mg-Si alloys containing excess Si was discussed in detail by Gupta et al. [18].



The decomposition begins with the formation of two types of (Mg+Si) clusters or zones. Firstly, coherent Si-rich cluster are enriched by Mg atoms forming Si-depleted plate-like or spherical co-clusters or GP(I) zones. As aging proceeds, the clusters and zones become ordered forming needle shaped GP(II)/  $\beta''$  phase. Following the  $\beta''$ ; numerous phases were identified by the researchers. Matsuda et al. [19] have suggested the precipitation of three different phases in addition to  $\beta'$  phase.

Three new types of metastable phases; Type-A, Type-B and Type-C are defined by Matsuda et al. which have different crystal structures from that of the  $\beta'$  phase. The atomic ratio of Mg and Si in the  $\beta'$  phase is about Mg/Si=1.68, while the Type-A and Type-B consists of ternary elements Al, Mg, Si in the atomic ratios of Al:Mg:Si 4:1:5 and 4:2:5 respectively. According to Matsuda; both the  $\beta'$  phase and the Type-B precipitate appear at the same time during aging and their amount and size increases as the aging continues. As aging progresses, the amount of  $\beta'$  phase increases to a maximum value then rapidly decreases whereas the amount of Type-B precipitate is almost constant. With further aging, the disappearance of  $\beta'$  phases and the termination of new Type-B formation is followed by the rapid precipitation of Type-A precipitates and a decrease in Type-B precipitates. At the same time, small amount of heterogeneous Type-C precipitates form in the matrix. In the overaged condition; Type-A disappears and equilibrium  $\beta$  ( $\text{Mg}_2\text{Si}$ ) and Si phases are dominant [19].

The formation of elemental Si precipitates in the final structure was explained by Murayama et al. [20]. According to their investigations; separate Mg and Si clusters in the as-quenched state forms Mg-Si co-clusters by aggregation of Mg and Si atoms during aging. With further aging GP zones and  $\beta''$  precipitates forms. The atomic ratios of Mg and Si of co-clusters, GP zones and the  $\beta''$  precipitates in the Si-excess alloy are found as 1:1. In contrast the ratio is closer to the one expected from the equilibrium  $\beta$  phase,  $\text{Mg}_2\text{Si}$  for balance alloys. Figure 2.8 shows the schematic atomic ratios for GP zones and  $\beta''$  phases for balance and Si-excess alloys. It is seen from figure that the densities of the co-clusters, GP zones and the  $\beta''$  are all determined by the available number of Si atoms, rather than Mg atom number. Hence higher densities of GP zones and  $\beta''$  phases precipitates in the Si-excess alloy. As the aging continues; the atomic ratio of Mg:Si in more stable precipitates such as  $\beta'$  should be closer to 2:1 due to the stoichiometric composition of the equilibrium  $\beta$  phase ( $\text{Mg}_2\text{Si}$ ). This eventually results the precipitation of elemental Si from the excess amount of Si; obtaining  $\beta + \text{Si}$  in the overaged alloys [20].

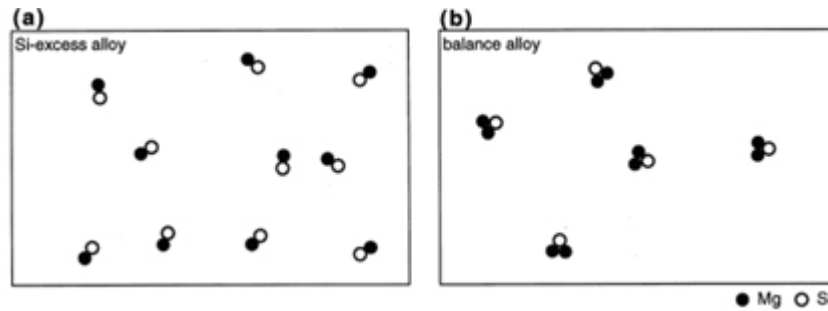


**Figure 2.8 Schematic representation of clusters GP zones for (a) Si-excess alloy, (b) balance alloy [20]**

### 2.2.3.2. Sequence with Cu

The investigations on the effect of Cu on the precipitation sequence of Al-Mg-Si have showed that; Cu addition enhances the precipitation kinetics due to microstructure refinement and precipitation sequence changes [12,21,22].

The surveys show the presence of precipitates apart from the previously mentioned precipitates in Al-Mg-Si system. Cu-containing precipitates such as  $\theta$  and its precursor metastable phases, as well as Q and its precursor metastable phases have also been observed in the precipitation sequence of Al-Mg-Si-Cu alloys.  $\theta$  is body centered tetragonal  $\text{Al}_2\text{Cu}$  with lattice parameter  $a=b=0.607\text{nm}$  and  $c=0.487\text{nm}$ . The Q phase is a quaternary phase consisting of Al-Mg-Si-Cu and its structure has been proposed to be hexagonal with  $a=1.04$  and  $c=0.405\text{nm}$  [12].

The first stage in the precipitation sequence, i.e. GP zone or cluster formation is thought to be same for alloys with or without Cu. Clusters of Si atoms, clusters of Mg atoms and co-clusters of Mg and Si atoms compete with each other. In the second stage of sequence, needle-like  $\beta''$  is the dominant intermediate phase for both Al-Mg-Si and Al-Mg-Si-Cu alloys. The only difference has been found to the variation of lattice parameters due to the Cu atoms incorporated into the needle-like  $\beta''$ , which is thought to be the precursor of the metastable phase of Q. The metastable phase of Q appears to be formed in the third stage of sequence [12]. This metastable phase has been thought to be the B' phase, which has been behaved like the rod-like  $\beta'$  phase in Al-Mg-Si alloys. Later on this phase has been called the Q' phase by

some authors being the metastable version of the equilibrium quaternary phase Q. The Q' phase has a lath morphology and a hexagonal structure, which is oriented parallel to the  $\langle 100 \rangle_{Al}$  directions and  $\{150\}_{Al}$  habit planes of matrix. The final stage has been reported to be the equilibrium Q phase with hexagonal crystal structure and composition of  $Al_4Cu_2Mg_8Si_7$  [22].

Another interesting result has been proposed by Matsuda et al. [22], showing the orientation relationships between Type-C precipitate and the Q' precipitate. Type-C precipitate is an Al-Mg-Si ternary phase for Si-excess alloys and the Q' precipitate is the Al-Mg-Si-Cu quaternary for Cu-containing ones. But it has been reported by Miao [12] that, the formation of Q' is kinetically favored compared with other competing phases.

The overall sequence with Cu has been summarized by Miao [12] as follows:

- For small amount of Cu;

$\alpha$  (sss)  $\rightarrow$  GP zones  $\rightarrow$  needle-like  $\beta''$   $\rightarrow$  rod-like  $\beta'$  + lath-shaped Q'  $\rightarrow$  platelet  $\beta$  + Si

- For higher amounts of Cu;

$\alpha$  (sss)  $\rightarrow$  GP zones  $\rightarrow$  needle-like  $\beta''$   $\rightarrow$  lath-shaped Q'  $\rightarrow$  lath-like Q + Si

- For Cu and excess Si containing alloys [23]:

$\alpha$  (sss)  $\rightarrow$  GP zones  $\rightarrow$  needle-like  $\beta''$   $\rightarrow$  rod-like  $\beta'$  + lath-shaped Q'  $\rightarrow$  Q +  $\beta$  +  $\theta$  + Si

where Q ( $Al_4Cu_2Mg_8Si_7$ ),  $\beta$  ( $Mg_2Si$ ) and  $\theta$  ( $Al_2Cu$ )

Due to numerous alloying additions; many precipitation sequences and lots of transition and metastable phases has been observed. All the phases observed in the sequences have been collected by Ravi and Wolerton [24]. They have tabulated the findings of all authors' including the crystal structure and morphology. This survey was presented in Table A. 1 at the appendix on page 98.

The types of metastable phases for the three main classes of 6xxx alloys: balance alloy, Si-excess alloy and the Cu-containing alloy were summarized by Matsuda [22] in Table 2.5.

**Table 2.5 Types of transition and metastable phases in Al-Mg-Si alloys [22]**

<i>Phase</i>	<i>Balanced Alloy</i>	<i>Excess Si Alloy</i>	<i>Alloy with Copper</i>
Transition	random type	random type	random type
	parallelogram type	parallelogram type *	parallelogram type
		$\beta''$ phase	$\beta''$ phase *
	$\beta'$ phase	type-A	$\beta'$ phase *
		type-B	type-C with Q'
		type-C *	

\* A minor phase

#### 2.2.4. Strengthening in 6xxx

During aging, formation of stable and metastable phases affects the material properties. The change from totally coherent to semi-coherent and incoherent precipitates (Table 2.6) is important in terms of strengthening [6].

**Table 2.6 Coherency of phases formed during aging of 6000 series aluminum alloys**

<i>Phases</i>	<i>Coherency</i>	<i>Remarks</i>
GP Zones	Coherent	Spherical
$\beta''$	Coherent	Needles with spherical cross-section; totally coherent in Al-matrix
$\beta'$	Semi-coherent	Rods with ellipsoidal cross-section; mostly coherent, but end of rods are incoherent to Al-matrix
$\beta$	Incoherent	Plates; totally incoherent to Al-matrix

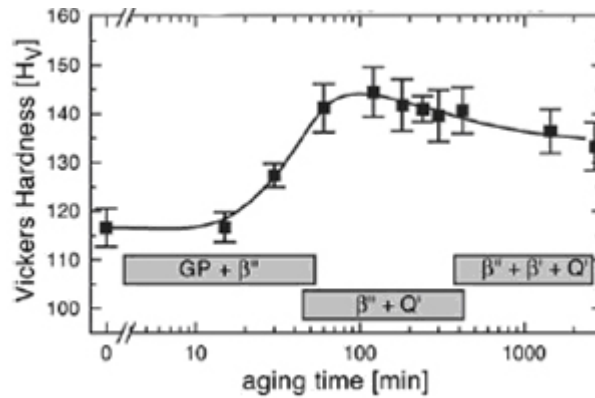


**Figure 2.9** Aging curve and relevant phases during heat treatment at 190°C [6]

After solutionizing, the main resistance to dislocation movement is the solid solution hardening. As GP zones form, the hardness increases due to the extra stress required forcing dislocations through the coherent zones. Tensile strength continues to increase with the formation of coherent  $\beta''$  precipitates, because dislocations must be forced through highly strained matrix resulting from the misfit perpendicular to the  $\beta''$  precipitates. As aging continues needle-like  $\beta''$  becomes thicker and transforms to  $\beta'$  rods. Therefore, the force needed for precipitate shearing increases. With the progressing of aging,  $\beta'$  thickens and transforms to  $\beta$  rods. At that time, precipitates coarsen, which results in a lower particle density and large inter-particle distance. The dislocations can squeeze themselves between precipitates and less force will be required for dislocation movement [25].

There are many articles in literature modeling the dependence of engineering strength on microstructure namely characteristics, sizes and shapes of precipitates [26]. Since the morphology of precipitates change from needles to plates, the aspect ratio variation affects the strengthening in terms of particle-dislocation interactions. The change in aspect ratio during precipitation is shown in Figure 2.10.

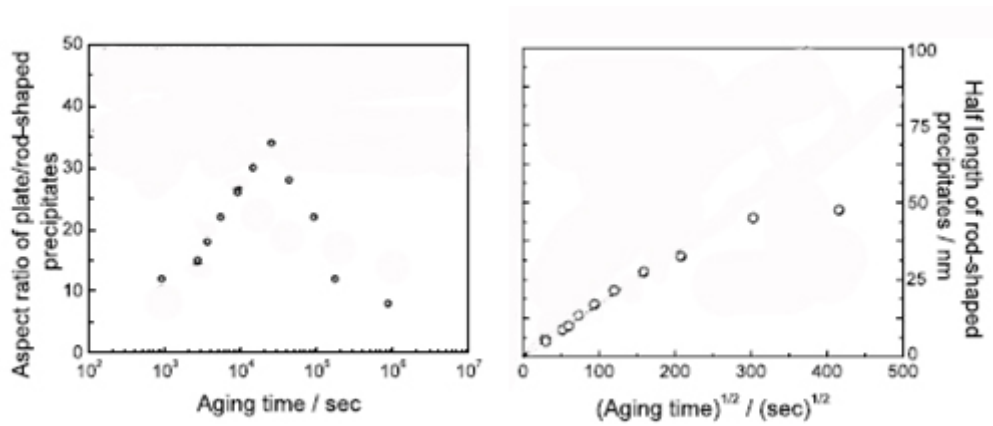


Figure 2.10 Aspect ratio change during aging [26]

Except from hardening precipitates; insoluble  $Mg_2Si$  and intermetallics formed during casting. Coarse iron bearing intermetallics (A),  $Mg_2Si$  particles formed during extrusion (B) and the hardening  $\beta'$  precipitates (C) can be observed in a typical TEM micrograph (Figure 2.11) [27].

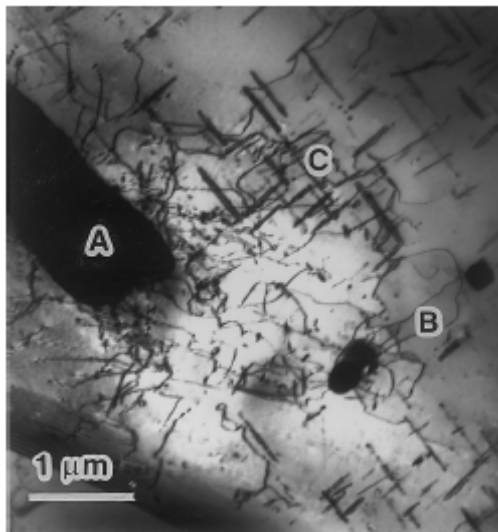


Figure 2.11 TEM micrograph in the peakaged condition [27]

Any deformation applied in the production sequence affects the dislocation-precipitation interactions. Cold working prior to aging [28-29], change in the extrusion ratio [30], cooling rate after extrusion [31] are all effective in strengthening.

### 2.3. Precipitation Hardening Mechanisms

The strength increase of an age-hardenable alloy is due to the interaction of the dispersed precipitate phase with dislocation. The interaction of glissile dislocations with the dispersed second phase will increase the critical resolved shear stress by a number of mechanisms. Three groups can be formed depending on how the dislocation manages to penetrate the dispersed particle: Dislocation can loop the particle; cut through the particle or cross slip around particle [32].

Particle looping (also referred as Orowan looping) is the mechanism in which the dislocation firstly bows out, and then is separated from the looped region leaving one loop around particle (Figure 2.12 a). A loop is formed around each precipitate every time a dislocation passes the precipitates. This mechanism becomes effective for small spacing between precipitates having small diameters.

Particle cutting mechanism on the other hand is applicable for small sized particles in which dislocations are not stopped at the particle-dislocation contact and glide right through the particle (Figure 2.12 b).

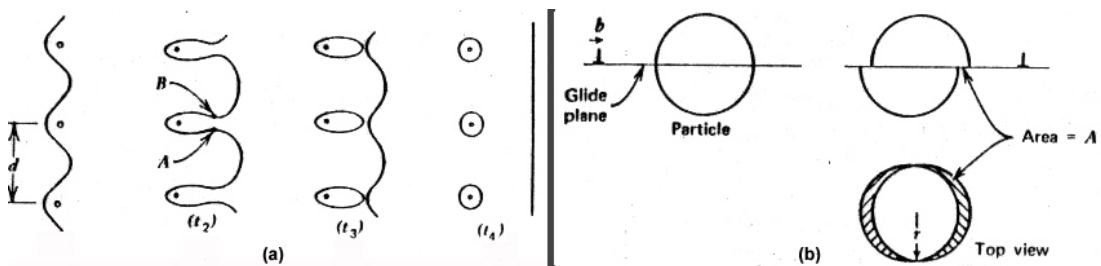
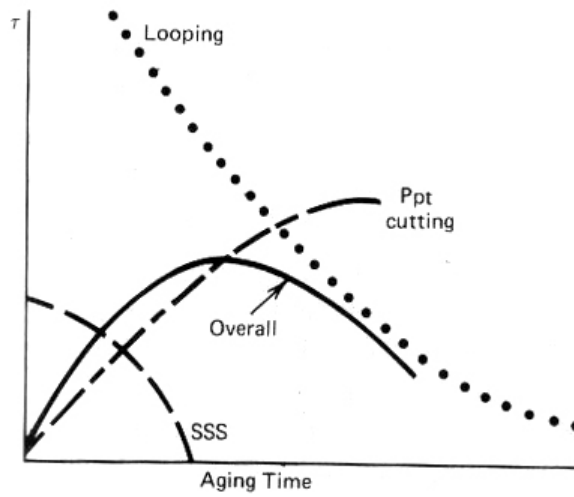


Figure 2.12 Particle – dislocation interactions (a)Orowan looping, (b)particle cutting [32]

During aging process, initially particle cutting mechanism operates due to small precipitate sizes. As aging continues, particle radii increase looping becomes easier [33]. The role of hardening mechanisms during aging is schematically shown in Figure 2.13.



**Figure 2.13 Role of major hardening mechanisms during age hardening [33]**

## CHAPTER 3

### EXPERIMENTAL PROCEDURE

In this study; the aging and deformation behavior of aluminum AA6066 (Al-Mg-Si-Cu) alloy was investigated. The microstructural and mechanical characterization of this alloy under different deformation and heat treatment conditions were studied. Figure 3.1 shows the details of the experimental studies.

#### 3.1. Material Used

This research was conducted using a wrought aluminum rod with the dimensions of  $\varnothing = 46\text{mm}$  and  $l = 200\text{mm}$  which was received from MKE. The as received rod was in hot-extruded and annealed condition. The chemical composition of the rod, which was determined via spectral analysis, was represented in Table 3.1.

**Table 3.1 Spectral analysis of alloy and the composition ranges of Standard AA6066**

	<i>Si %</i>	<i>Mg %</i>	<i>Cu %</i>	<i>Mn %</i>	<i>Fe %</i>	<i>Cr %</i>	<i>Zn %</i>	<i>Ti %</i>	<i>Al %</i>
<b>Al rods</b>	1.21	0.92	0.82	0.65	0.26	$\approx 0$	0.010	0.013	bal.
<b>AA6066</b>	0.9	0.8	0.7	0.6	0.5	0.4	0.25	0.2	bal.
	1.8	1.4	1.2	1.1	max	max	max	max	

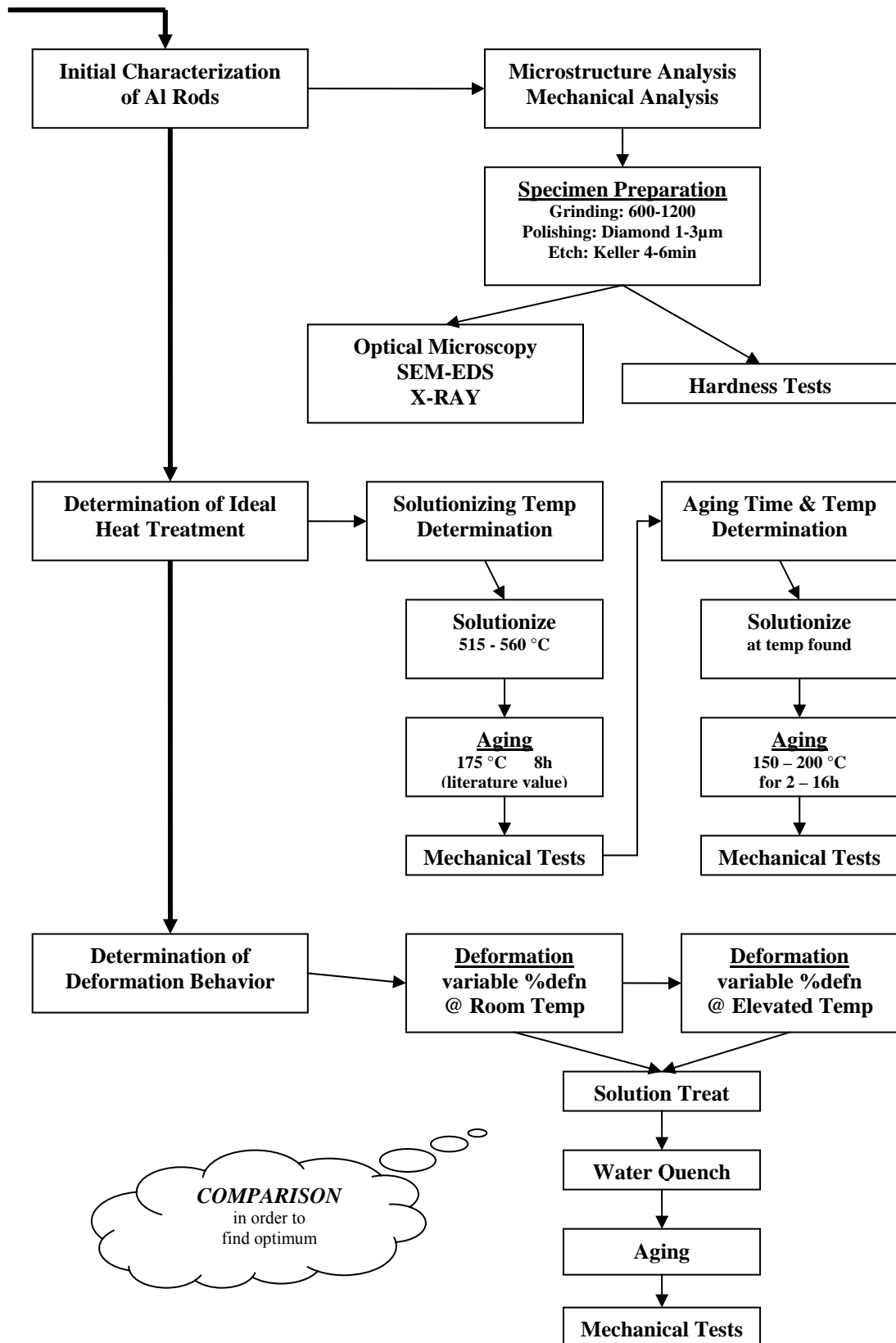


Figure 3.1 General experimental layout

As seen from table, the received bar is of AA.6066 type. The chemical composition ranges and some mechanical properties of Al.6066 are given in Table 3.1 and Table 3.2 respectively.

**Table 3.2 Mechanical properties of Al6066**

<i>Mechanical Properties</i>		<i>Al.6066</i>
Tensile Strength (MPa)	O temper	150
	T4, T451 tempers	360
	T6, T651 tempers	395
Yield Strength (MPa)	O temper	83
	T4, T451 tempers	207
	T6, T651 tempers	359
Elongation (%)	O temper	18
	T4, T451 tempers	18
	T6, T651 tempers	12
Hardness (HB)	O temper	43
	T4, T451 tempers	90
	T6, T651 tempers	120
Elastic Modulus (GPa)		69
Fatigue Strength (MPa)		110

### **3.2. Initial Characterization**

During “initial characterization step”, mechanical tests (tensile, hardness) and microstructural studies were carried out.

For mechanical testing, the specimens were prepared from  $\varnothing = 20\text{mm}$  rod according to ASTM E8 standard [34]. They were heat treated in accordance with the heat treatment procedure of Al.6066 [4]. Several specimens were solutionized at 530°C for 70 minutes and quenched. Several others were artificially aged at 175°C for 8

hours after quenching. As a result, three sets were achieved which were in O, T4 and T6 condition. Before tensile test, samples at a height of 15 mm were cut from the tension bars for microstructural investigations and hardness measurements. The tension test experiments were performed in a hydraulically activated, load controlled ALSA universal testing machine. For hardness measurements, Heckert analogue hardness tester was used. The surface, which was etched with Keller's reagent (2.5% $\text{HNO}_3$  – 1.5% $\text{HCl}$  – 1% $\text{HF}$  – water), was characterized by using optical microscope, SEM with EDS and X-ray methods.

During this initial characterization step; the microstructural features, UTS, yield strength, %elongation and hardness were obtained for as-received, as-solutionized and as-aged samples.

### ***3.3. Determination of Ideal Heat Treatment***

The effect of temperature and time during solutionizing and aging were examined. For that purpose; the as-received rods were cut into 40 pieces. The samples were first solutionized at various temperatures for various times. After solutionizing, all samples were quenched to water at room temperature. Ice was used to keep the temperature at about  $20 \pm 2^\circ\text{C}$ . During quenching; the medium is stirred to achieve temperature homogeneity. Aging was the last step.

It must be noted that, after solutionizing treatment, the samples were always kept in freezer which was kept at about  $-18^\circ\text{C}$  to eliminate the detrimental effect of natural aging.

#### **3.3.1. Solutionizing Temperature Determination**

For solution heat treatment; the soak times were determined according to their thickness. According to Table 3.3; the ideal soak time was 95 – 105 min for air furnace and 65 – 75 min for salt bath and the ideal temperature was also reported as  $530^\circ\text{C}$  [3].

**Table 3.3 Soak times and max quench delays for solutionizing [3]**

<i>Thickness (mm)</i>	<i>Soak Times (min)</i>				<i>Max. Quench Delay (sec)</i>
	<i>Air Furnace</i>		<i>Salt Bath</i>		
	<i>min</i>	<i>max</i>	<i>min</i>	<i>max</i>	
6.35 – 12.7	65	75	45	55	15
For each additional 12.7 or fraction	+30	+30	+20	+20	15

In order to investigate the effect of solutionizing temperature; the samples were solutionized for 95 minutes at eight different temperatures (515, 520, 525, 530, 535, 540, 550, 560°C). Also two different soak times (95 minutes & 12 hours) were tried for temperatures 515, 530, 540 and 550°C. All solutionizing treatments were done in a muffle furnace (Figure 3.2). Another trial was also established in a salt bath with circulation (stirring) equipment (Figure 3.3) at 530°C. After solutionizing; all the samples were quenched and peak aged at 175°C for 8 hours in an oil bath. These studies were summarized in Table 3.4.



**Figure 3.2 Muffle furnace for solutionizing**



**Figure 3.3 Salt bath for solutionizing**

**Table 3.4 Different solutionizing trials before quenching and aging at 175°C for 8 hours**

<i>Solutionizing Trials</i>	<i>Device</i>	<i>Solutionizing Temperature (°C)</i>	<i>Soak Time (min)</i>
1	Muffle Furnace	515	95
2		520	95
3		525	95
4		530	95
5		535	95
6		540	95
7		550	95
8		560	95
9	Muffle Furnace	515	720
10		530	720
11		540	720
12		550	720
13	Salt Bath	530	65

The specimens prepared using the temperature and time interval given in Table 3.4 were subjected to metallographic inspection and hardness measurements.

### 3.3.2. Aging Time and Temperature Determination

In this part of the work; 40 different sets of aging trial were carried out. The aging temperatures were selected as 150, 165, 175, 185 and 200°C. The specimens were hold at these temperatures in a range from 2 to 16 hours. Before aging; all sets are solutionized at 530°C for 95 min and quenched. The aging treatments were carried out in Julabo heating circulator oil bath (Figure 3.4) which operates within 0.1°C accuracy. The medium was commercial Julabo Thermal H oil (polydimethylsiloxan with stabilizing agent; viscosity < 50mPas [35]).



**Figure 3.4 Julabo heating circulator for aging**

**Table 3.5 Different aging trials followed by solutionizing at 530°C for 95min and quenched**

<i>Aging Trials</i>	<i>Aging</i>	
	<i>Temperature (°C)</i>	<i>Aging Durations (hour)</i>
1	150	
2	165	
3	175	2, 4, 6, 8, 10, 12, 14, 16
4	185	
5	200	

Metallographic and hardness investigations were performed after heat treatment.

### **3.4. Deformation Tests**

The deformation process was done by using Fenn rotary die swager. These swagers were used to obtain reduced round cross sections of the samples. The operation was schematically shown in Figure 3.5. The swager used, has two set of dies with exit diameters of 19.2 and 15.2mm. The swager and the dies were shown in Figure 3.6.



**Figure 3.5 Operation scheme of swager**



**Figure 3.6 Swager and the dies used**

From the as-received Al rods with  $\text{Ø} = 46\text{mm}$ ; all the rods were machined with four different diameters in such a manner that approximately 10%, 20%, 30% and 40% deformation (reduction in area) could be established. One pass had been enough for 10%, 20% and 30% deformation with the use of either smaller or the bigger die. However for 40% deformation; the samples were swaged from both die. The initial diameters and the deformation scheme were presented in Table 3.6.

<b>Table 3.6 Initial diameters of specimens and deformation scheme</b>			
<i>Deformation</i>	<i>Specimen Diameter (mm)</i>	<i>Exit Diameter (mm)</i>	<i>Dies Used</i>
10%	20.2	19.2	big die
20%	17.2	15.4	small die
30%	18.4	15.4	small die
40%	19.9	19.2	big die +
		15.4	small die

Four different temperatures were chosen, namely RT, 200, 300 and 400°C for the deformation. For the hot deformation processes; muffle furnace was used. The specimens were held in the furnace for 90 minutes at given temperatures and directly swaged.

Single pass deformation for 40% reduction was tried. Although deformations at 400°C and 300°C were succeeded; the sample was failed in the 200°C process (Figure 3.7). Hence two pass system was selected for 40% reductions. A set of specimens after deformation was presented in Figure 3.8.



**Figure 3.7 Failure of 40% deformation at 200°C with single pass**

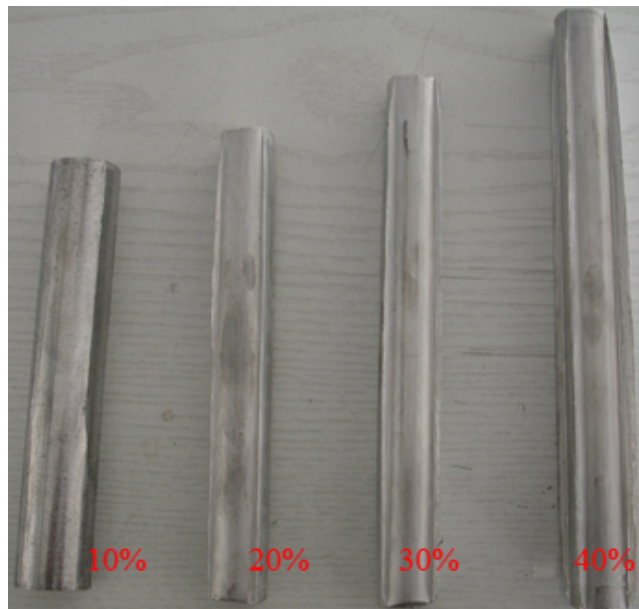


**Figure 3.8 Swaged aluminum rods**

The deformed rods were sliced into pieces of 15mm for age hardening treatment. Some of them were solutionized at 530°C for 95 min and quenched; then aged at 175°C in the range 4 – 12 hours. Seven sets of specimens were prepared irrespective to deformation. (Table 3.7)

**Table 3.7 Sets of deformed samples**

<i>Sets</i>	<i>Deformed</i>	<i>Solutionized</i> <i>530°C 95 min</i>	<i>Aged</i> <i>175°C</i>
1	√		
2	√	√	
3	√	√	4 hour
4	√	√	6 hour
5	√	√	8 hour
6	√	√	10 hour
7	√	√	12 hour

Microstructural evaluation and hardness measurements were carried out for all the sets. Also the specimens aged for 8 hour were subjected to tensile testing.

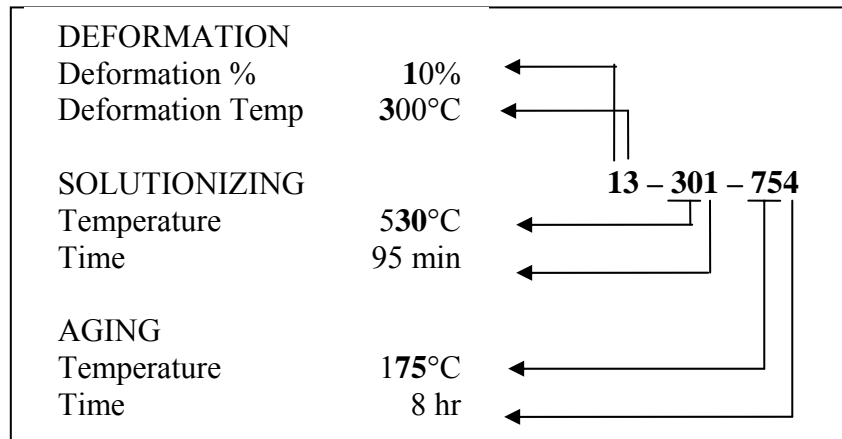
### **3.5. Specimen Notations**

In order to prevent specimen loss and mismatch; specimen notation system was developed and these notations were hammered on the specimens after each processes. The notation system was explained in Table 3.8.

**Table 3.8 The specimen notation system**

Deformation %		Deformation Temp (°C)		Solutionizing Temp (°C)		Soln Time		Age Temp (°C)		Age Time (h)	
0	Not			0	Not			0	Not		
1	10	0	RT	15	515	1	95 min	50	150	1	2
2	20	2	200	20	520	2	12 h	65	165	2	4
3	30	3	300	25	525	3	Salt bath	75	175	3	6
4	40	4	400	30	530			85	185	4	8
				35	535			00	200	5	10
				40	540					6	12
				50	550					7	14
				60	560						

Deformation%Temp–SolutionizingTempTime–AgeTempTime  
 eg. 13–301–754



All the investigations and test were carried on specimens obtained from the 46 mm diameter extruded bars. The cutting directions and orientations of the test specimens were schematically shown in the Figure A. 5 at appendix.

### 3.6. Microstructural Characterization

Metallographic preparation should be done with utmost care due to the softness of studied alloy. The surface of the specimens was grinded with 600 and 1200 grit emery papers respectively. For polishing; 3 μm and then 1 μm diamond paste was used. After polishing; the surface was cleaned with detergent.

For microstructural characterization; optical microscopy, scanning electron microscope (JEOL JSM 6400® equipped with Noran® EDS system) and Rigaku XRD unit were used. Grain size measurements were carried out with the use of Clemex Vision Professional software. At least 100 grains were counted and measured for each 200X magnified micrographs (Figure 3.9) and the grain size distribution was calculated.

Optical microscopy and SEM studies were done on as-polished and on etched surfaces. The etchant with the composition given in Table 3.9, was used for detection of microscopic features.

**Table 3.9 Composition of the etchant used**

<i>Ingredients</i>	<i>Volume (ml)</i>
HF (48%)	5
H <sub>2</sub> SO <sub>4</sub>	10
H <sub>2</sub> O	85

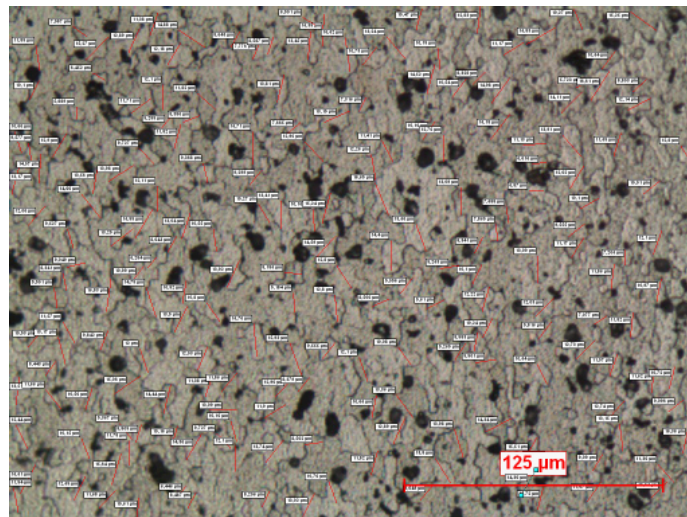


**Figure 3.9 Grain size measurement with clemex software**

### **3.7. Mechanical Characterization**

#### **3.7.1. Hardness Tests**

For hardness measurements; EMCO universal digital hardness testing machine was used. Brinell hardness numbers were obtained using 2.5mm ball indenter under 613N load. Hardness was taken from polished surfaces. During ideal aging determination; six indentations were made on each sample where two samples were used for each treatment. On the other hand; at least three indentations were made for deformed samples. Average hardness and the standard deviation were calculated using these data.

#### **3.7.2. Tensile Tests**

Tensile test specimens for the deformed samples were prepared according to aluminum tensile testing standard of ASTM (B557M-02a) [36]. “Small-size specimens proportional to standard” were prepared from the deformed rods. (Figure 3.10 and Figure 3.11) The rods were solutionized at 530°C for 65 min, quenched and aged at 175°C for 8h before testing.



**Figure 3.10 Small-sized specimen proportional to standard tension specimen**

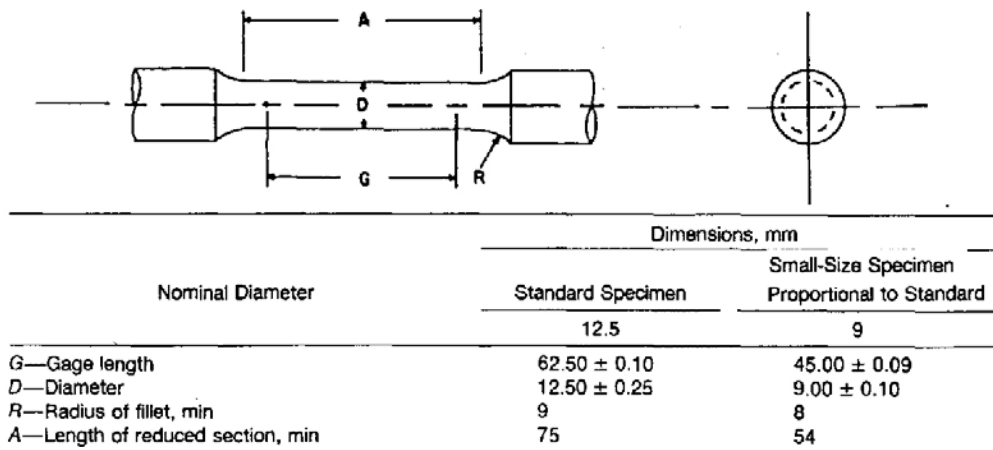


Figure 3.11 Specimen dimensions according to ASTM B557M [36]

Tensile tests were performed in a Dartec servo-hydraulic universal testing machine with 250kN capacity, interfaced with a computer for data acquisition. Constant elongation (0.015mm/sec stroke) was used throughout the tests. The yield strength, determined as the 0.2% strain offset, as well as the tensile strength were obtained from the resulting stress-strain plots.

## CHAPTER 4

### RESULTS AND DISCUSSION

The aim of this study was to characterize the AA6066 alloy having the nominal composition in Table 3.1. After a detailed microstructural study, the age hardening characteristics of the alloy is examined. The effect of hot and cold deformation on age hardening characteristics and resulting mechanical properties was also investigated by applying a series of deformation process at the onset of solutionizing treatment.

In the following section the alloy was characterized. The microstructural features were presented via optical and scanning electron microscope images. Tensile properties and hardness values were tabulated for T0, T4 and T6 tempers. Secondly; the effect of solutionizing temperature on properties was investigated via hardness measurements and micrographs. For aging trials; the hardness measurements were tabulated. Finally the effect of initial deformation on mechanical properties and microstructure was evaluated with the use of optical microstructures, tensile test results and hardness values. The tabulated hardness values were also presented graphically for comparison purposes.

#### ***4.1. Characterization of Al 6066***

##### **4.1.1. Microstructural Investigations**

According to the spectral analysis carried out; the as received Al alloy was composed of mainly silicon, magnesium, copper and iron. The overview of the as-received alloy and at T6 temper condition can be seen in Figure 4.1 and Figure 4.2 respectively. Metallographic inspections revealed the presence of dark particles

throughout the structure. XRD analysis was carried out in order to determine the phases present in the structure. However, the results of the analysis (Figure 4.3) showed no eligible information. The detection of small peaks near aluminum peaks were unsuccessful. Actually this was due to low concentration of alloying elements ( $\text{wt}\% \leq 1$ ); causing lower intensity peaks. However, the studies on as-polished surfaces showed the presence of tiny ( $5\text{--}10\mu\text{m}$ ) gray script-like particles near dark particles. (Figure 4.4)



**Figure 4.1 Microstructure of as-received Al 6066 (200X)  
Dark phases present throughout the surface**



**Figure 4.2 Microstructure of Al 6066 – T6 (200X)**  
Grain boundaries can be observed easily in T6 condition

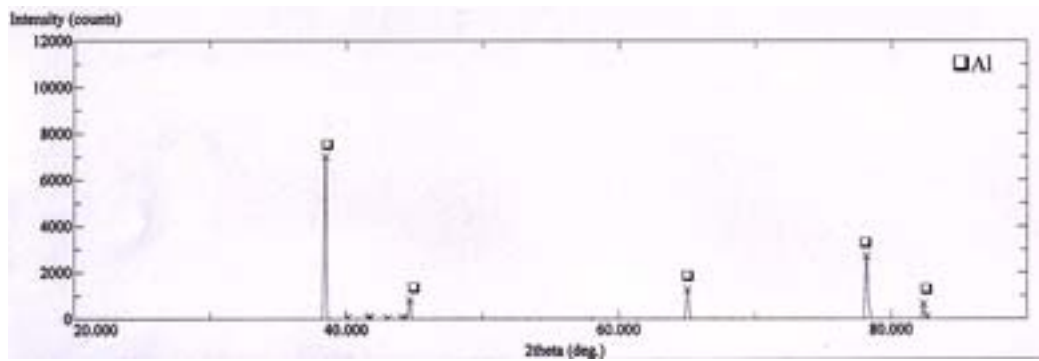


**Figure 4.3 XRD of the as-received alloy**

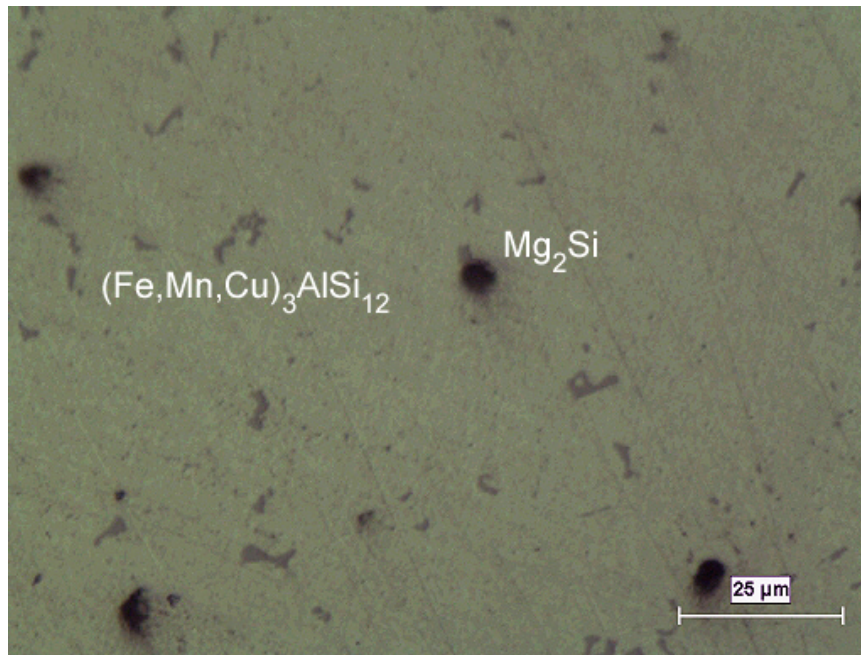


**Figure 4.4** The optical micrograph of as polished surface of the as-received alloy  
Two type of phases namely  $\text{Mg}_2\text{Si}$  and  $(\text{Fe,Mn,Cu})_3\text{AlSi}_{12}$  can be seen

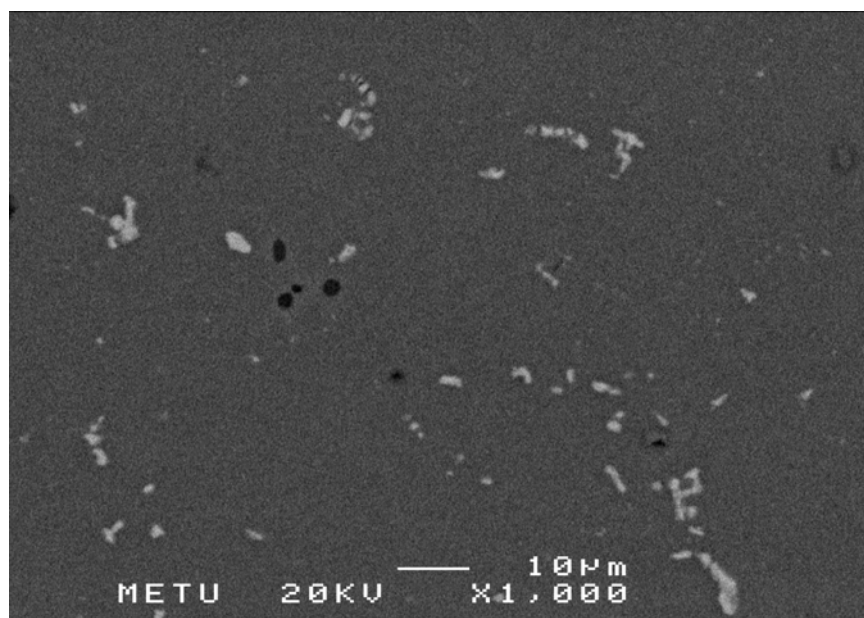


**Figure 4.5** Backscatter SEM image of the alloy

In order to investigate the nature of these particles; as-polished surfaces were examined under scanning electron microscopy. With the use of attached EDS; it was seen that the large black ones were of  $Mg_2Si$  type and the gray script-like ones were of  $(Fe,Mn,Cu)_3SiAl_{12}$  type. It is also concluded that most of the dark regions observed under optic microscope were voids. The detection of  $Mg_2Si$  inside these voids is due to that hard  $Mg_2Si$  particle pull-out from the soft aluminum matrix during metallographic preparation (grinding and/or polishing). All the particle characterizations were established on the as-polished surfaces; since it is known that; they are readily dissolved during etching. The back-scatter SEM image and the EDS analysis were presented in Figure 4.5, Figure 4.6 and Figure 4.7. The composition yielding the stoichiometric formulations of the phases was tabulated at Table 4.1.

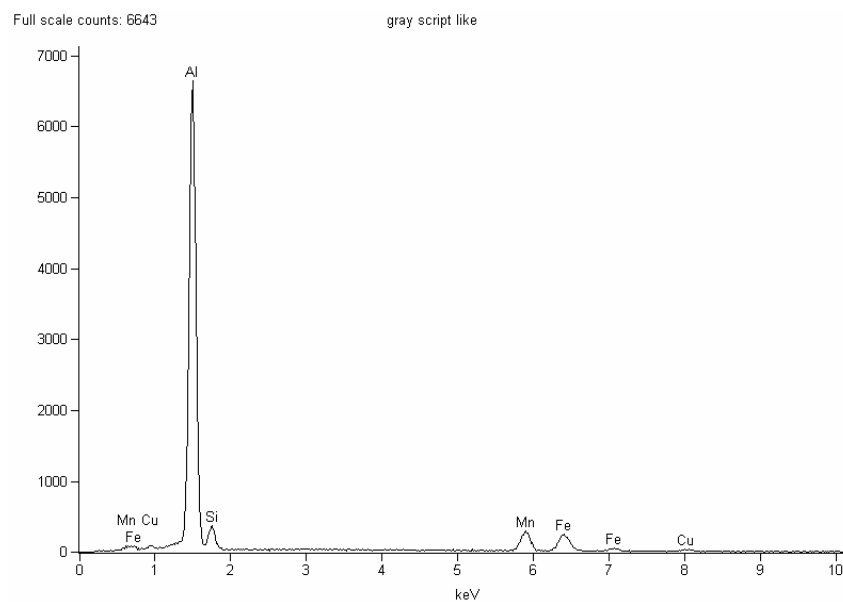


**Figure 4.6 The EDS analysis of gray script-like particles, which yielded  $(Fe,Mn,Cu)_3SiAl_{12}$  type precipitates**

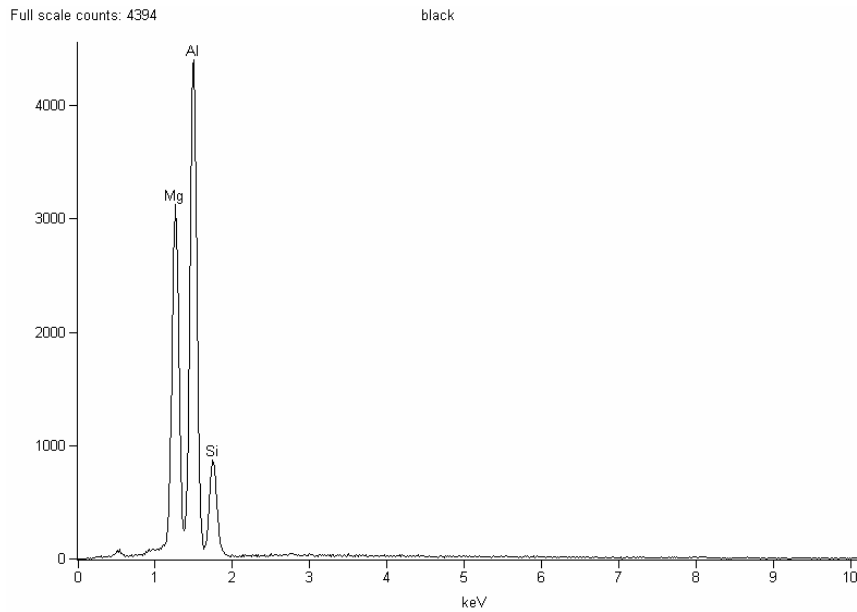


**Figure 4.7 The EDS analysis of black particles, has shown that they are of Mg<sub>2</sub>Si type**

**Table 4.1 The chemical compositions of the particles analysed with EDS**

$(\text{Fe}, \text{Mn}, \text{Cu})_3\text{SiAl}_{12}$			$\text{Mg}_2\text{Si}$		
<i>Element</i>	<i>Weight Conc %</i>	<i>Atom Conc %</i>	<i>Element</i>	<i>Weight Conc %</i>	<i>Atom Conc %</i>
Al	86.58	91.91	Mg	25.92	28.16
Si	2.52	2.57	Al	56.59	55.39
Mn	4.41	2.30	Si	17.49	16.45
Fe	4.72	2.42			
Cu	1.78	0.80			

#### 4.1.2. Mechanical Properties

For determination of some basic mechanical properties, tensile tests and hardness measurements were carried out for three tempers namely annealed (O), solutionized (T4) and aged (T6). The results were summarized in Table 4.2. In that table, the nominal properties given by Aluminum Association (AA) were also presented for comparison purposes. It was evident that; the alloy used, had higher mechanical properties than the standard one. It seems that higher alloying element additions, i.e. copper in this case, most probably yields a better the performance of the alloy during aging.

**Table 4.2 Mechanical test results for O, T4 and T6 tempers**  
**The nominal data given by AA is also tabulated for comparison purposes.**

Temper	<i>6066 Alloy Used</i>				<i>Standard Alloy (AA6066)[3]</i>			
	Brinell Hardness	Yield Strength (MPa)	UTS (MPa)	% EL	Brinell Hardness	Yield Strength (MPa)	UTS (MPa)	% EL
O	57	175	220	18	43	82	152	18
T4	102	317	442	15	90	207	359	18
T6	140	451	472	9	120	359	393	12

The alloy showed ~10 %elongation in the T6 temper and ~18 % in the annealed condition. Fracture surfaces of the specimen were observed on tensile test specimen surfaces. Figure 4.8, shows the macroscopic fracture surface, which indicates a ductile behavior. Shear deformation at an angle of about 45° with the tensile axis and the perfect cup-and-cone structure can be seen in Figure 4.8.



**Figure 4.8 Macroscopic fracture surfaces**  
**Cup and cone structure indicates the ductile fracture behavior**

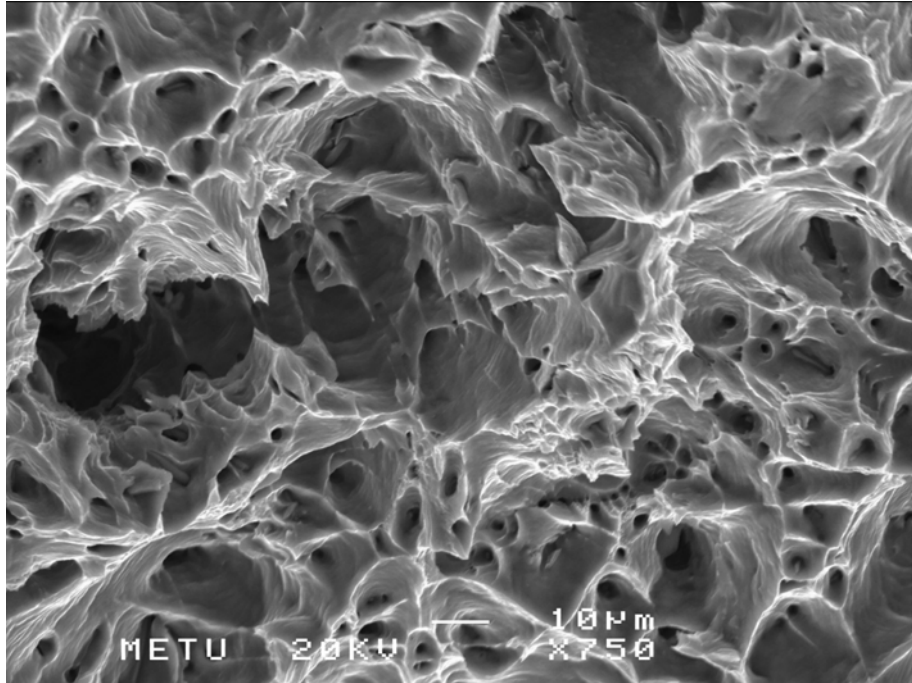


**Figure 4.9 Fracture surface of as-received alloy**

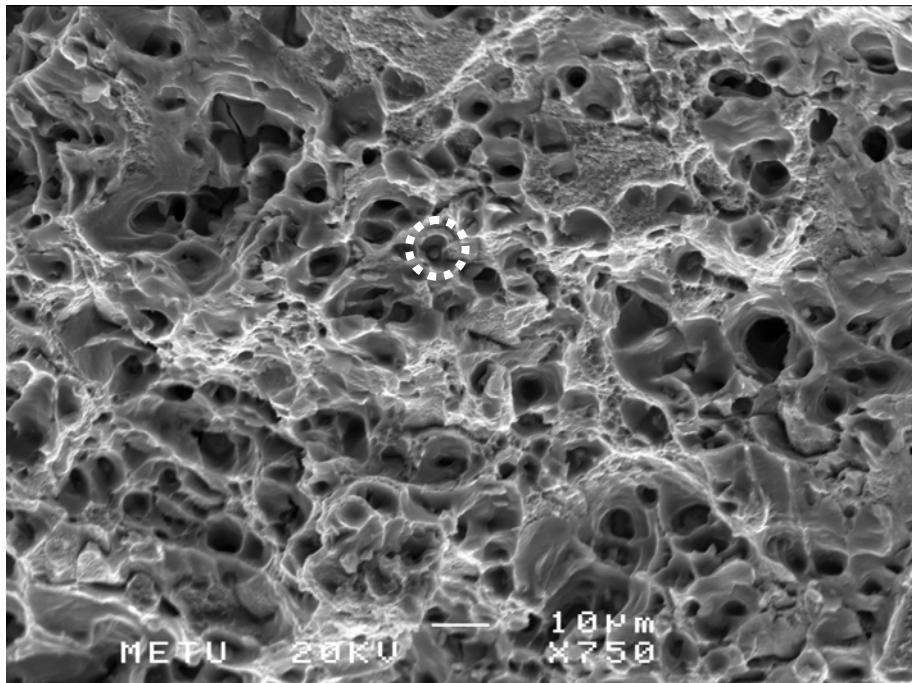


**Figure 4.10 Fracture surface of peak-aged alloy**

The dimples, which were an indication of ductile fracture, could be observed under SEM. Fracture surfaces were shown in Figure 4.9 and Figure 4.10. Inside the dimples; the complex alloy particles were detected. An example  $((\text{Fe},\text{Mn},\text{Cu})_3\text{SiAl}_{12})$  was shown within white dashed circle in Figure 4.10. The investigations demonstrated that mainly transgranular dimpled shear rupture structure was observed in both cases. After aging, the size of dimples got smaller as compared to that of as-received one. This was possibly due to increase in the number of second-phase particles after aging, yielding more microvoid coalescence during tension test. Another feature that could be observed from Figure 4.10 was the presence of intergranular dimpled regions together with transgranular ones. These finding were also confirmed by the studies of Munitz on AA6063 [25].

## **4.2. Heat Treatment Studies**

### **4.2.1. Effect of Solutionizing Treatment**

Solutionizing is the main step the precipitation hardening. It must be carried out carefully to choose higher temperatures for dissolving maximum amount of particles to achieve a homogenous solid solution. However, the grain boundary melting due to overheating should be also taken into consideration.

The as received specimen in the annealed temper, having a hardness of 57HB, was treated at different temperatures and for different time intervals prior to artificial aging at 175°C for 8 h. Hardness measurements were tabulated in Table A. 2 at the appendix and summarized in Table 4.3. Also, the effect of solutionizing treatment on hardness was illustrated via column chart in Figure 4.11.

**Table 4.3 Tabulated Brinell hardness values for different solutionizing treatment**

<i>Device</i>	<i>Solutionizing Process</i>	<i>HB</i>	<i>STD</i>	<i>HB</i>	<i>STD</i>
		<i>solutionized</i>		<i>aged</i>	
Muffle Furnace	515°C – 95 min	94	± 2.34	131	± 4.59
	520°C – 95 min	94	± 3.39	135	± 1.79
	525°C – 95 min	93	± 3.06	138	± 1.64
	530°C – 95 min	95	± 1.55	139	± 1.38
	535°C – 95 min	93	± 1.83	140	± 5.06
	540°C – 95 min	96	± 1.83	142	± 3.66
	550°C – 95 min	99	± 3.13	144	± 2.58
	560°C – 95 min	98	± 2.25	145	± 2.58
	515°C – 720 min	93	± 0.98	134	± 1.72
	530°C – 720 min	83	± 2.07	145	± 2.58
	540°C – 720 min	98	± 1.97	139	± 3.46
	550°C – 720 min	95	± 1.55	139	± 2.58
Salt Bath	530°C – 65 min	95	± 1.22	138	± 1.63

The samples heat treated in salt bath provided the same results as the samples heat treated in muffle furnace. Hence, for the remaining part of the experiments; the muffle furnace was chosen as the solutionizing medium. It was shown that; the peak hardness was achieved after solutionizing at 530°C for 12 h. The chart demonstrated that; as the solutionizing temperature increased, the hardness increased from 131 HB to 145 HB in the case of 95 minute soaking time. As temperature increased more solid dissolved in matrix for super saturation due to increased diffusion kinetics and higher solubility limits at higher temperatures. After 530°C the loss of hardness for long soaking times might be interrelated to the most probable grain growth tendency. Since the hardness values were closer to each other; 95min duration at 530°C could be chosen as solutionizing treatment for the alloy. Similar results were obtained by Zhen et al. [37]

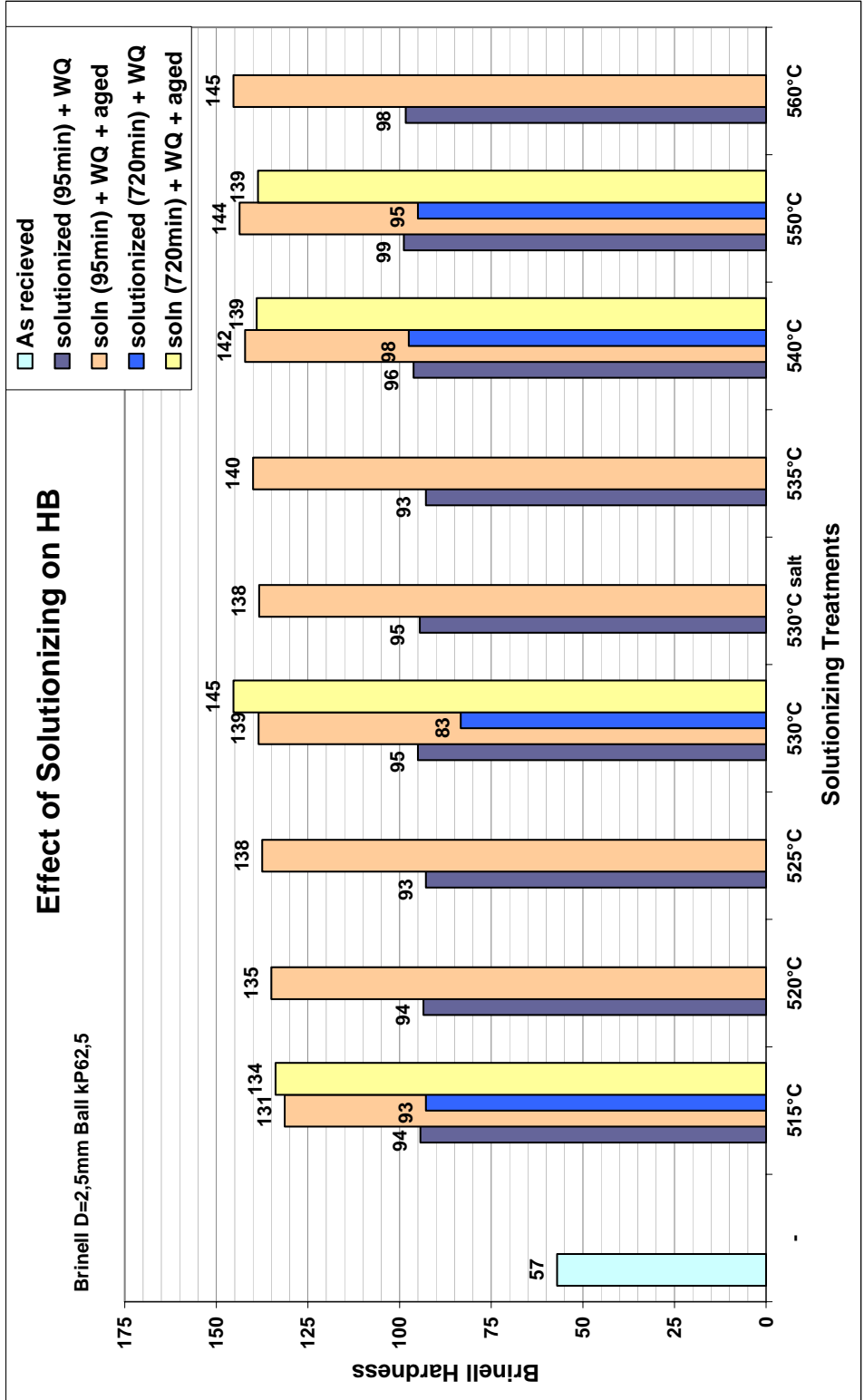


Figure 4.11 Effect of solutionizing treatment on Brinell Hardness

#### 4.2.2. Aging Behavior of the Alloy

Since 530°C was selected as optimum solutionizing temperature; different aging treatments were tried on the samples solutionized at 530°C for 95 min. Totally 40 sets of aging treatments were applied between 150°C and 200°C for the periods of time ranging from 2 hour to 16 hour. All hardness measurements were tabulated in Table A. 3 at the appendix and summarized in Table 4.4. Also, the aging behavior of alloy was presented in the form of charts in Figure 4.12.

**Table 4.4 Hardness values for different aging treatments**

<i>Aging Temperature</i>		<i>Aging Time (hour)</i>							
		<i>2</i>	<i>4</i>	<i>6</i>	<i>8</i>	<i>10</i>	<i>12</i>	<i>14</i>	<i>16</i>
150°C	Hardness	100	106	110	116	120	126	127	130
	STD	1.44	1.61	1.88	1.73	1.07	1.24	2.07	1.44
165°C	Hardness	118	132	135	138	139	140	138	138
	STD	1.72	1.48	1.28	1.19	1.31	1.73	0.78	1.97
175°C	Hardness	129	136	136	140	139	137	136	137
	STD	1.38	2.11	2.38	1.17	2.97	1.82	2.09	1.42
185°C	Hardness	143	141	142	140	137	136	135	135
	STD	2.21	1.71	1.53	2.20	1.98	1.96	1.24	1.64
200°C	Hardness	132	129	128	124	122	121	119	116
	STD	1.68	1.44	2.37	1.60	2.54	1.27	2.09	3.45

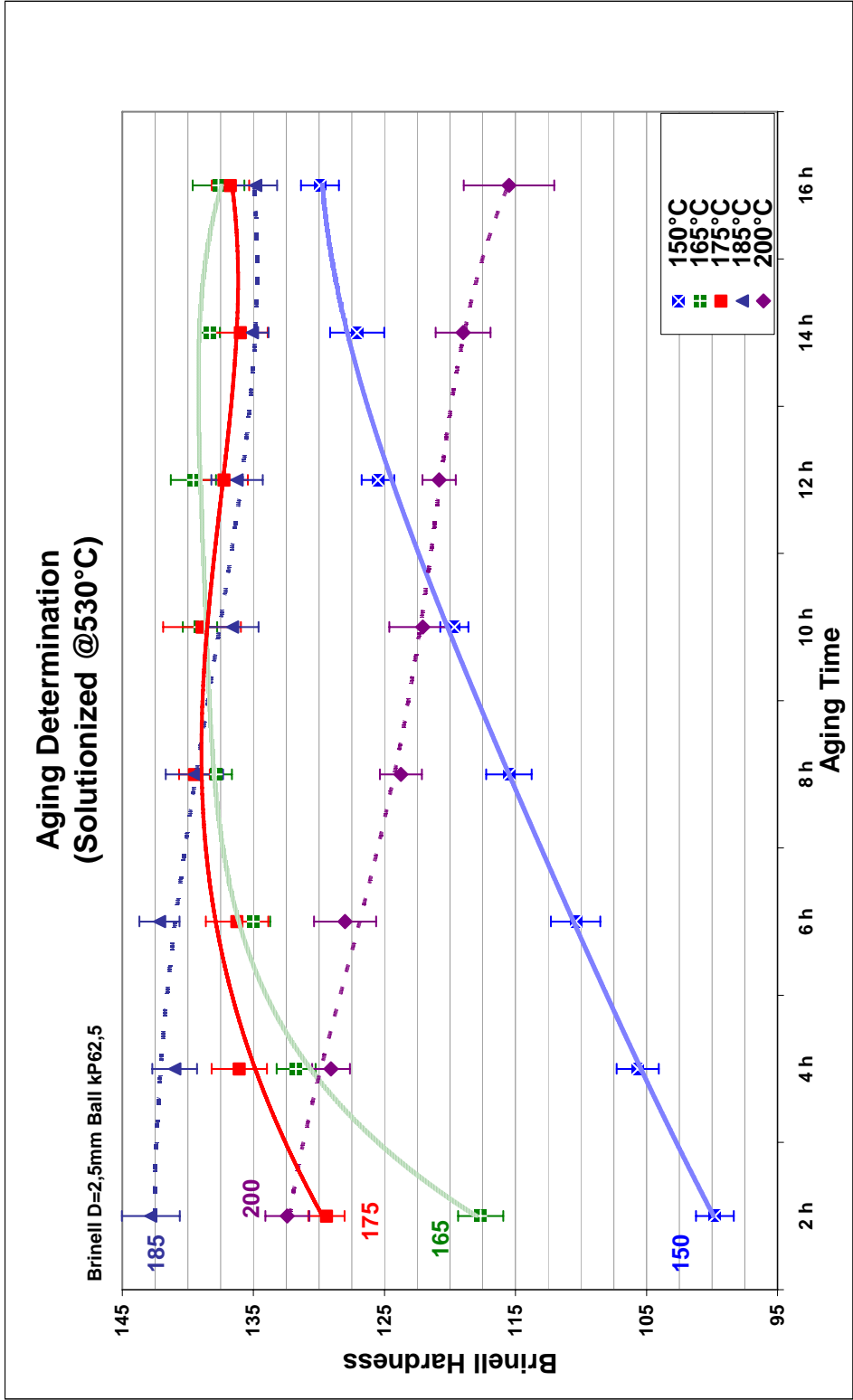


Figure 4.12 Aging response of alloy solutionized at 530°C for 95 min

The figure showed typical hardness curves of solutionized alloys after artificial aging at elevated temperatures. Accordingly; a peak hardness of 140 HB was reached after 8 h of aging at 175°C and then a slight decrease was followed. The curve for 185°C and 200°C did not show a peak hardness which most probably due to overaging. On the other hand; for the specimens aged at 150°C and 165°C, a continuous increase in hardness was observed throughout the 2 -16 hour interval. The effect of slow kinetics could be the reason of such a trend. As seen in Figure 4.12, the aging at 175°C yields the optimum temperature for the alloy; since the peak of 140 HB after aging 8 hours could be obtained.

Maximum hardness could be reached in the case of forming fine dispersed needle-shaped ( $\beta''$ ) phase with equal sizes, small spatial distances and high volume fraction [38]. This was most probably obtained by aging at 175°C at 8 hour. For higher times and temperatures, much larger precipitates with larger spatial distance would appear resulting a lower hardness.

### ***4.3. Effect of Deformation***

6000 series aluminum alloys were used for general extrusion purposes. The effect of microstructure i.e. grain size and nucleation sites for precipitates [39-40] on the final mechanical properties is obvious. Hence the effect of deformation prior to heat treatment must be considered, in terms of amount of deformation [41] and deformation temperature.

The as-received specimen was in hot-extruded condition. Initially, the microstructure of the bar is examined in detail. Then a set of different deformation process was applied to observe the effect of deformation on mechanical properties and heat treatment.

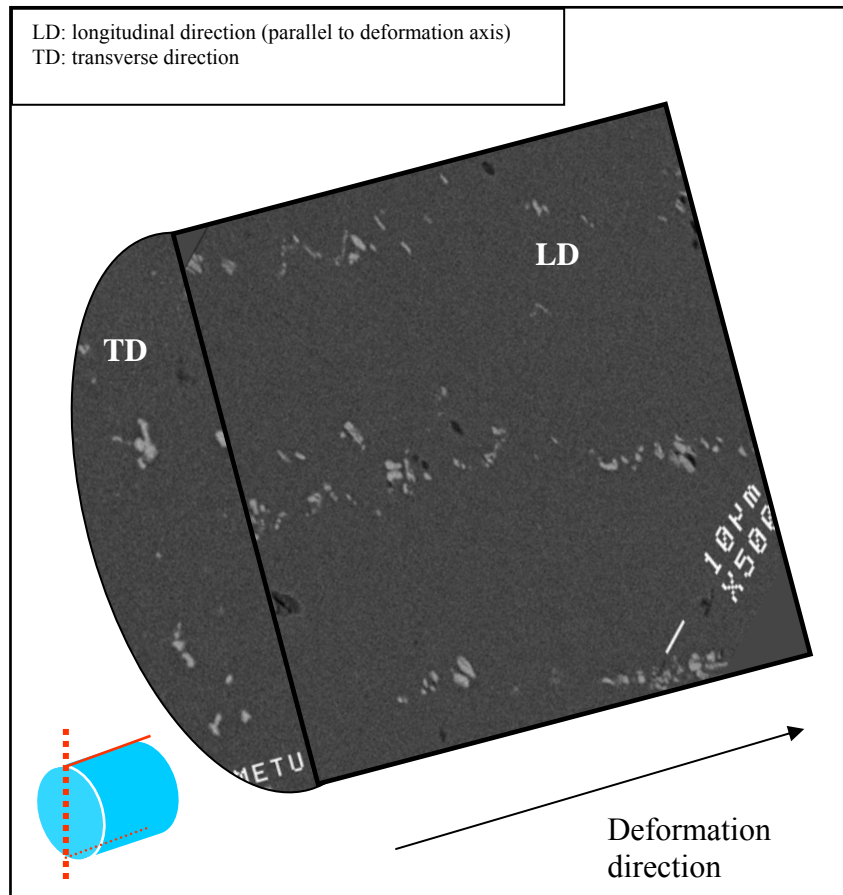


Figure 4.13 Backscatter SEM image of a deformed sample

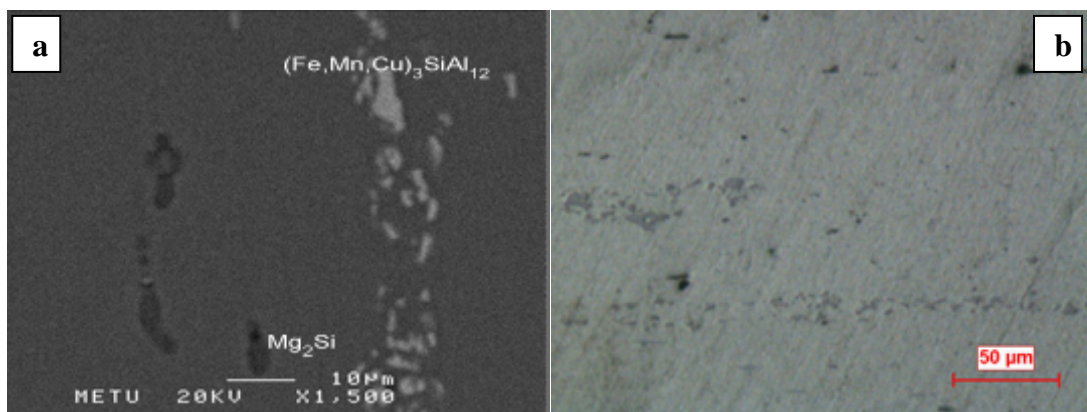
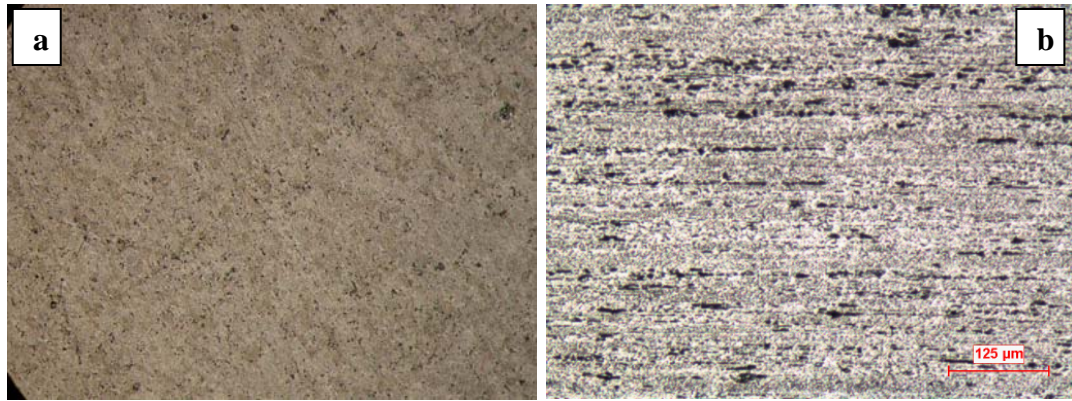


Figure 4.14 (a) Back-scatter SEM image and (b) optical micrograph of as-received samples showing the particles on as-polished surface parallel to the deformation axis (LD)



**Figure 4.15** Optic micrographs from etched surfaces of as-received samples (a) TD, (b) LD

After deformation; only as-polished surfaces revealed valuable information: the particles in Figure 4.14 were broken and formed stringers along the deformation direction. But; the grains (elongated grains) could not be observed from the etched surfaces as shown in Figure 4.15. Only finding was the presence of lines showing the deformation direction on LD surfaces. This might be possibly due to the small separation between high amount of boundaries (cell and/or grain) preventing the contrast formation during etching.

#### **4.3.1. Effect of Deformation on Microstructure**

The mechanical properties of the final products were greatly influenced by their final microstructures. An example for development of microstructure for cold deformed specimens was presented in Figure 4.16. All the surfaces were obtained from TD. Although, the aged samples are never examined under optical microscope, the observation of grain boundaries become easier due to high contrast within grains.

When directions are concerned; the information from longitudinal direction (LD) was more important than the transverse direction (TD), since the effect of deformation and effect of recrystallization could be easily recognized at the LD direction. On the other hand; the TD sections were used as the crack growth planes during tensile testing. For this reason; from this point forward, the discussions regarding tensile behavior were based on observations on TD sections; whereas the ones regarding recrystallization behavior were based on LD sections.

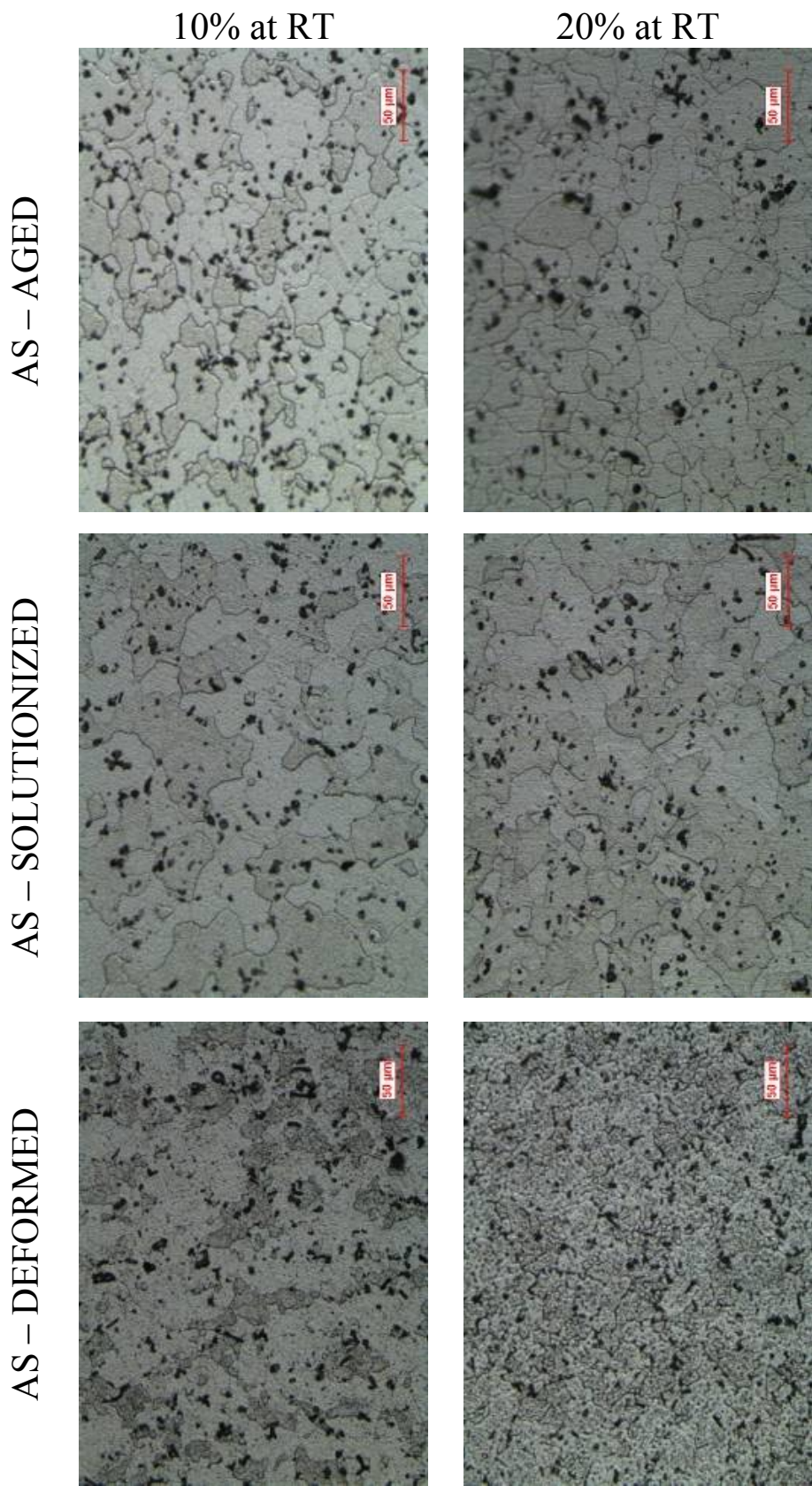


Figure 4.16 The optical micrographs of cold deformed samples (TD)

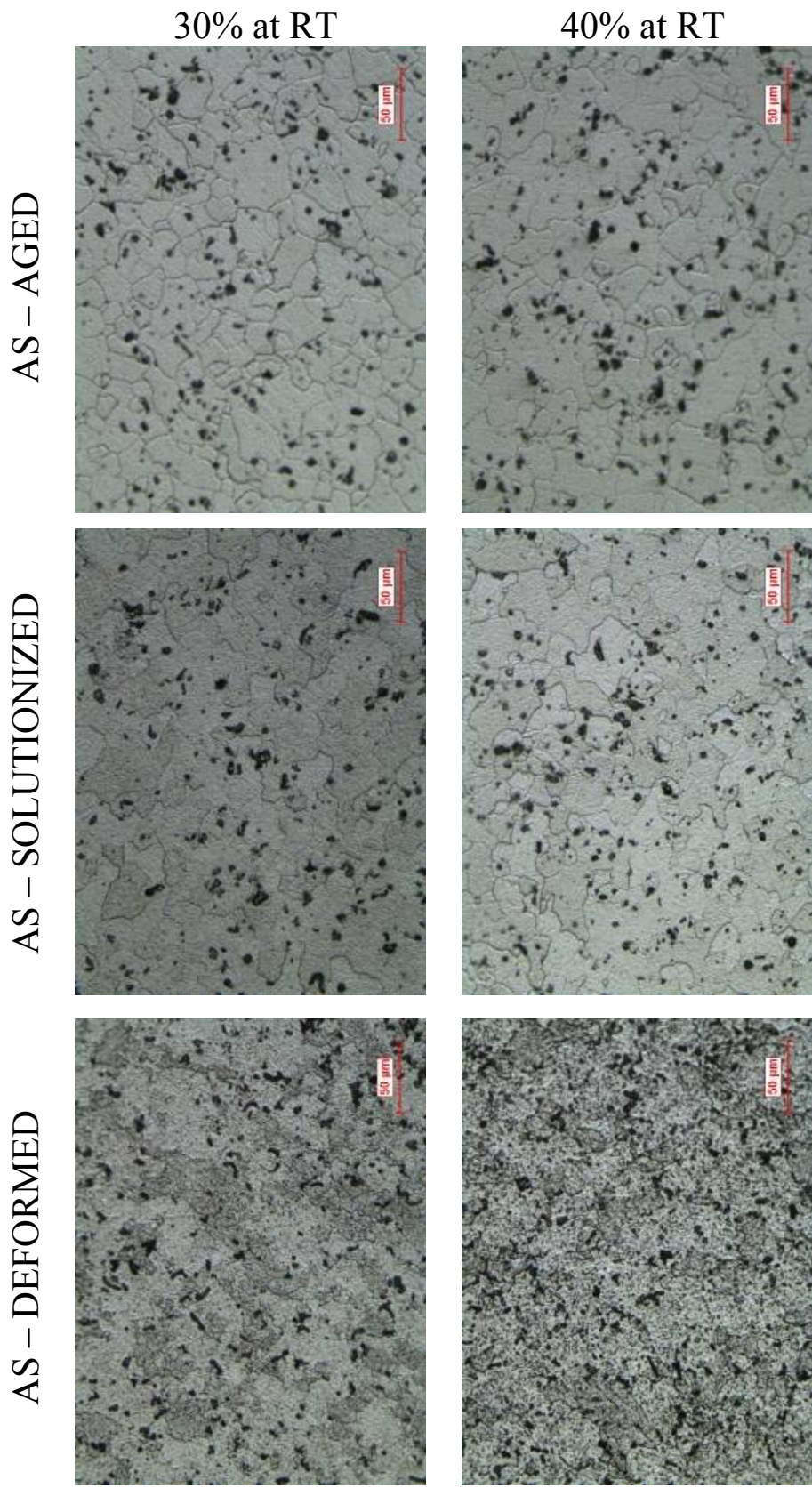
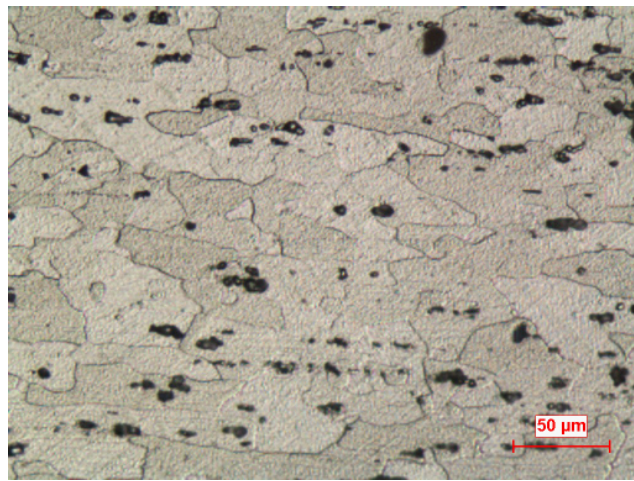


Figure 4.16 (cont'd)

#### 4.3.1.1. Recrystallization Behavior

After a deformation (shaping) process, it is expected that a solutionizing treatment will alter the grain morphology via recrystallization. Moreover, for hot deformation processes; the recrystallization temperature must be taken into consideration. Three sets of alloys were prepared from 40% cold deformed specimen: 1) 40% cold deformed then treated at 530°C; 2) 40% cold deformed then treated at 450°C and 3) 40% cold deformed then treated at 350°C. The resultant micrographs were presented in Figure 4.17 to Figure 4.19.



**Figure 4.17** Sample treated at 530°C for 65 min after 40% cold deformation (LD)

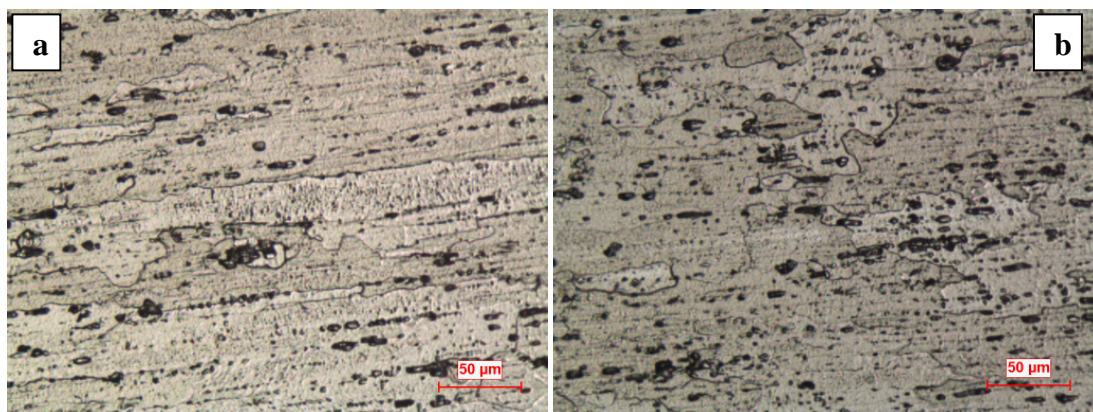


**Figure 4.18** Sample treated at 450°C for 1 hr after 40% cold deformation (LD)  
a)center b)near rim

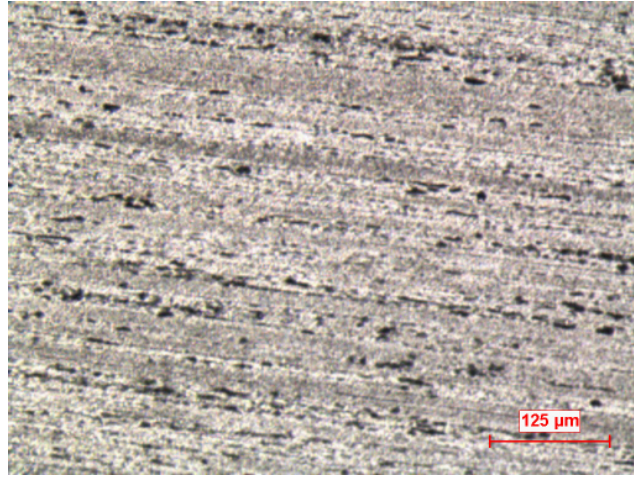


**Figure 4.19 Sample treated at 350°C for 1 hr after 40% cold deformation (LD)**

As far as the results are concerned, it can be concluded that, no recrystallization was occurred upon heating to 350°C whereas a partial recrystallization was obtained at 450°C. On the other hand, fully recrystallized microstructure could be observed at 530°C. So it seems that the alloy started to recrystallize at about 400°C and fully recrystallized at around 500°C. The results obtained were parallel to the findings of Park et al. on drawn 6063 tubes [42].

#### 4.3.1.2. Grain Morphology

Due to combination of deformation and heat treatment; the microstructure of the specimens were forced to change as shown in previous section. The strong relation between microstructure and the final properties necessitates the investigations of this morphology.

An investigation on LD surfaces revealed two different morphologies for the specimens which were solutionized followed by a 10% cold-deformation step (Figure 4.20). Although the region near to rim had an equiaxed grain structure; inside the specimen some elongated grains (pan-cake grains) were present. Low reduction rates might be responsible for such a grain morphology difference at the center and at the surface of the bar. However, in the 40% cold deformed specimens there was no grain morphology difference between the center and the surface of the bar. Most

probably due to lower stored strain energy in the 10% cold deformed ones; the growth was hindered by the particles and the grains were grown between these aligned particles during recrystallization process in the solutionizing period. A study by Lillywhite et al. [43] showed that the recrystallization behavior was affected by particle stimulated nucleation or Zener pinning mechanisms due to the presence of intermetallics and small precipitates in the matrix.

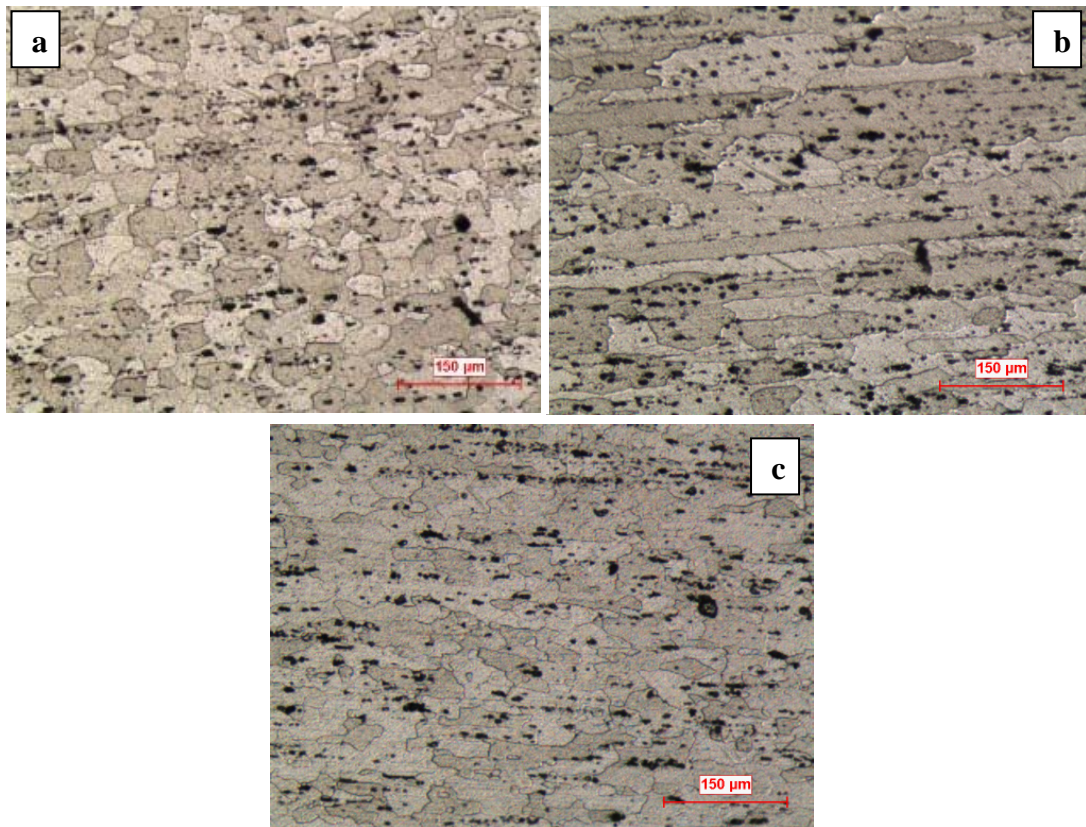


**Figure 4.20 LD surface showing different grain**  
**(a) near rim 10% cold deformed + soln, (b) center region 10% cold deformed + soln**  
**(c) all regions 40% cold deformed + soln**

Apart from grain shapes; different grain sizes were obtained by changing deformation route. All the grain size measurements were done with the use of optical micrographs obtained from rim regions of the specimens in the as-solutionized condition because of the fact explained previously. For cold-deformed specimens;

the microstructure and the relevant grain size distributions for both LD sections and TD sections were presented in Figure 4.21 and Figure 4.22 respectively. For hot deformed cases, the measurements regarding to the TD sections were carried out (Figure 4.23 - Figure 4.25). The mean grain sizes obtained from the image analyzer were tabulated in Table 4.5 and the effect of deformation on the TD section grain size was plotted in Figure 4.26.

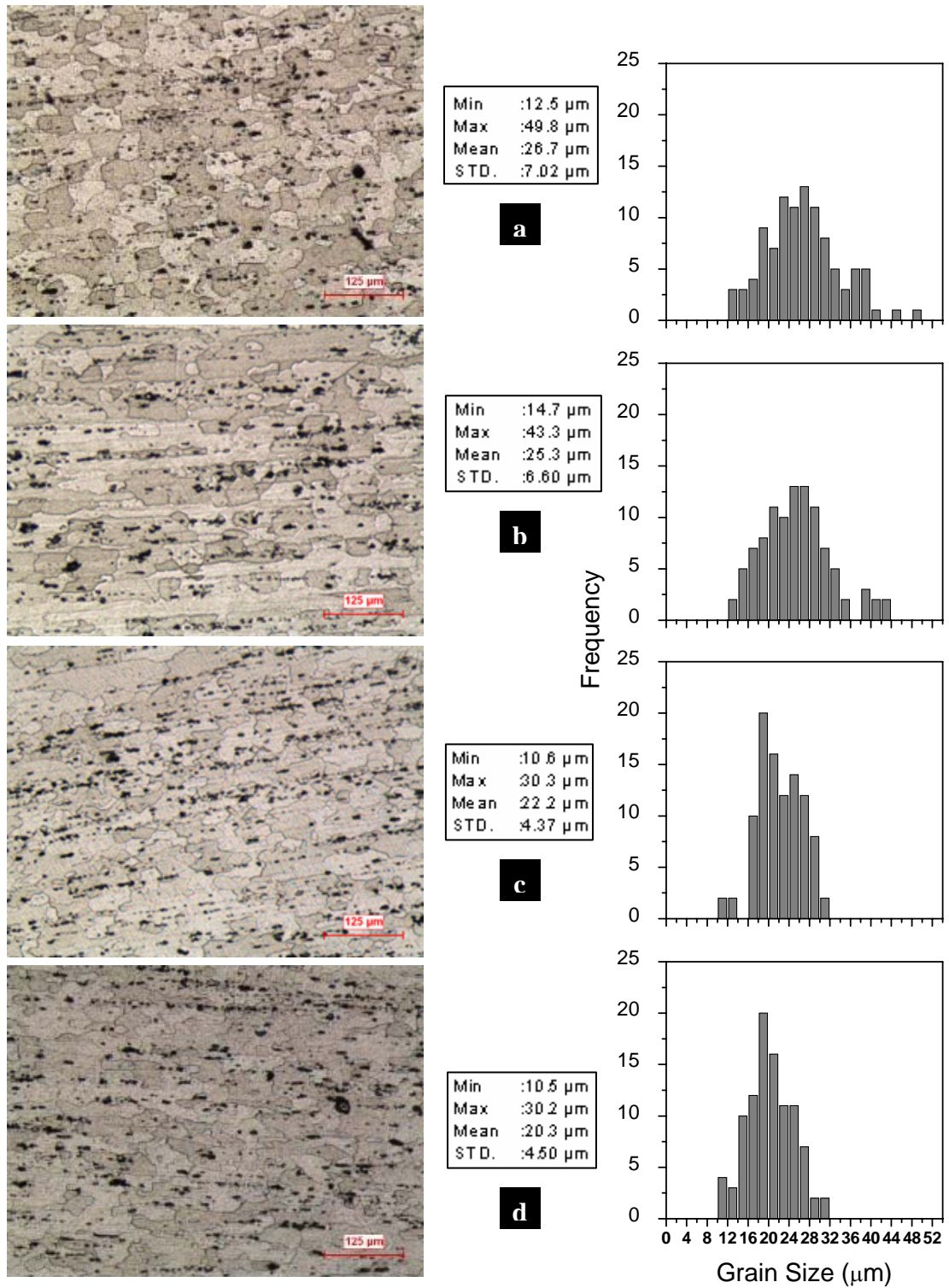


**Figure 4.21 Optic micrographs obtained from LD sections of the specimens solutionized at 530°C and the corresponding grain size distributions; a)10% b)20% c)30% d)40% cold-deformed samples**

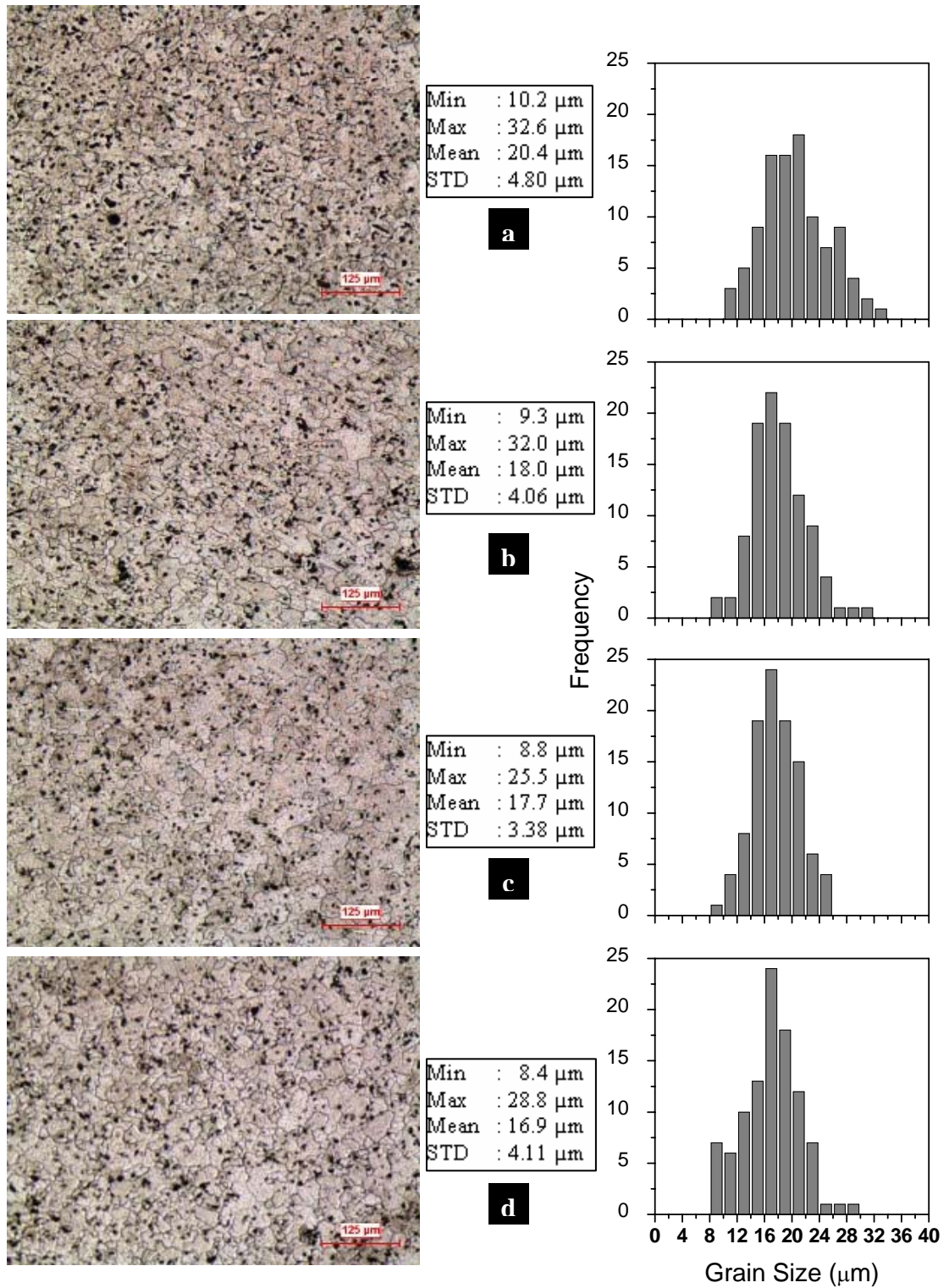
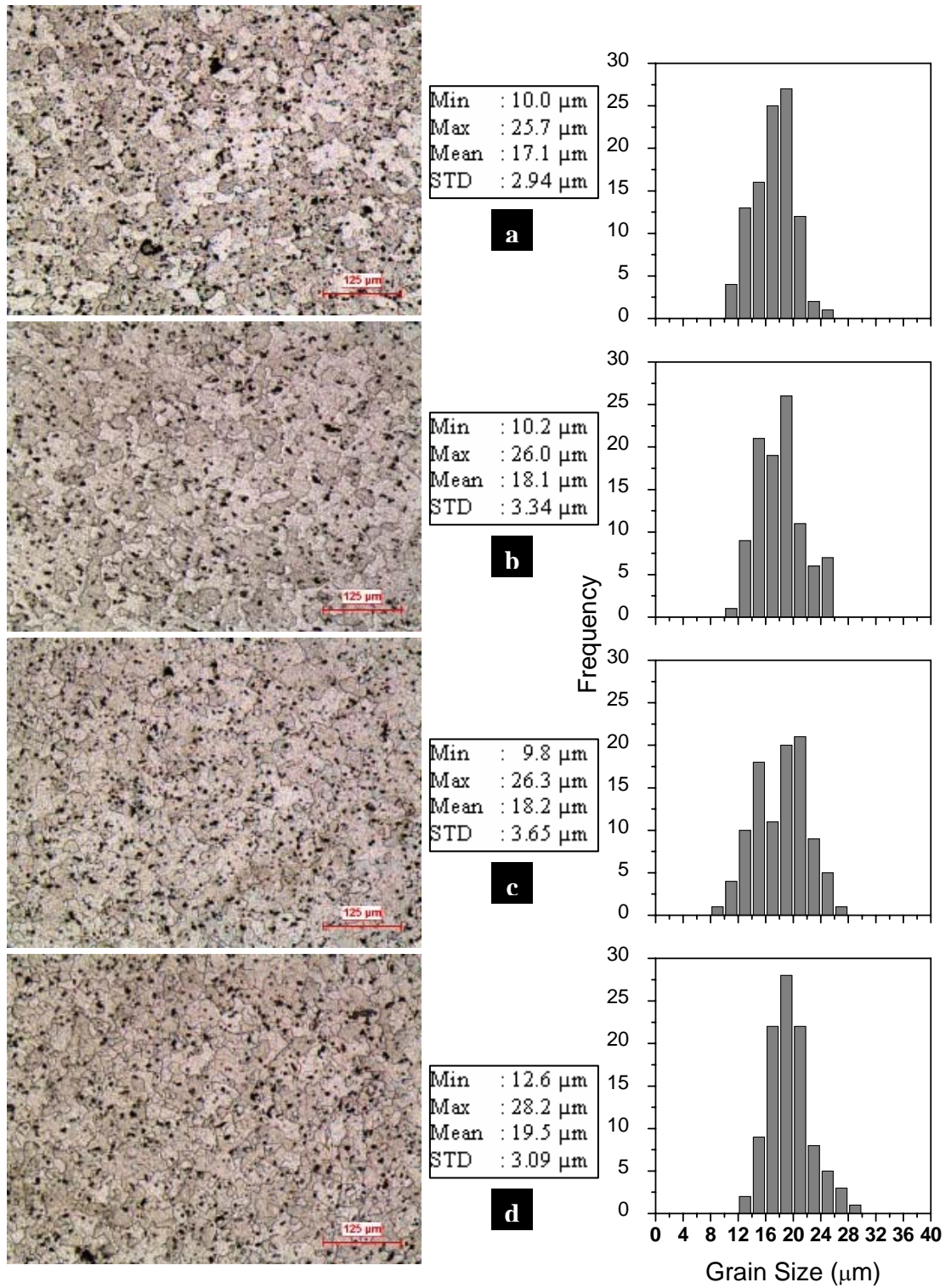
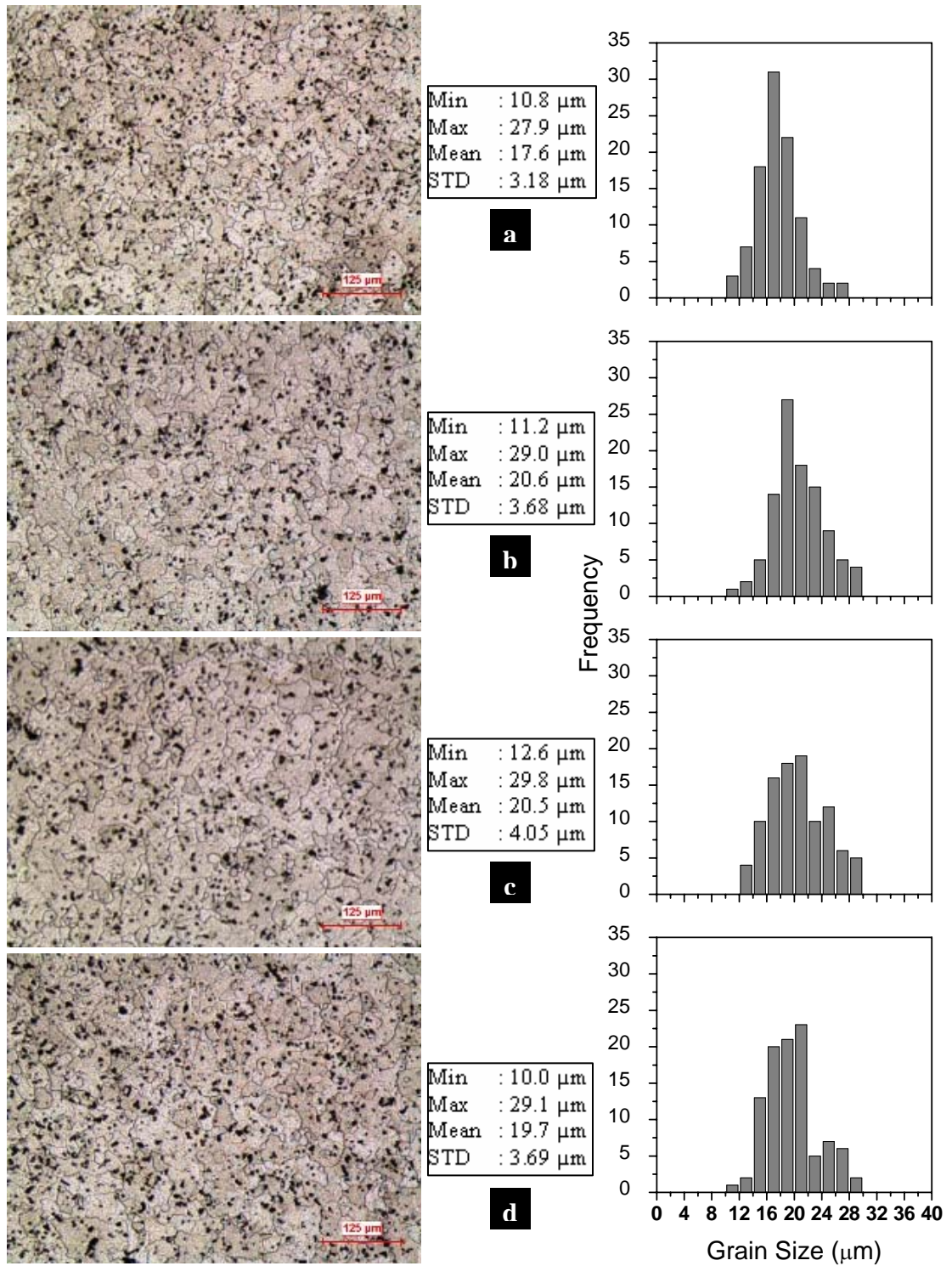


Figure 4.22 Optic micrographs after solutionizing at 530°C and the corresponding grain size distributions; TD sections obtained from the specimens a)10% b)20% c)30% d)40% cold deformed



**Figure 4.23** Optic micrographs after solutionizing at 530°C and the corresponding grain size distributions; TD sections obtained from the specimens a)10% b)20% c)30% d)40% deformed at 200°C



**Figure 4.24** Optic micrographs after solutionizing at 530°C and the corresponding grain size distributions; TD sections obtained from the specimens a)10% b)20% c)30% d)40% deformed at 300°C

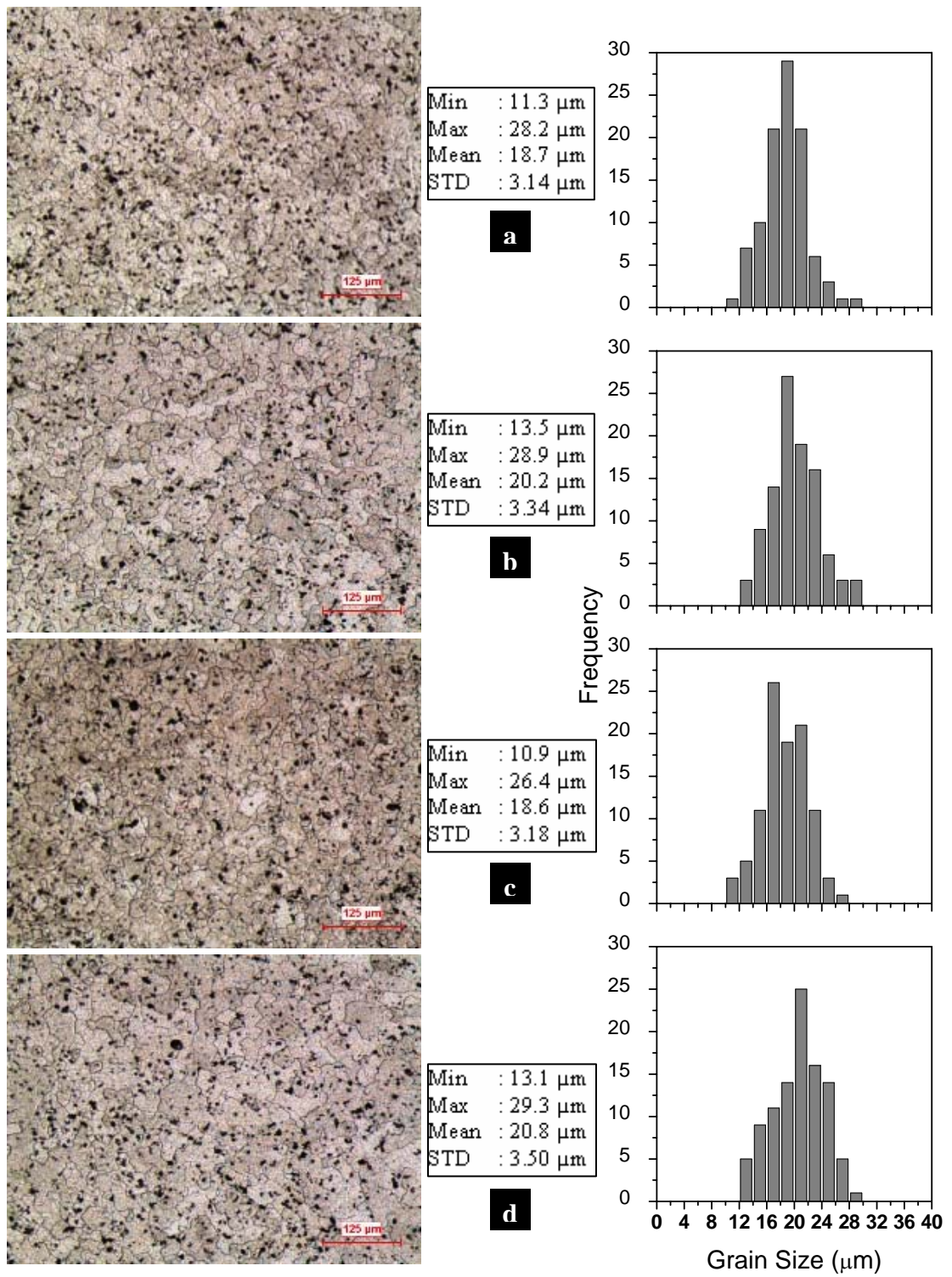


**Figure 4.25** Optic micrographs after solutionizing at 530°C and the corresponding grain size distributions; TD sections obtained from the specimens a)10% b)20% c)30% d)40% deformed at 400°C

**Table 4.5 The effect of deformation route on grain size**

<i>Deformation</i>		<i>Grain Size (<math>\mu\text{m}</math>)</i>			
		<i>TD</i>		<i>LD</i>	
NON		11.4	$\pm$ 2.49	18	$\pm$ 4.77
RT	10%	20.4	$\pm$ 4.80	26.7	$\pm$ 7.02
	20%	18.0	$\pm$ 4.06	25.3	$\pm$ 6.60
	30%	17.7	$\pm$ 3.38	22.2	$\pm$ 4.37
	40%	16.9	$\pm$ 4.11	20.5	$\pm$ 4.72
200°C	10%	17.1	$\pm$ 2.94		
	20%	18.1	$\pm$ 3.34		
	30%	18.2	$\pm$ 3.65		
	40%	19.5	$\pm$ 3.09		
300°C	10%	17.6	$\pm$ 3.18		
	20%	20.6	$\pm$ 3.68		
	30%	20.5	$\pm$ 4.05		
	40%	19.7	$\pm$ 3.69		
400°C	10%	18.7	$\pm$ 3.14		
	20%	20.2	$\pm$ 3.34		
	30%	20.6	$\pm$ 3.82		
	40%	20.8	$\pm$ 3.50		

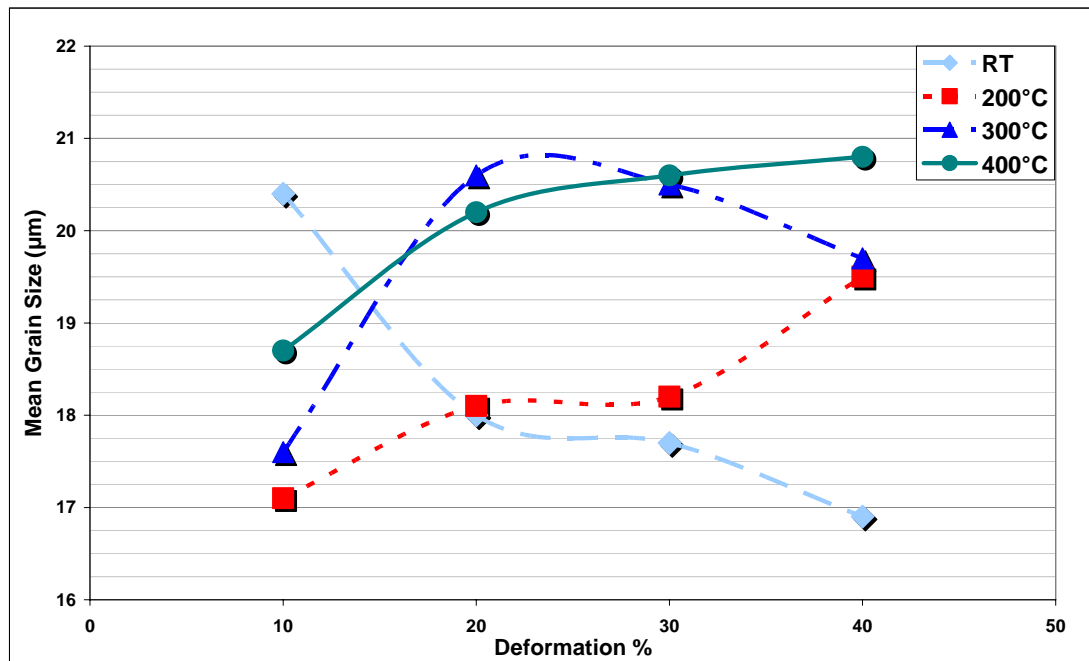


**Figure 4.26 Variation of grain size of TD sections obtained from hot deformed specimens prior to soln and aging (All specimens are aged at 175°C for 8h)**

The effect of recrystallization was easily observed from grain sizes of cold deformed specimens at LD sections. After solutionizing, 10% cold deformed sample yielded a grain size in the order of  $26.7 \pm 7.02 \mu\text{m}$ . On the other hand, an average grain size of  $20.5 \pm 4.72 \mu\text{m}$  was found for the 40% deformed one. It is common that; deformation leads energy storage in the form of lattice defect creation, i.e. dislocations. During solutionizing at temperatures of  $530^\circ\text{C}$ ; the cold-deformed specimens were recrystallized. As a result, the higher strain energy stored specimens would yield a finer grain size.

On the other hand according to the line chart of TD sections, it could be seen that the grain sizes were all in the range of  $17 - 21 \mu\text{m}$ . When the STD values were concerned, it would be difficult to indicate a change in grain size.

### **4.3.2. Effect of Deformation on Mechanical Properties**

#### **4.3.2.1. Tensile Testing**

In the previous section the optimum solutionizing and aging treatment temperatures were selected as  $530^\circ\text{C}$  and  $175^\circ\text{C}$  respectively. An ultimate tensile strength of 470 MPa and a hardness of 140 HB was reached after this heat treatment. Microstructural changes due to different deformation cycles would possibly affect the tensile strength and hardness values. As mentioned previously, several specimens were hot or cold deformed prior to a solutionizing and aging treatment. The amount of deformation was given as 10%, 20%, 30% or 40%. The deformation treatments were carried out at either room temperature,  $200^\circ\text{C}$ ,  $300^\circ\text{C}$  or  $400^\circ\text{C}$ . The effect of various treatment cycles on mechanical properties were given in Table 4.6. The variation of tensile strength and yield strength of the 6066 alloy with deformation temperature and deformation amount could be seen from the plots in Figure 4.27 and Figure 4.28. All the values presented were related to the final product properties namely the properties of deformed + solutionized + 8 hours-aged specimens.

**Table 4.6 Tensile test results for aged specimens subjected to various deformation routes**

<i>Deformation Status</i>	<i>UTS (MPa)</i>	<i>Yield (MPa)</i>	<i>% EL</i>
NON	470	450	9.2
10% RT	376	295	12.5
20% RT	380	298	12.3
30% RT	383	300	14.5
40% RT	418	319	11.2
10% 200°C	431	336	9.9
20% 200°C	375	285	12.5
30% 200°C	373	283	12.8
40% 200°C	363	255	14.3
10% 300°C	434	352	13.0
20% 300°C	364	245	16.5
30% 300°C	361	240	12.3
40% 300°C	403	296	17.7
10% 400°C	443	335	11.0
20% 400°C	414	309	10.1
30% 400°C	370	276	13.5
40% 400°C	350	230	15.0

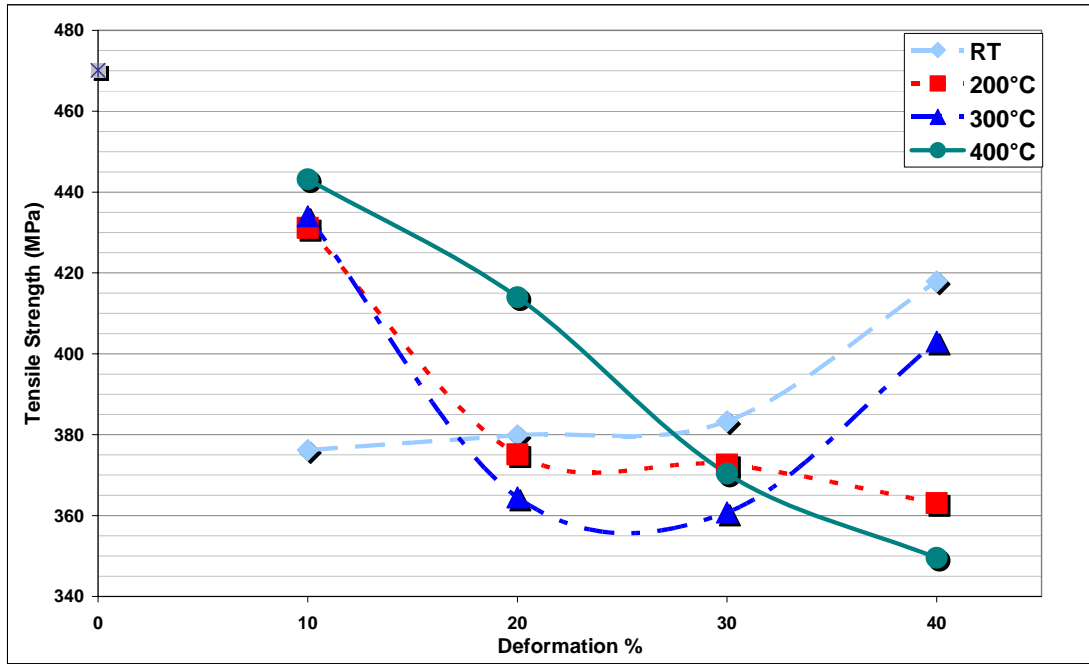


Figure 4.27 Change of tensile strength of hot deformed specimens prior to soln and aging (All specimens are aged at 175°C for 8h)

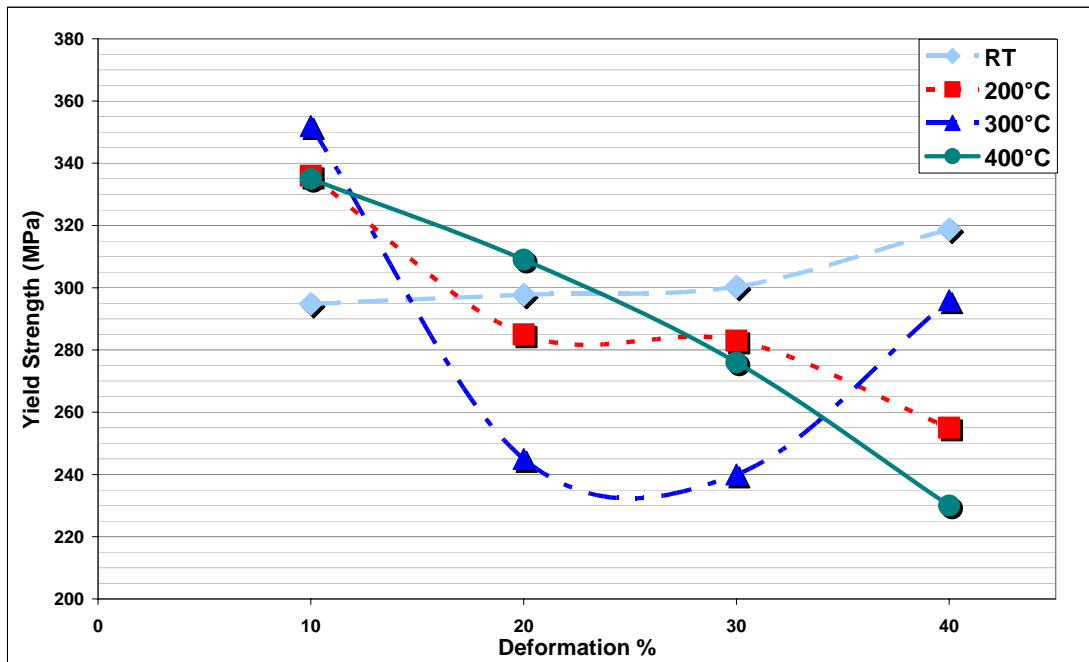


Figure 4.28 Change of yield strength of hot deformed specimens prior to soln and aging (0.2% offset) (All specimens are aged at 175°C for 8h)

When the plots given in Figure 4.27 and Figure 4.28 are examined it is seen that a deformation process prior to solutionizing causes an overall decrease in strength values attained. The tensile strength was decreased from 460 MPa (no deformation) to 418 MPa upon 40% cold deformation and 350 MPa upon 40% deformation at 400°C. Same trend was observed in the yield strengths. Yield strength of 450 MPa was obtained after peak-aging of the as-received alloy; whereas the yield strength of the 40% hot-worked and peak-aged specimen was only 230 MPa. On the other hand percent elongation increased from 9.2% to 15% upon hot-deformation.

For the specimens deformed at room temperature; the trend was an increase in strength with an increase in deformation percent; whereas the tendency was vice versa for hot deformations. As seen from figures; the strength loss was maximized for treatments at high temperatures and higher percent reductions, as in the case of 40% deformation at 400°C yielding a tensile strength of only 349 MPa.

The reason for deterioration of properties was most probably due to the destruction of the as-received (hot-extruded) microstructure during deformation and heat treatment. A detailed discussion will be made in the following sections.

#### 4.3.2.2. Hardness Measurements

After deformation and solutionizing, specimens were artificially aged at 175°C (the ideal temperature) for 4, 6, 8, 10 and 12 hour. The effect of deformation on the aging response was examined by hardness testing of these specimens. The values were tabulated in Table A. 4 at appendix; and the results were summarized in Table 4.7 to Table 4.10. The effect of deformation temperature on hardness curves were shown in Figure 4.29 - Figure 4.32. In these plots, the aging curve of non-deformed sample was also presented for comparison purposes.

**Table 4.7 Effect of 10% deformation on hardness of alloy**

<i>Process</i>			<i>Brinell Hardness</i>		
<i>Deformation %</i>	<i>Temp</i>	<i>Age Time</i>			
10%	RT	Deformed	73	±	1.17
		Solutionized	84	±	1.04
		8 h	139	±	1.15
	200	Deformed	71	±	0.26
		Solutionized	90	±	0.58
		8 h	140	±	0.58
	300	Deformed	60	±	0.42
		Solutionized	83	±	1.48
		8 h	141	±	0.58
	400	Deformed	66	±	0.75
		Solutionized	87	±	1.19
		8 h	134	±	1.00

**Table 4.8 Effect of 20% deformation on hardness of alloy**

<i>Process</i>			<i>Brinell Hardness</i>		
<i>Deformation %</i>	<i>Temp</i>	<i>Age Time</i>			
20%	RT	Deformed	79	±	0.44
		Solutionized	82	±	2.10
		8 h	133	±	1.00
	200	Deformed	78	±	0.66
		Solutionized	82	±	1.55
		8 h	137	±	1.73
	300	Deformed	65	±	0.40
		Solutionized	83	±	1.00
		8 h	130	±	0.58
	400	Deformed	69	±	0.85
		Solutionized	85	±	1.33
		8 h	134	±	2.89

**Table 4.9 Effect of 30% deformation on hardness of alloy**

		<i>Process</i>		<i>Brinell Hardness</i>		
<i>Deformation %</i>	<i>Temp</i>	<i>Age Time</i>				
30%	RT	Deformed		82	±	0.26
		Solutionized		85	±	0.91
		8 h		135	±	0.00
	200	Deformed		75	±	0.75
		Solutionized		87	±	0.53
		8 h		134	±	3.21
	300	Deformed		63	±	0.46
		Solutionized		81	±	1.37
		8 h		130	±	1.15
	400	Deformed		66	±	0.93
		Solutionized		79	±	0.87
		8 h		134	±	1.15

**Table 4.10 Effect of 40% deformation on hardness of alloy**

		<i>Process</i>		<i>Brinell Hardness</i>		
<i>Deformation %</i>	<i>Temp</i>	<i>Age Time</i>				
40%	RT	Deformed		80	±	2.51
		Solutionized		83	±	0.40
		8 h		139	±	0.00
	200	Deformed		78	±	0.52
		Solutionized		78	±	0.80
		8 h		134	±	1.15
	300	Deformed		63	±	0.79
		Solutionized		77	±	2.25
		8 h		131	±	0.58
	400	Deformed		64	±	0.25
		Solutionized		85	±	0.49
		8 h		140	±	1.73

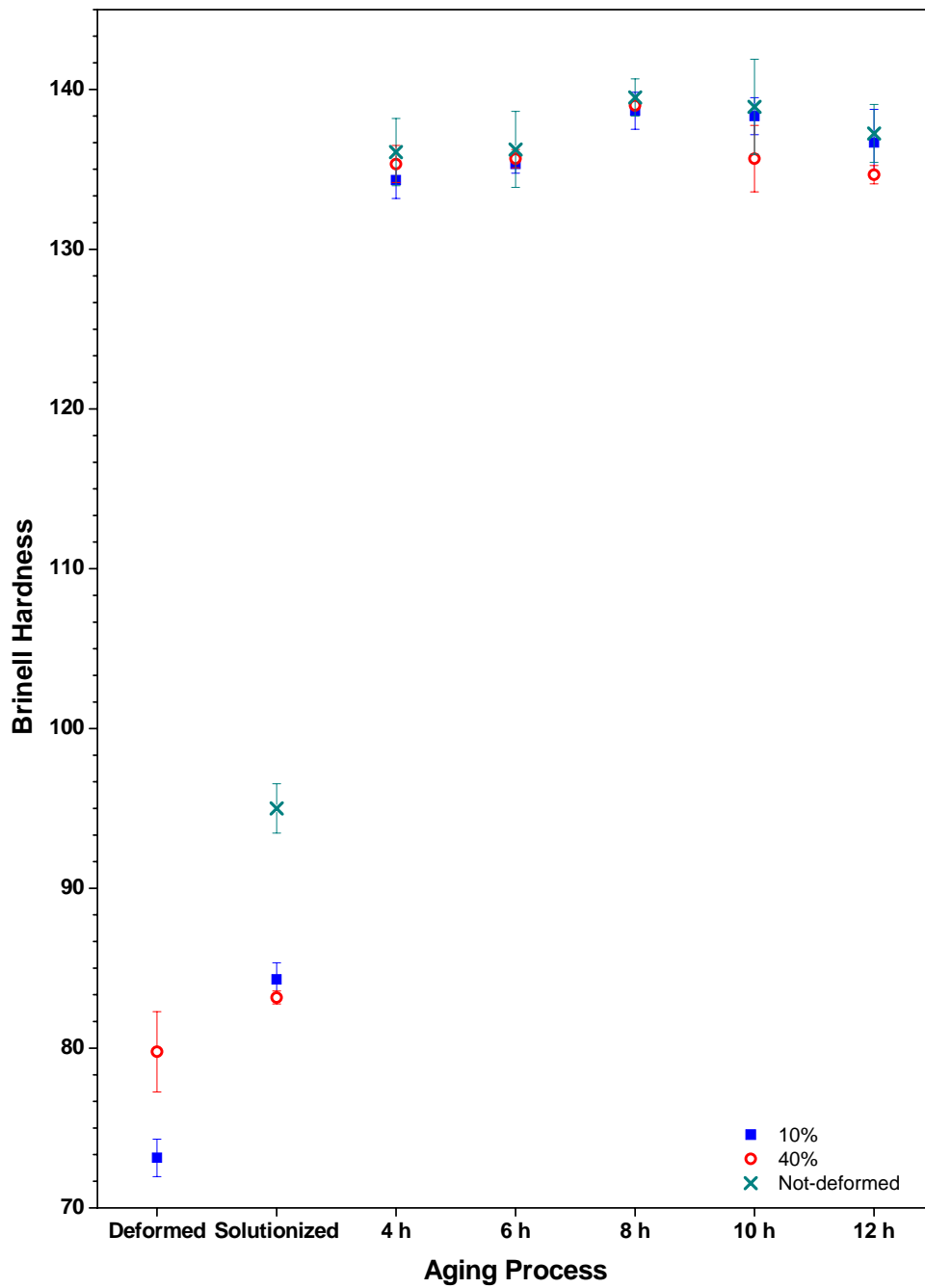


Figure 4.29 Effect of cold deformation with various %deformation on hardness

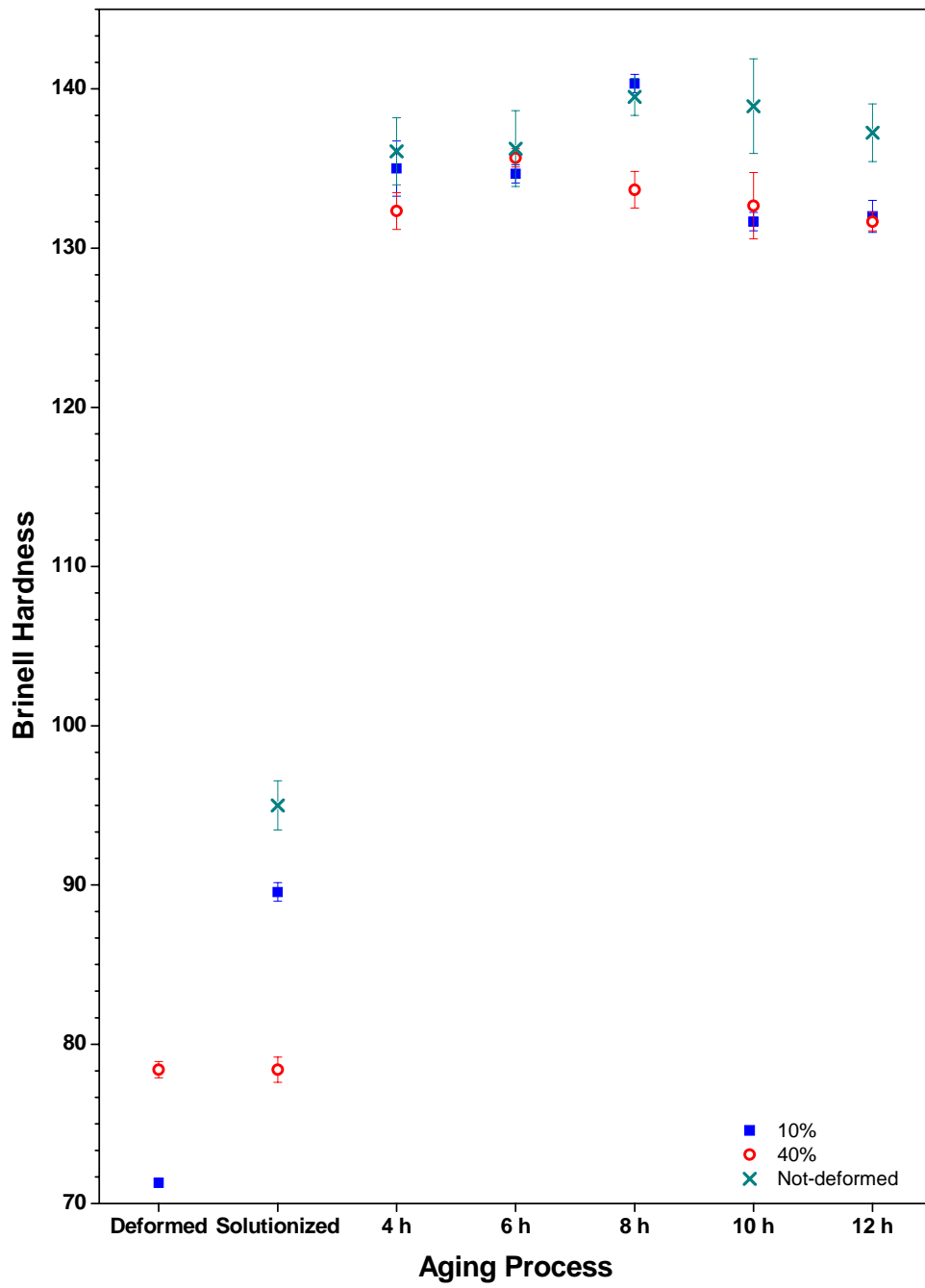


Figure 4.30 Effect of deformation at 200°C with various %deformation on hardness

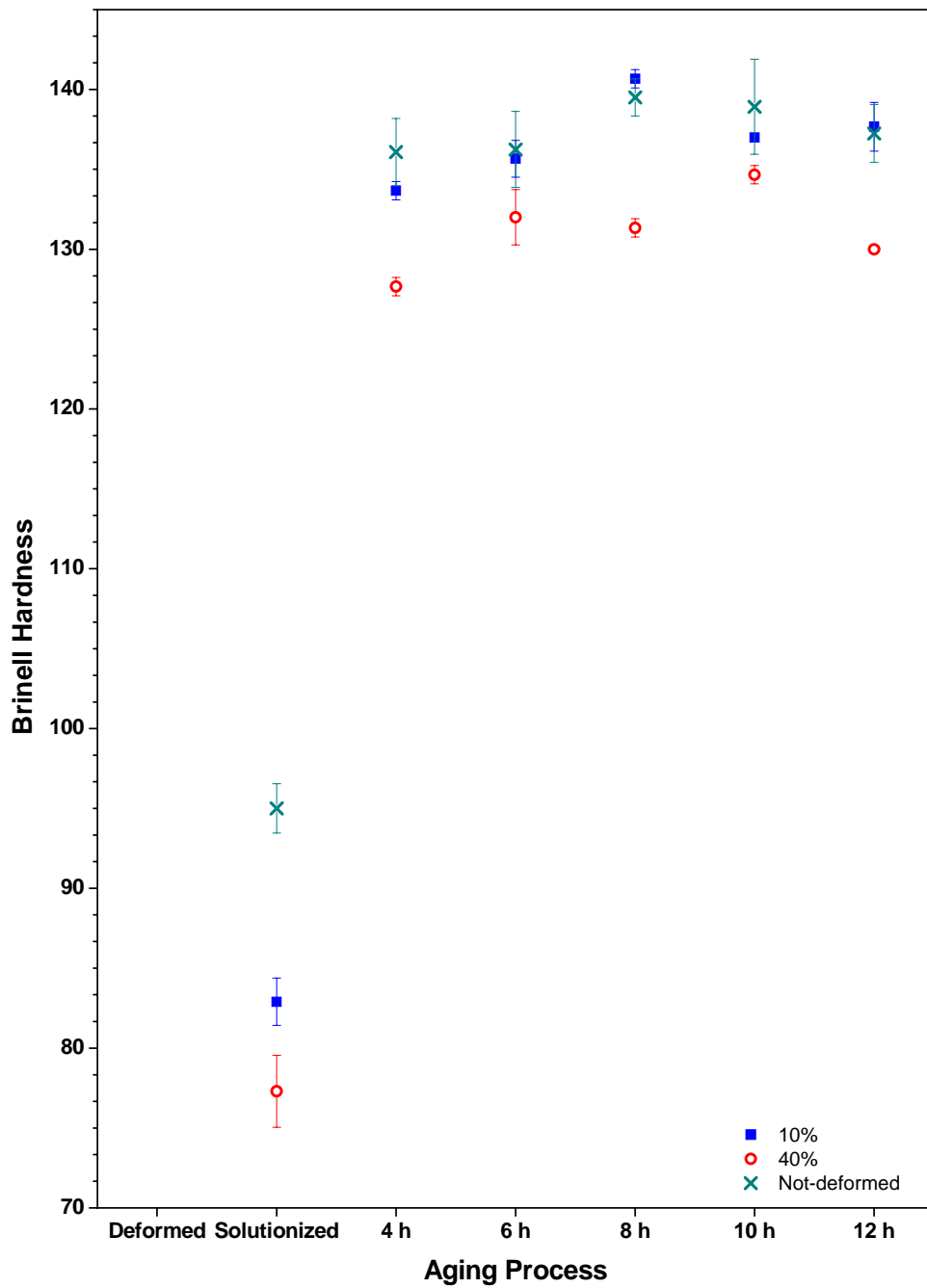


Figure 4.31 Effect of deformation at 300°C with various %deformation on hardness

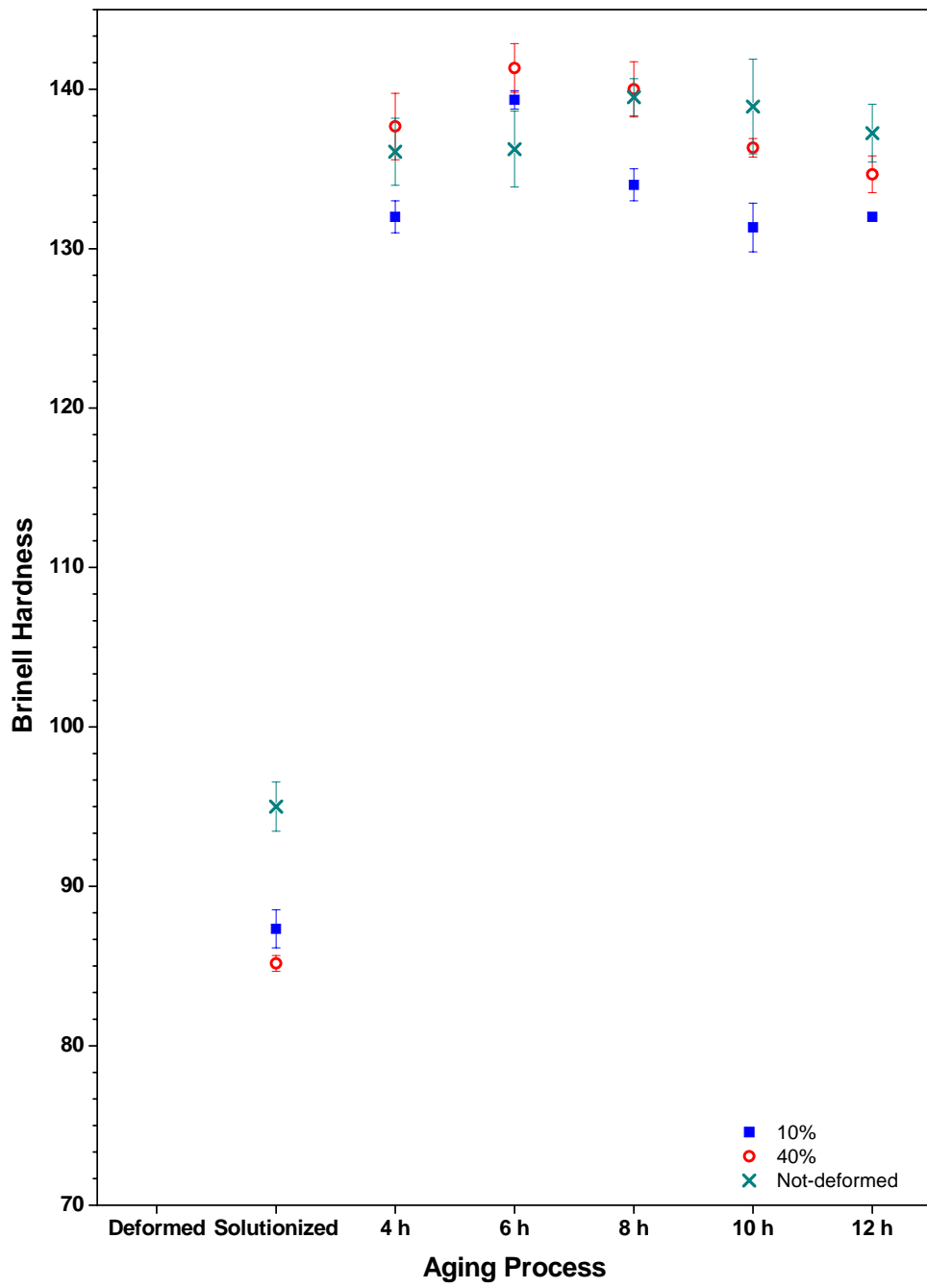


Figure 4.32 Effect of deformation at 400°C with various %deformation on hardness

As far as the hardness curves are compared, it is seen that the peak hardness is attained at 175°C after aging 8 hours. After a deformation process, aging 6 hours was enough for most of the sets; overaging afterwards. This was most probably due to the presence of dislocations remained in the matrix after solutionizing; which were most likely to serve as nucleation sites for precipitates enhancing the rate.

It was observed that; when deformation was applied, an 8 hr aging caused overaging. When deformation was carried out after solutionizing; the overaging became more detrimental after 8 hours (Table 4.11) due to the increased precipitation rate.

**Table 4.11 Effect of deformation's order in the whole sequence**

<i>Solutionizing</i>	<i>10% Deformation</i>	<i>Solutionizing</i>	<i>Aging</i>	<i>Hardness after 4h</i>	<i>Hardness after 8h</i>
		√	√	136	140
	√	√	√	134	139
√	√		√	135	132

#### **4.4. An Overview of Results**

It seems that there is a relation between mechanical properties and microstructures. Besides the microstructural features; it is known that the average grain size in a metal had an effect on mechanical properties by famous Hall-Patch relation. Due to higher grain boundary area; a fine-grained material would be harder and stronger than the coarse grained ones. According to the relation the strength of a metal is proportional to the inverse square-root of grain diameter. But for the precipitation strengthening alloys (like the one in this case), size, shape and distribution of features contribute to the strengthening by pinning dislocation motion.

$$\sigma = \sigma_{\text{due to GB}} + \sigma_{\text{due to intermetallics}} + \sigma_{\text{due to precipitates}}$$

**Table 4.12 Variation of mechanical properties and grain sizes with deformation**

<i>Deformation Status</i>	<i>UTS</i> <sup>†</sup> <i>(MPa)</i>	<i>Yield</i> <sup>†</sup> <i>(MPa)</i>	<i>% EL</i> <sup>†</sup>	<i>Hardness</i> <sup>†</sup> <i>HB</i>	<i>Average Grain Size (TD)(<math>\mu\text{m}</math>)</i> <sup>‡</sup>
NON	470	450	9.2	140	11.4 ± 2.49
10% RT	376	295	12.5	139	20.4 ± 4.80
20% RT	379	298	12.3	133	18.0 ± 4.06
30% RT	383	300	14.5	135	17.7 ± 3.38
40% RT	418	319	11.2	139	16.9 ± 4.11
10% 200°C	431	336	9.9	140	17.1 ± 2.94
20% 200°C	375	285	12.5	137	18.1 ± 3.34
30% 200°C	372	283	12.8	134	18.2 ± 3.65
40% 200°C	363	255	14.3	134	19.5 ± 3.09
10% 300°C	434	352	13.0	141	17.6 ± 3.18
20% 300°C	364	245	16.5	130	20.6 ± 3.68
30% 300°C	360	240	12.3	130	20.5 ± 4.05
40% 300°C	403	296	17.7	131	19.7 ± 3.69
10% 400°C	443	335	11.0	134	18.7 ± 3.14
20% 400°C	414	309	10.1	134	20.2 ± 3.34
30% 400°C	370	276	13.5	134	20.6 ± 3.82
40% 400°C	349	230	15.0	140	20.8 ± 3.50

The mechanical data and microstructural results were summarized in Table 4.12. It was explained above that strengthening was achieved by creating obstacles to dislocation motion. Leaving the solid solution strengthening, which was applicable in the as-solutionized state, to a side; grain size and precipitation hardening must be considered for strengthening. When Table 4.12 was investigated; a variation of mechanical properties and grain sizes with deformation were observed. However, as discussed previously; the change in the grain sizes was too small for compensating

<sup>†</sup> Values corresponds to the data obtained after deformation + solutionizing + quenching + 8h-aging

<sup>‡</sup> Values corresponds to the data obtained after deformation + solutionizing + quenching

the big change in strength. Actually, the little grain size dependence of flow stress, namely the lower efficiency in Hall-Patch relation, was emphasized by many authors like Embury [44]. According to Bratland [45], the grain and sub-grain structures had a secondary influence on strength; and they might influence other properties such as fracture and corrosion. So precipitation hardening would be the operative mechanism for aluminum alloys.

At that time the nature of point obstacles (precipitates and coarse intermetallics) and the dislocation-obstacle interactions would be effective. Number density of obstacles, mean free path between obstacles and strength of each obstacle became the parameters affecting the strength. However, the number densities of obstacles and the obstacle – dislocation interaction have been forced to change by the continuum deformation and aging processes. Crushing of intermetallics, creation of strain energies as new dislocations during deformation and the mechanism change from precipitate cutting to Orowan looping during aging gather attention. Concerning these fundamentals; the effect of deformation on the strength would be discussed below for cold and hot deformations separately.

#### Cold deformation

For the cold shaping process; the strength loss was decreased by increasing the percent deformation. A tensile strength of 376 MPa was obtained after a 10% cold work; whereas the tensile strength of the 40% cold worked specimen increased to 418 MPa. One reason can be the increase of stored elastic energy in the form of dislocations with deformation percent increase. Recrystallization was most likely enhanced by this stored energy during solutionizing step which was carried afterwards. Also; the remaining dislocation density might increase dislocation-dislocation interactions; most probably leading to an increase of strength with percent deformation.

#### Hot deformation

For the hot shaping process; much lower tensile strength values were obtained and the strength loss increased with an increase in percent deformation. A tensile strength

of 431 MPa was obtained after a 10% hot work at 200°C; whereas the tensile strength of the 40% hot worked specimen decreased to 363 MPa. The decrease in strength was much higher as deformation temperature was increased. The tensile strength was decreased to 349 MPa after a 40% hot work at 400°C. The strength loss was more pronounced for the specimens directly aged without being deformed. A tensile strength of 470 MPa and a yield strength of 450 MPa was obtained for this type of specimens.

It is possible that precipitation of a phase during hot-deformation process can lead to deterioration of the properties. It was thought that the precipitation in the form of coarse equilibrium precipitates was the consequence of the fact; by decreasing the amount of solute available for the continuing solutionizing and precipitation hardening. As discussed above, the coarser the precipitate size; the less the strength (hardness) would be obtained. Table 4.13 shows the as-deformed hardness ranges for deformation processes. It could be seen that, hardness was in the range of 73–80 HB in the RT deformed specimens. On the other hand it was in the range of 64–69 HB in the specimens deformed at 400°C. This drop in the hardness was most probably due to the fact suggested above.

**Table 4.13 Brinell hardness ranges obtained after various deformations**

<i>Deformation Temperature</i>	<i>Brinell Hardness</i>
RT	73–80
200°C	71-78
400°C	64–69

In order to clarify the detrimental effect of heating time prior to deformation; a set of samples were heated to the temperature of deformation and air cooled to room temperature without being deformed. The results were tabulated in Table 4.14. As

discussed above; hardness was decreased most probably due to formation of coarse precipitates during heating.

**Table 4.14 Effect of heating to deformation and air-cooling on hardness**

<i>Heat &amp; Air Cooled</i>	<i>Brinell Hardness</i>
-	60 ± 0.85
200°C	66 ± 1.39
300°C	57 ± 0.25
400°C	55 ± 0.61

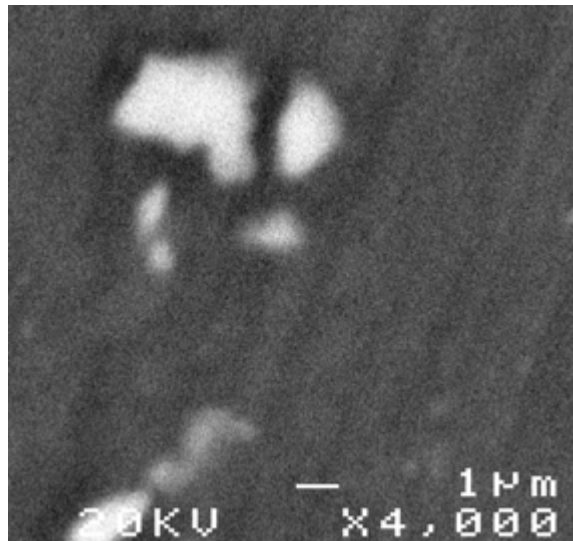


**Figure 4.33 Back-scatter SEM image of complex intermetallic broken during deformation**

Another possibility for the strength loss might be due to the complex intermetallics, which were formed during solidification from the cast. It was found that the iron bearing complex intermetallics crack during deformation. These irregular shaped phases (Figure 4.33) have been shown to be the nucleation sites of voids during high temperature deformation [46]. For hot deformation cases; a decrease in strength was observed with an increase in percent deformation. Hence; the presence of

intermetallics in the structure was most probably the explanation of this fact. The more intermetallics broken down to finer sized particles with an increase of deformation percent would probably cause more microvoid formation during the deformation.

Throughout the study it was observed that; a deformation process, whether cold or hot, found detrimental to the mechanical properties. For precipitation hardened materials, this phenomenon was generally related to the lower number density of precipitates [43,45]. The increased dislocation density; in the deformed cases was most likely responsible for this lower precipitate number density in such a way. In a study with the introduction of deformation, defects were created which might not be removed completely during solutionizing [37]. The remaining defects (dislocations) were presumably served as the nucleation sites for the precipitates leading to an increase in diffusion rate and heterogeneous nucleation. Therefore precipitation rate was increased leading to a decrease in precipitation temperature. Hence; coarse precipitates and reduced number density was obtained by applying same aging time-temperature as the non-deformed ones [37-46]. Actually this overaging phenomenon could also be observed in this study, as far as the hardness curves of deformed specimens are concerned. The peak hardness could be attained in 4-6 hours in the deformed specimens; whereas peak hardness was shifted to 8 hour aging for non-deformed specimens.

The processes and resulting microstructural evolution during thermomechanical treatment of 6000 series aluminum alloys were schematically summarized in Figure 4.34 which indicates the effect of nucleation sites on the final properties. The amounts of Mg, Si, and Cu in solid solution were important for final properties but an unknown fraction might be tied up in the form of different phases (Fe-Mn containing intermetallics and coarse  $Mg_2Si$  particles) which were present in the matrix. These were believed to be the sites for non hardening  $\beta'$  formation during the time passed for air cooling from deformation temperature. This might lead to a loss in solute content in the matrix and eventually to a reduced strength in the aged condition. [45]

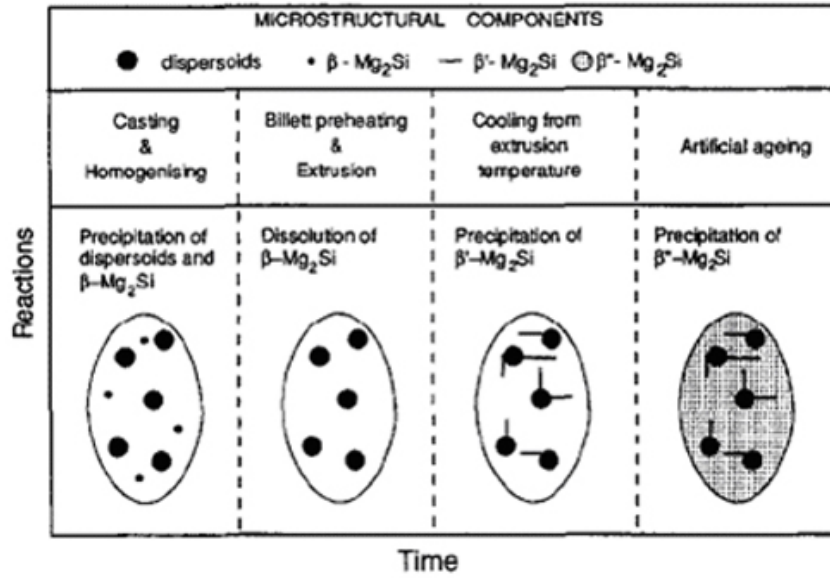


Figure 4.34 Evolution of microstructure during thermo-mechanical treatment of 6xxx [28]

Consequently; although hardness values and some UTS values were in the range of standards; none of the deformation schedules were succeeded for meeting the yield strength requirements of Aluminum Association (given in Table 3.2).

Table 4.15 Summary of yield and tensile strength values obtained in the study

Deformation Status <sup>§</sup>		10%	20%	30%	40%
RT	$\sigma_{\text{uts}}$	376	379	383	418
	$\sigma_{\text{y}}$	295	298	300	319
200°C	$\sigma_{\text{uts}}$	431	375	372	363
	$\sigma_{\text{y}}$	336	285	283	255
300°C	$\sigma_{\text{uts}}$	434	364	360	403
	$\sigma_{\text{y}}$	352	245	240	296
400°C	$\sigma_{\text{uts}}$	443	414	370	349
	$\sigma_{\text{y}}$	335	309	276	230

<sup>§</sup> The shaded values were the ones which meets the specification

## CHAPTER 5

### CONCLUSION

In this study; the effect of deformation on mechanical properties of 6066 aluminum alloy was investigated. In view of the results obtained, the following conclusions can be withdrawn;

- ✓ The microstructure of 6066 aluminum alloy contains  $Mg_2Si$  and  $(Fe,Mn,Cu)_3SiAl_{12}$  complex intermetallic particles. These particles are distributed homogeneously in an aluminum matrix.
- ✓ The ideal solutionizing temperature was found as  $530^{\circ}C$ . Below  $530^{\circ}C$ ; there was an increase in the hardness with an increase in soaking time; whereas the trend was vice versa for higher temperatures.
- ✓ Aging trials between  $150 - 200^{\circ}C$  showed that; a peak hardness of 140HB was reached after an aging treatment at  $175^{\circ}C$  for 8 hours. The hardness attained was considerably higher than specified by Aluminum Association, which was given as 120HB.
- ✓ The swaged and peak-aged specimens had lower mechanical properties as compared to the non-deformed and peak-aged ones. This was most probably due to destruction of initial as-received microstructure of the alloy.
- ✓ Recrystallization temperature for the alloy after a cold deformation of 40% was found to be in the order of  $450^{\circ}C$ .
- ✓ If a cold working operation is applied prior to solutionizing; as deformation percent is increased from 10% to 40%; the final strength of the solutionized and aged alloy increased from 376 MPa to 418 MPa. However, at all cold working levels, the strength values attained were lower than non-deformed samples.

- ✓ If a hot-deformation operation is applied prior to solutionizing at 400°C; as deformation percent is increased from 10% to 40%; the final strength of the solutionized and aged alloy decreased from 443 MPa to 349 MPa. The same trend is observed for lower reduction ratios, but a lower extent.

## REFERENCES

- 1** Altenpohl, Dietrich G., “Aluminum: Technology, Applications and Environment”, Aluminum Association, 1999
- 2** Van Horn K. R., “Aluminum, Vol I. Properties, Physical Metallurgy and Phase Diagrams”, American Society for Metals, 1968
- 3** ASM Specialty Handbook, “Aluminum and Aluminum Alloys”, Materials Information Society, 1996
- 4** ASM Handbook, “Heat Treating of Aluminum Alloys, Vol 4”, ASM International, 1991
- 5** Starke Jr E.A.; “Encyclopedia of Materials: Science and Technology; Aluminum Alloys: Thermal Treatments”; Elsevier Science Ltd.; 116-118; 2001
- 6** Staab T.E.M., Krause-Rehberg R., Hornauer U., Zschech E.; “Study of Artificial Aging in AlMgSi (6061) and AlMgSiCu (6013) Alloys by Positron Annihilation”; Journal of Materials Science; 41; 1059-1066; 2006
- 7** Troeger L.P., Starke E.F.; “Microstructural and Mechanical Characterization of a Superplastic 6xxx Aluminum Alloy”; Materials Science and Engineering A; A277; 102-113; 2000
- 8** Dorward R.C., Bouvier C.; “A Rationalization of Factors Affecting Strength, Ductility and Toughness of AA6061-type Al-Mg-Si-(Cu) Alloys”; Materials Science and Engineering A; A254; 33-44; 1998
- 9** Hirth S.M., Marshall G.J., Court S.A., Lloyd D.J.; “Effect of Si on the Aging Behavior and Formability of Aluminum Alloys Based on AA6016”; Materials Science and Engineering A; A319-321; 452-456; 2001
- 10** Gupta A.K., Lloyd D.J., Court S.A.; “Precipitation Hardening in Al-Mg-Si Alloys with and without Excess Si”; Materials Science and Engineering A; A316; 11-17; 2001
- 11** Matsuda K., Teguri D., Uetani Y., Sato T., Ikeno S; “Cu-segregation at the Q'/ $\alpha$ -Al Interface in Al-Mg-Si-Cu Alloys”; Scripta Materialia; 47; 833-837; 2002

- 12** Miao W.F., Laughlin D.E.; “Effect of Cu Content and Preaging on Precipitation Characteristics in Aluminum Alloy 6022”; Metallurgical and Materials Transactions A; 31A; 361-371; 2000
- 13** Hsu C., O’Reilly K.A.Q., Cantor B., Hamerton R.; “Non-equilibrium Reactions in 6xxx Series Al Alloys”; Material Science and Engineering A; A304-306; 119-124; 2001
- 14** Sha G., O’Reilly K., Cantor B., Worth J., Hamerton R.; “Growth Related Metastable Phase Selection in 6xxx Series Wrought Aluminum Alloy”; Materials Science and Engineering A; A304-306; 612-616; 2001
- 15** Liu Y.L., Kang S.B., Kim H.W.; “The complex microstructures in As-Cast Al-Mg-Si Alloy”; Materials Letters; 41; 267-272; 1999
- 16** Avner S.H.; “Introduction to Physical Metallurgy”; McGraw Hill; 1974
- 17** Chackrabarti D.J., Laughlin D.E.; “Phase Relation and Precipitation in Al-Mg-Si Alloys with Cu Additions”; Progress in Materials Science; 49; 389-410; 2004
- 18** Gupta A.K., Lloyd D.J., Court S.A.; “Precipitation Hardening Process in an Al-0.4%Mg-1.3%Si-0.25%Fe Aluminum Alloy”; Materials Science and Engineering; A301; 140-146; 2001
- 19** Matsuda K., Sakaguchi Y., Miyata Y., Uteni Y., Sato T., Kamio A. Ikeno S.; “Precipitation Sequence of Various Kinds of Metastable Phases in Al-1.0mass%Mg2Si-0.4mass%Si Alloy”; Journal of Materials Science; 35; 179-189; 2000
- 20** Murayama M., Hono K.; “Pre-precipitate Clusters and Precipitation Process in Al-Mg-Si Alloys”; Acta Materialia; 47-5; 1537-1548; 1999
- 21** Murayama M., Hono K., Miao W.F., Laughlin D.E.; “The Effect of Cu Additions on the Precipitation Kinetics in an Al-Mg-Si Alloy with Excess Si”; Metallurgical and Materials Transactions A; 32A; 239-246; 2001
- 22** Matsuda K., Uetani Y., Sato T., Ikeno S.; “Metastable Phases in an Al-Mg-Si Alloy Containing Copper”; Metallurgical and Materials Transactions A; 32A; 1293-1299; 2001
- 23** Chakrabarti D.J., Peng Y.G., Laughlin D.E.; “Precipitation in Al-Mg-Si Alloys with Cu Additions and the Role of the Q’ and Related Phases”; Materials Science Forum; 396-4; 857-862; 2002
- 24** Ravi C., Wolverton C.; “First Principles Study of Crystal Structure and Stability of Al-Mg-Si-(Cu) Precipitates”; Acta Materialia; 52; 4213-4227; 2004

- 25** Munitz A., Cotler C., Talianker M.; “Aging Impact on Mechanical Properties and Microstructure of Al-6063”; *Journal of Materials Science*; 35; 2529-2538; 2000
- 26** Liu G., Zhang G.J., Ding X.D., Sun J., Chen K.H.; “Modeling the Strengthening Response to Aging Process of Heat Treatable Aluminum Alloys Containing Plate/Disc- or Rod/Needle-Shaped Precipitates”; *Materials Science and Engineering A*; A344; 113-124; 2003
- 27** Urreta S.E., Louchet F., Ghilarducci A.; “Fracture Behavior of an Al-Mg-Si Industrial Alloy”; *Materials Science and Engineering A*; A302; 300-307; 2001
- 28** Quainoo G.K., Yannacopoulos S.; “The Effect of Cold Work on the Precipitation Kinetics of AA6111 Aluminum”; *Journal of Materials Science*; 39; 6495-6502; 2004
- 29** Dutkiewicz J., Litynska L.; “The Effect of Plastic Deformation on Structure and Properties of Chosen 6000 Series Aluminum Alloys”; *Materials Science and Engineering A*; A324; 239-243; 2002
- 30** Karabay S., Yilmaz M., Zeren M.; “Investigation of Extrusion Ratio Effect on Mechanical Behavior of Extruded Alloy AA-6101 from the Billets Homogenized-Rapid Quenched and As-cast Conditions”; *Journal of Materials Processing Technology*; 160; 138-147; 2005
- 31** Cavazos J.L., Cola R.; “Precipitation in a heat-treatable Aluminum Alloy Cooled at Different Rates”; *Materials Characterization*; 47; 175-179; 2001
- 32** Verhoeven J.D.; “Fundamentals of Physical Metallurgy”; John Wiley & Sons; 1975
- 33** Hertzberg R.W.; “Deformation and Fracture Mechanics of Engineering Materials”; John Wiley & Sons; 1996
- 34** ASTM Standard, “E 8M Tension Testing of Metallic Materials”, 1993
- 35** Julabo Labortechnik, “Julabo Thermal H”, [http://www.julabo.de/Download/Julabo\\_Thermal\\_H\\_e.pdf](http://www.julabo.de/Download/Julabo_Thermal_H_e.pdf); “Last accessed date”: September 2006
- 36** ASTM Standard, “B557M Tension Testing Wrought and Cast Aluminum and Magnesium-Alloy Products”, 2002
- 37** Zhen L., Fei W.D., Kong S.B., Kim H.W.; “Precipitation Behavior of Al-Mg-Si Alloys with High Silicon Content”; *Journal of Materials Science*; 32; 1895-1902; 1997

- 38** Ber L.B.; “Accelerated Artificial Aging Regimes of Commercial Aluminum Alloys”; *Materials Science and Engineering A*; A280; 91-96; 2000
- 39** Singh R.K., Singh A.K., Prasad N.E.; “Texture and Mechanical Property Anisotropy in an Al-Mg-Si-Cu Alloy”; *Materials Science and Engineering A*; A277; 114-122; 2000
- 40** Singh R.K., Singh A.K.; “Evolution of Texture During Thermo-Mechanical Processing of an Al-Mg-Si-Cu Alloy”; *Scripta Materialia*; 38; 1299-1306; 1998
- 41** Lee Y., Kwon Y., Lee J., Park C., Kim S.; “Effects of Strain and Strain Rate on Tensile Behavior of Hot-Forged Al 6061-T6”; *Materials Science and Engineering A*; A362; 187-191; 2003
- 42** Park H., Lee D.N.; “Deformation and Annealing Textures of Drawn Al-Mg-Si Alloy Tubes”; *Journal of Materials Processing Technology*; 113; 551-555; 2001
- 43** Lillywhite S.J., Prangnell P.B., Humphreys F.J.; “Interactions Between Precipitation and Recrystallization in an Al-Mg-Si Alloy”; *Material Science and Technology*; 16; 1112-1120; 2000
- 44** Poole W.J., Lloyd D.J., Embury J.D.; “The Effect of Natural Aging on the Evolution of Yield Strength During Artificial Aging for Al-Mg-Si-Cu Alloys”; *Material Science and Engineering A*; A234-236; 306-309; 1997
- 45** Brathland D.H., Grong Ø., Shercliff H., Myhr O.R., Tjøtta S.; “Modelling of Precipitation Reactions in Industrial Processing”; *Acta Metallurgica*; 45; 1-22; 1997
- 46** Troeger L.P., Starke Jr E.A.; “Particle Stimulated Nucleation of Recrystallization for Grain-Size Control and Superplasticity in an Al-Mg-Si-Cu Alloy”; *Material Science and Technology A*; A293; 19-29; 2000

## APPENDIX

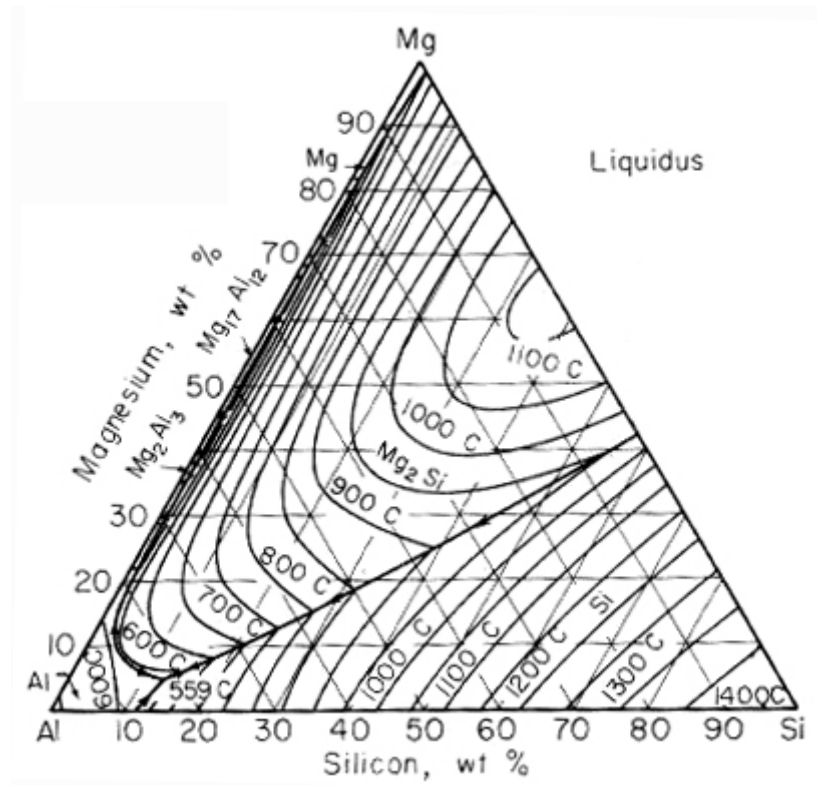


Figure A. 1 Al-Mg-Si phase diagram (liquidus) [2]

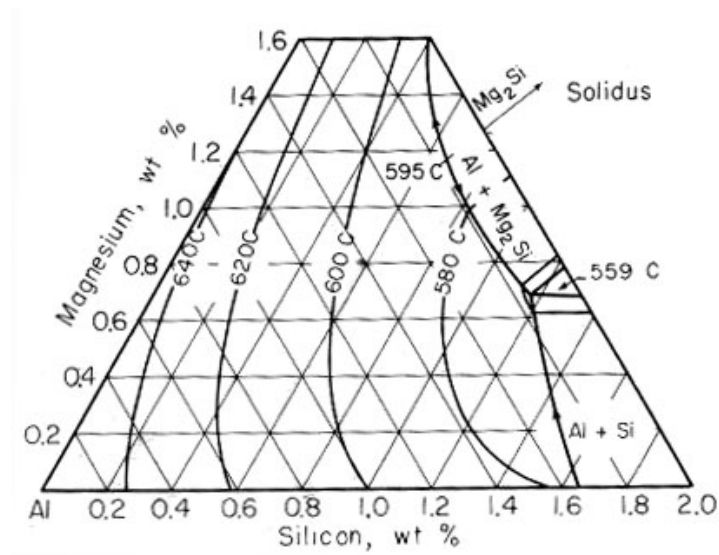


Figure A. 2 Al-rich portion of Al-Mg-Si system (solidus) [2]

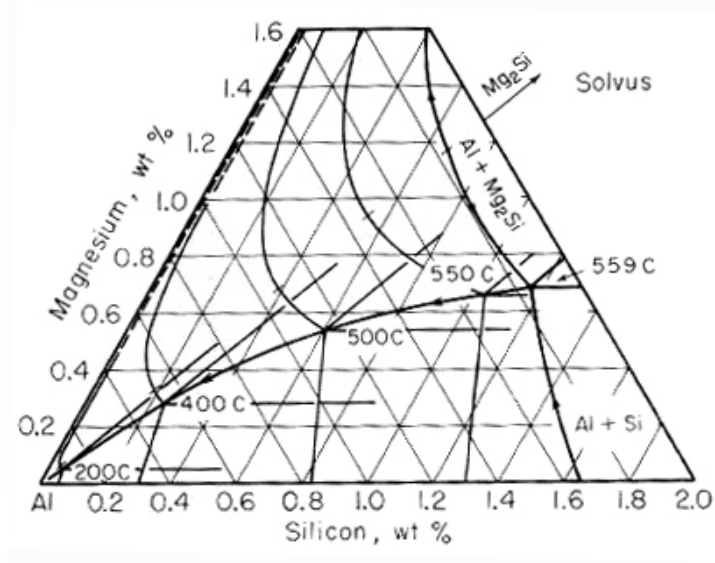


Figure A. 3 Al-rich portion of Al-Mg-Si system (solvus) [2]

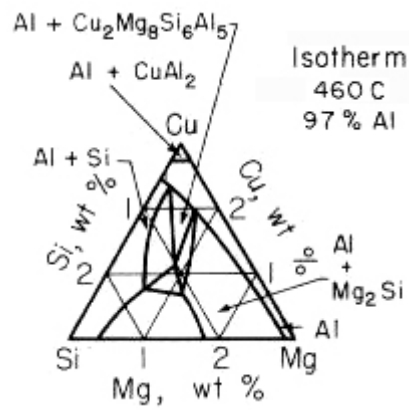


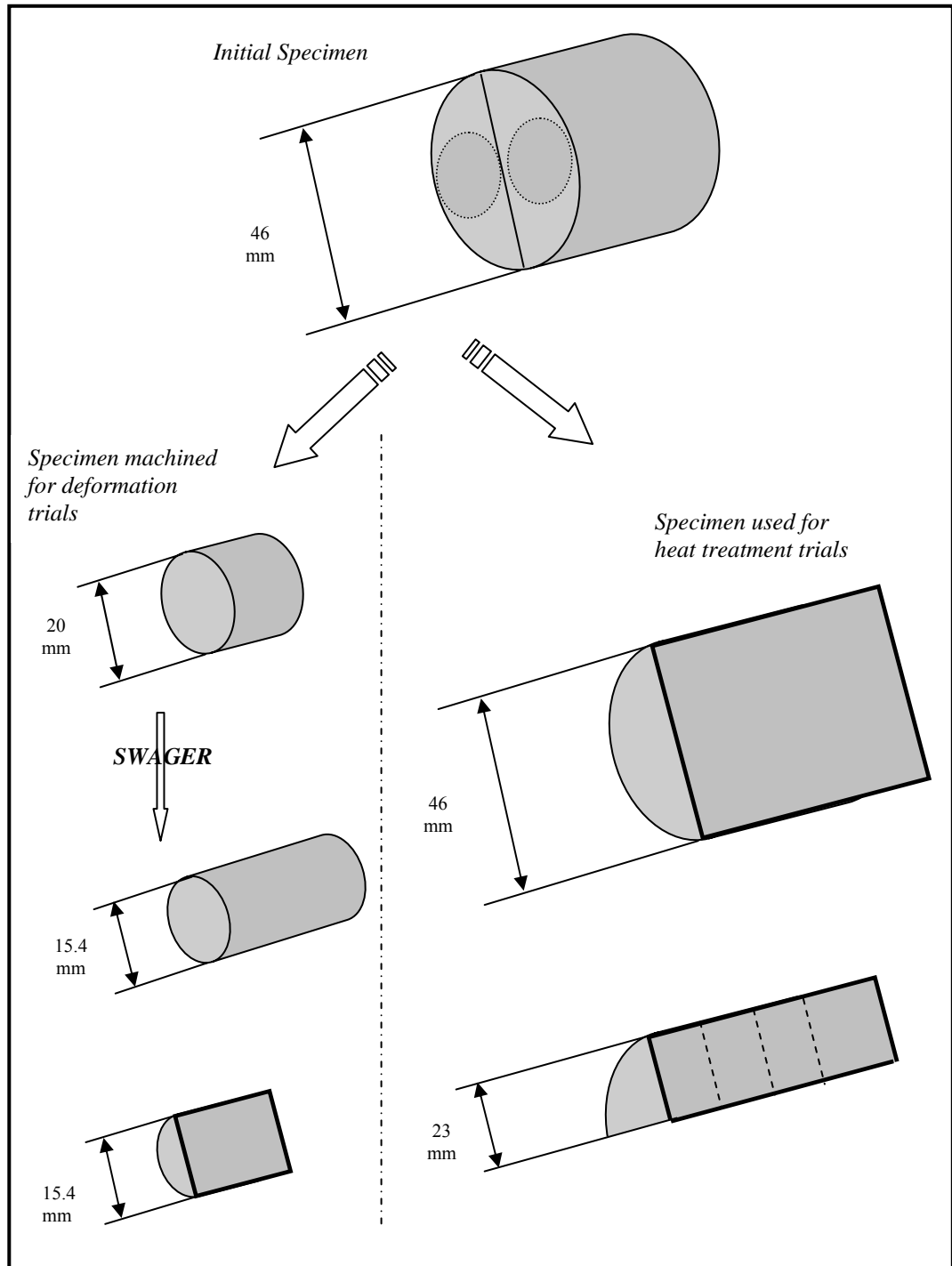
Figure A. 4 Al-Cu-Mg-Si system (97% Al section) [2]

Table A. 1 Survey of reported crystal structures of Al-Mg-Si-Cu alloy [24]

Phase	Structure	Notes	Mg/Si (wt.%)
GP zone	fcc based orthorhombic super cell Mg:Si = 2:1 $a = 8.08 \text{ \AA}$ , $b = 8.74 \text{ \AA}$ , $c = 4.05 \text{ \AA}$	Alternate stacking of two rows of Mg and one row of Si on (011) Al-matrix planes along [100]; same stacking as MoPt <sub>2</sub> structure	1.59
GP zone	fcc based cubic Mg:Si = 1:1 $a = 4.05 \text{ \AA}$	Alternating rows of Mg and Si along [100] with a spacing of 4.050 Å on Al lattice	1.73
GP zone (pre-β <sup>0</sup> )	fcc based base-centered monoclinic (Al + Mg) <sub>5</sub> Si <sub>6</sub> $a = 14.78 \text{ \AA}$ , $b = 4.05 \text{ \AA}$ , $c = 6.74 \text{ \AA}$ , $\beta = 106.8^\circ$	Complete crystal structure reported	0.67
β <sup>0</sup>	Base-centered monoclinic (C2/m) Mg <sub>5</sub> Si <sub>6</sub> $a = 15.16 \text{ \AA}$ , $b = 4.050 \text{ \AA}$ $c = 6.74 \text{ \AA}$ , $\beta = 105.3^\circ$	Complete crystal structure reported	0.94
β <sup>0</sup>	Base-centered monoclinic $a = 15.34 \text{ \AA}$ , $b = 4.05 \text{ \AA}$ $c = 6.83 \text{ \AA}$ , $\beta = 106^\circ$	Needles of β <sup>0</sup> precipitates	1.01
β <sup>0</sup>	Monoclinic $a = b = 6.16 \text{ \AA}$ , $c = 7.10 \text{ \AA}$ , $\alpha = \beta = 90^\circ$ , $\gamma = 82^\circ$	Selected area electron diffraction (SAED) patterns of needle precipitates, stereographic projection	0.09
β <sup>0</sup>	Monoclinic $a = 3.00 \text{ \AA}$ , $b = 3.30 \text{ \AA}$ , $c = 4.00 \text{ \AA}$ $\alpha = \beta = 90^\circ$ , $\gamma = 71^\circ$	Needles of β <sup>0</sup> precipitates	1.73
β <sup>0</sup>	Monoclinic	Needles of β <sup>0</sup> , TEM	0.45
β <sup>0</sup>	Monoclinic $a = 6.50 \text{ \AA}$ , $b = 7.60 \text{ \AA}$ $c = 4.05 \text{ \AA}$ , $\gamma = 70^\circ$	HRTEM, SAED, Needle morphology	1.54
β <sup>0</sup>	Monoclinic (P2/m) Al:Mg:Si = 3:1:6 $a = 7.70 \text{ \AA}$ , $b = 6.70 \text{ \AA}$ $c = 2.03 \text{ \AA}$ , $\gamma = 75^\circ$	HRTEM, SAED, Microbeam diffraction, (MBD), and energy dispersive X-ray, (EDX)	0.83
β <sup>1</sup>	Hexagonal $a = b = 7.05 \text{ \AA}$ , $c = 4.05 \text{ \AA}$	Rods of β <sup>1</sup> precipitates	1.73
β <sup>1</sup>	Hexagonal Mg <sub>44</sub> Si $a = b = 7.08 \text{ \AA}$ , $c = 4.05 \text{ \AA}$	Rods of β <sup>1</sup> precipitates	1.73
β <sup>1</sup>	Hexagonal Mg:Si = 2:1 $a = b = 7.10 \text{ \AA}$ , $c = 4.05 \text{ \AA}$	Sketch of unit cell model and projected atomic positions on (0001)	0.83
β <sup>1</sup>	Hexagonal $a = b = 7.15 \text{ \AA}$ , $c = 4.05 \text{ \AA}$	Complete crystal structure available	1.8
β	Hexagonal $a = b = 4.07 \text{ \AA}$ , $c = 4.05 \text{ \AA}$	Latent lattice for β <sup>1</sup>	1.54
β <sup>1</sup>	Hexagonal (P6̄2m) $a = b = 7.10 \text{ \AA}$ , $c = 4.05 \text{ \AA}$	Atomic coordinates reported	1.54
'u-phase'	Hexagonal $a = b = 6.70 \text{ \AA}$ , $c = 8.08 \text{ \AA}$	Al-Mg-Si alloys with Mn and/or Cr	0.64
Type B	Orthorhombic Al:Mg:Si = 4:2:5, $a = 6.83 \text{ \AA}$ , $b = 7.94 \text{ \AA}$ , $c = 4.05 \text{ \AA}$	Sketch of unit cell model	0.83
U2	Orthorhombic (Pnma) Al:Mg:Si = 4:4:4, $a = 6.75 \text{ \AA}$ , $b = 4.05 \text{ \AA}$ , $c = 7.94 \text{ \AA}$	Atomic coordinates reported	0.66

Table A. 1(cont'd)

Phase	Structure	Notes	Mg/Si (wt.%)
Type A	Hexagonal(P $\bar{6}2m$ ) Al:Mg:Si = 4:1:5 $a = b = 4.05 \text{ \AA}$ , $c = 6.70 \text{ \AA}$	Sketch of unit cell model	0.83
U1	Trigonal (P $\bar{3}m1$ ) Al:Mg:Si = 2:1:2 $a = b = 4.05 \text{ \AA}$ , $c = 6.74 \text{ \AA}$	Al <sub>2</sub> CaSi <sub>2</sub> (La <sub>2</sub> O <sub>3</sub> ) type	0.66
Type C	Hexagonal $a = b = 10.40 \text{ \AA}$ , $c = 4.05 \text{ \AA}$	HRTEM image + EDS profile	0.83
B'	Hexagonal $a = 10.4 \text{ \AA}$ , $c = 4.05 \text{ \AA}$	TEM, lath-like. The reported hexagonal cell is considered as a special case of a possible base-centered orthorhombic structure of B'	1.67
B'	Hexagonal $a = b = 10.50 \text{ \AA}$ , $c = 4.05 \text{ \AA}$	Laths of B', TEM	1.01
M	Hexagonal $a = 10.30 \text{ \AA}$ , $b = 4.05 \text{ \AA}$	HREM and SAED analysis	0.91
QP	Hexagonal $a = b = 3.95 \text{ \AA}$ , $c = 4.05 \text{ \AA}$	Latent lattice for QC, space group reported Structure involves mixed and partial occupancy	1.54
QC	Hexagonal $a = b = 7.10 \text{ \AA}$ , $c = 4.05 \text{ \AA}$	Latent lattice for Q', space group reported Structure involves mixed and partial occupancy	1.54
Q'	Hexagonal	DSC and TEM images	0.44
Q	Hexagonal P( $\bar{6}$ ) Al <sub>4</sub> Cu <sub>2</sub> Mg <sub>3</sub> Si <sub>7</sub> $a = b = 10.39 \text{ \AA}$ , $c = 4.02 \text{ \AA}$	Atomic coordinates reported Single crystals from an alloy with (wt%): 13.8% Cu, 24.8% Mg, 22.2% Si, and 39.2% Al	1.12
$\beta$	Cubic Mg <sub>2</sub> Si, $a = 6.39 \text{ \AA}$	TEM, CaF <sub>2</sub> type, platelets	1.73
$\beta$	Cubic Mg <sub>2</sub> Si, $a = 6.40 \text{ \AA}$	X-ray diffraction, CaF <sub>2</sub> type, platelets	1.73



**Figure A. 5 Specimen orientations**

Table A. 2 Hardness values for different solutionizing trials

DEVICE	PROCESS		CODE	BRINELL HARDNESS	Datas: Brinell D=2,5mm Ball KP62,5										
					57	59	57	56	56	57	57	56	56	56	
Muffle Furnace	515	95 min	0-0-0	57 ± 1,22	91	96	97	93	93	96					
		95 min + Aged177 8h	0-151-778	94 ± 2,34	133	133	124	133	137	128					
	520	95 min	0-201-0	94 ± 3,39	98	93	96	88	93	93					
		95 min + Aged177 8h	0-201-778	135 ± 1,79	137	135	135	133	137	133					
	525	95 min	0-251-0	93 ± 3,06	93	88	96	96	93	91					
		95 min + Aged177 8h	0-251-778	138 ± 1,64	135	140	137	138	138	137					
	530	95 min	0-301-0	95 ± 1,55	93	96	93	96	96	96					
		95 min + Aged177 8h	0-301-778	139 ± 1,38	139	140	137	138	140	137					
	535	95 min	0-351-0	93 ± 1,83	91	91	93	93	93	96					
		95 min + Aged177 8h	0-351-778	140 ± 5,06	144	147	142	135	135	137					
	540	95 min	0-401-0	96 ± 1,83	98	98	96	96	96	93					
		95 min + Aged177 8h	0-401-778	142 ± 3,66	142	144	144	137	139	147					
	550	95 min	0-501-0	99 ± 3,13	96	104	101	96	96	98					
		95 min + Aged177 8h	0-501-778	144 ± 2,58	142	142	147	147	142	142					
560	95 min	0-601-0	98 ± 2,25	98	98	96	96	96	101						
	95 min + Aged177 8h	0-601-778	145 ± 2,58	147	147	147	142	142	147						
515	720 min	0-152-0	93 ± 0,98	91	93	93	93	94	93						
	720 min + Aged177 8h	0-152-778	134 ± 1,72	133	133	136	136	132	133						
530	720 min	0-302-0	83 ± 2,07	82	86	86	82	82	82						
	720 min + Aged177 8h	0-302-778	145 ± 2,58	142	147	147	142	147	147						
540	720 min	0-402-0	98 ± 1,97	96	98	96	96	98	101						
	720 min + Aged177 8h	0-402-778	139 ± 3,46	142	137	142	133	140	140						
550	720 min	0-502-0	95 ± 1,55	96	93	96	96	93	96						
	720 min + Aged177 8h	0-502-778	139 ± 2,58	137	142	137	137	137	142						
530	65 min	0-303-0	95 ± 1,22	93	95	93	95	96	95						
	65 min + Aged177 8h	0-303-778	138 ± 1,63	140	137	136	138	140	139						

Table A. 3 Hardness values for different aging trials

PROCESS	CODE	BRINELL HARDNESS	Data: Brinell D=2,5mm Ball kP62,5															
			102	100	101	102	99	97,3	98,6	99,5	98	100	100	100	100	100	100	
150°C	2 h	100 ± 1,44	102	100	101	102	99	97,3	98,6	99,5	98	100	100	100	100	100	100	
	4 h	106 ± 1,61	108	106	107	106	107	104	105	106	105	107	105	107	105	107	105	
	6 h	110 ± 1,88	111	109	108	110	108	108	113	113	113	112	110	112	111	112	111	
	8 h	116 ± 1,73	117	115	115	114	115	113	116	120	115	115	115	115	116	115	116	
	10 h	120 ± 1,07	119	120	122	118	119	119	121	120	119	120	120	120	119	120	120	
	12 h	126 ± 1,24	126	126	127	125	124	123	126	126	126	124	126	127	126	127	126	
	14 h	127 ± 2,07	126	126	129	132	126	124	126	128	126	126	126	126	128	128	128	
	16 h	130 ± 1,44	130	131	130	128	132	127	132	130	129	130	130	130	130	130	130	
165°C	2 h	118 ± 1,72	120	120	119	119	119	117	116	117	115	116	116	116	118	118	118	
	4 h	132 ± 1,48	134	134	132	131	133	130	130	130	133	131	132	131	132	131		
	6 h	135 ± 1,28	134	132	135	136	135	134	137	135	136	135	135	135	136	135		
	8 h	138 ± 1,19	138	135	139	137	137	139	139	139	138	138	138	138	137	137		
	10 h	139 ± 1,31	141	139	138	140	140	138	141	138	137	140	138	138	139	139		
	12 h	140 ± 1,73	140	140	139	142	138	137	138	139	138	142	140	142	140	142		
	14 h	138 ± 0,78	139	139	139	138	138	139	138	137	139	137	138	137	138	139		
	16 h	138 ± 1,97	137	138	139	133	137	138	141	137	140	137	138	137	138	137		
175°C	2 h	129 ± 1,38	131	131	131	130	128	130	129	128	128	131	128	128	128	128		
	4 h	136 ± 2,11	133	136	136	134	137	136	136	139	140	137	136	133	133			
	6 h	136 ± 2,38	133	136	136	135	135	137	141	133	140	136	136	137	137			
	8 h	140 ± 1,17	140	137	141	139	141	140	140	139	138	140	140	139	139			
	10 h	139 ± 2,97	136	139	137	135	135	137	144	140	143	141	140	140	140			
	12 h	137 ± 1,82	139	139	136	137	137	136	139	138	137	134	140	135	135			
	14 h	136 ± 2,09	137	138	133	137	133	133	138	137	135	136	136	139	139			
	16 h	137 ± 1,42	136	138	136	137	133	138	138	137	137	137	138	136	137			

Table A. 3 (cont'd)

PROCESS		CODE	BRINELL HARDNESS	Data: Brinell D=2,5mm Ball kP62,5															
185°C	2 h	0-501-851	143 ± 2,21	146	146	142	142	140	143	143	142	141	141	145	145	141	143	140	
	4 h	0-501-852	141 ± 1,71	139	141	143	141	143	143	142	141	140	141	141	138	142	143	139	
	6 h	0-501-853	142 ± 1,53	140	141	141	141	143	145	143	143	143	144	141	141	141	143	141	
	8 h	0-501-854	140 ± 2,20	139	143	143	143	142	140	139	140	140	138	137	137	139	137	137	
	10 h	0-501-855	137 ± 1,98	133	135	136	136	138	135	136	141	137	138	137	137	137	137	137	
	12 h	0-501-856	136 ± 1,96	136	134	133	133	137	137	134	138	140	136	136	136	136	136	138	
	14 h	0-501-857	135 ± 1,24	134	133	135	135	135	133	133	135	136	135	137	135	136	136	136	
	16 h	0-501-858	135 ± 1,64	137	132	135	135	136	134	134	135	137	135	132	135	132	135	134	
200°C	2 h	0-501-001	132 ± 1,68	133	137	132	132	133	132	130	132	132	132	133	132	131	132	132	
	4 h	0-501-002	129 ± 1,44	129	130	128	128	131	128	128	132	128	128	129	130	129	127	127	
	6 h	0-501-003	128 ± 2,37	129	132	129	129	131	130	129	125	126	126	125	126	125	126	126	
	8 h	0-501-004	124 ± 1,60	124	124	124	124	126	125	126	124	121	121	121	123	123	124	124	
	10 h	0-501-005	122 ± 2,54	123	123	125	125	126	123	123	125	121	118	119	120	122	120	120	
	12 h	0-501-006	121 ± 1,27	123	123	122	121	121	120	120	120	119	120	121	120	121	120	120	
	14 h	0-501-007	119 ± 2,09	120	120	121	121	120	121	121	122	120	117	116	116	117	116	118	
	16 h	0-501-008	116 ± 3,45	120	121	119	119	118	115	117	112	112	115	111	112	112	112	114	

Table A. 4 Hardness values for different deformation steps

PROCESS			CODE	BRINELL HARDNESS	Data: Brinell D=2,5mm Ball kP62,5		
Deformation %	Temp	Age Time					
10%	RT	Deformed	10-0-0	73 ± 1,17	72,9	72,1	74,4
		Solutionized	10-301-0	84 ± 1,04	83,1	85	84,8
		4 h	10-301-752	134 ± 1,15	135	133	135
		6 h	10-301-753	135 ± 0,58	135	135	136
		8 h	10-301-754	139 ± 1,15	138	138	140
		10 h	10-301-755	138 ± 1,15	139	139	137
		12 h	10-301-756	137 ± 2,08	136	139	135
	200	Deformed	12-0-0	71 ± 0,26	71,5	71,4	71
		Solutionized	12-301-0	90 ± 0,58	88,9	89,9	89,9
		4 h	12-301-752	135 ± 1,73	137	134	134
		6 h	12-301-753	135 ± 0,58	135	135	134
		8 h	12-301-754	140 ± 0,58	140	141	140
		10 h	12-301-755	132 ± 0,58	131	132	132
		12 h	12-301-756	132 ± 1,00	131	133	132
	300	Deformed	13-0-0	60 ± 0,42	60,9	60,3	60,1
		Solutionized	13-301-0	83 ± 1,48	83,9	81,2	83,6
		4 h	13-301-752	134 ± 0,58	134	133	134
		6 h	13-301-753	136 ± 1,15	137	135	135
		8 h	13-301-754	141 ± 0,58	140	141	141
		10 h	13-301-755	137 ± 0,00	137	137	137
		12 h	13-301-756	138 ± 1,53	136	139	138
	400	Deformed	14-0-0	66 ± 0,75	66,8	66	65,3
		Solutionized	14-301-0	87 ± 1,19	86,8	88,7	86,5
		4 h	14-301-752	132 ± 1,00	133	131	132
6 h		14-301-753	139 ± 0,58	139	140	139	
8 h		14-301-754	134 ± 1,00	135	133	134	
10 h		14-301-755	131 ± 1,53	130	133	131	
12 h		14-301-756	132 ± 0,00	132	132	132	
20%	RT	Deformed	20-0-0	79 ± 0,44	78,6	79,4	78,7
		Solutionized	20-301-0	82 ± 2,10	84,5	82,2	80,3
		4 h	20-301-752	130 ± 1,73	132	129	129
		6 h	20-301-753	133 ± 1,15	134	132	134
		8 h	20-301-754	133 ± 1,00	133	134	132
		10 h	20-301-755	133 ± 1,73	131	134	134
		12 h	20-301-756	137 ± 0,58	137	137	136
	200	Deformed	22-0-0	78 ± 0,66	78,6	78,1	77,3
		Solutionized	22-301-0	82 ± 1,55	81,4	80	83,1
		4 h	22-301-752	132 ± 1,15	131	131	133
		6 h	22-301-753	129 ± 1,53	131	129	128
		8 h	22-301-754	137 ± 1,73	138	138	135
		10 h	22-301-755	131 ± 0,58	132	131	131
		12 h	22-301-756	131 ± 1,00	132	130	131
	300	Deformed	23-0-0	65 ± 0,40	65,2	64,7	65,5
		Solutionized	23-301-0	83 ± 1,00	83,9	82,9	81,9
		4 h	23-301-752	128 ± 1,15	127	127	129
		6 h	23-301-753	130 ± 0,58	130	131	130
		8 h	23-301-754	130 ± 0,58	130	130	131
		10 h	23-301-755	129 ± 1,73	128	131	128
		12 h	23-301-756	126 ± 0,58	127	126	126
	400	Deformed	24-0-0	69 ± 0,85	69,6	68	68,3
		Solutionized	24-301-0	85 ± 1,33	86,1	83,8	86,1
		4 h	24-301-752	133 ± 1,53	135	133	132
6 h		24-301-753	132 ± 0,58	132	132	133	
8 h		24-301-754	134 ± 2,89	132	132	137	
10 h		24-301-755	133 ± 2,08	131	135	132	
12 h		24-301-756	130 ± 1,00	130	129	131	

Table A. 4 (cont'd)

PROCESS			CODE	BRINELL HARDNESS	Data: Brinell D=2,5mm Ball kP62,5		
Deformation %	Temp	Age Time					
30%	RT	Deformed	30-0-0	82 ± 0,26	81,5	82	81,9
		Solutionized	30-301-0	85 ± 0,91	85,9	84,1	85,2
		4 h	30-301-752	132 ± 1,53	131	134	132
		6 h	30-301-753	135 ± 0,58	136	135	135
		8 h	30-301-754	135 ± 0,00	135	135	135
		10 h	30-301-755	131 ± 1,15	130	132	130
	200	12 h	30-301-756	132 ± 0,58	132	132	133
		Deformed	32-0-0	75 ± 0,75	75,4	76,1	74,6
		Solutionized	32-301-0	87 ± 0,53	86,8	87,8	87,6
		4 h	32-301-752	135 ± 1,15	136	134	134
		6 h	32-301-753	135 ± 3,06	138	132	134
		8 h	32-301-754	134 ± 3,21	133	138	132
	300	10 h	32-301-755	133 ± 1,53	132	133	135
		12 h	32-301-756	132 ± 0,58	133	132	132
		Deformed	33-0-0	63 ± 0,46	62,7	63,5	63,5
		Solutionized	33-301-0	81 ± 1,37	80,2	82,9	81,2
		4 h	33-301-752	127 ± 1,15	128	126	128
		6 h	33-301-753	133 ± 2,08	131	135	132
	400	8 h	33-301-754	130 ± 1,15	131	131	129
		10 h	33-301-755	128 ± 1,53	128	130	127
		12 h	33-301-756	125 ± 1,15	126	124	126
		Deformed	34-0-0	66 ± 0,93	66,6	64,9	65,1
		Solutionized	34-301-0	79 ± 0,87	79,9	79,9	78,4
		4 h	34-301-752	132 ± 1,53	130	133	132
40%	RT	6 h	34-301-753	134 ± 0,58	133	134	134
		8 h	34-301-754	134 ± 1,15	133	135	135
		10 h	34-301-755	134 ± 2,08	132	136	135
		12 h	34-301-756	131 ± 2,65	128	133	132
		Deformed	40-0-0	80 ± 2,51	82,4	79,5	77,4
		Solutionized	40-301-0	83 ± 0,40	82,7	83,4	83,4
	200	4 h	40-301-752	135 ± 1,15	136	134	136
		6 h	40-301-753	136 ± 0,58	136	136	135
		8 h	40-301-754	139 ± 0,00	139	139	139
		10 h	40-301-755	136 ± 2,08	138	134	135
		12 h	40-301-756	135 ± 0,58	135	134	135
		Deformed	42-0-0	78 ± 0,52	77,8	78,7	78,7
	300	Solutionized	42-301-0	78 ± 0,80	79,2	77,6	78,4
		4 h	42-301-752	132 ± 1,15	131	133	133
		6 h	42-301-753	136 ± 0,58	136	136	135
		8 h	42-301-754	134 ± 1,15	135	133	133
		10 h	42-301-755	133 ± 2,08	131	135	132
		12 h	42-301-756	132 ± 0,58	131	132	132
	400	Deformed	43-0-0	63 ± 0,79	63,5	62	63,2
		Solutionized	43-301-0	77 ± 2,25	76,1	79,9	75,9
		4 h	43-301-752	128 ± 0,58	128	128	127
		6 h	43-301-753	132 ± 1,73	133	130	133
		8 h	43-301-754	131 ± 0,58	131	132	131
		10 h	43-301-755	135 ± 0,58	135	135	134
200	12 h	43-301-756	130 ± 0,00	130	130	130	
	Deformed	44-0-0	64 ± 0,25	63,8	63,5	63,3	
	Solutionized	44-301-0	85 ± 0,49	85,4	84,6	85,5	
	4 h	44-301-752	138 ± 2,08	140	137	136	
	6 h	44-301-753	141 ± 1,53	140	141	143	
	8 h	44-301-754	140 ± 1,73	138	141	141	
300	10 h	44-301-755	136 ± 0,58	136	136	137	
	12 h	44-301-756	135 ± 1,15	134	136	134	